

Regional Analysis of Maize-Based Land Use Systems for Early Warning Applications

Denis Rugege

Promotors: Prof. Dr Ir J. Bouma
Professor of Soil Inventarization and Land Evaluation
Wageningen University

Prof. Dr A.K. Skidmore
Professor of Vegetation and Agricultural Land Use Survey
ITC, Enschede, and Wageningen University

Co-promotor: Prof. Dr Ir P.M. Driessen
Professor of Modelling for Quantitative Land Evaluation
ITC, Enschede, and Wageningen University

Examining Committee:

Assoc.Prof.Dr J.R. Milford	University of Zimbabwe, Harare
Prof.Dr H.A. Savenije	IHE, Delft
Prof.Dr Ir.H. van Keulen	Wageningen University
Prof.Dr A. Meijerink	ITC, Enschede

Regional Analysis of Maize-Based Land Use Systems for Early Warning Applications

Denis Rugege

Thesis

to fulfill the requirements for the degree of doctor
on the authority of the Rector Magnificus of Wageningen University,
Prof.Dr Ir.L.Speelman, to be publicly defended
on Wednesday 20 March 2002
at 15.00 hrs in the auditorium
of ITC, Enschede.

Doctoral thesis (2002) ISBN 90-5808-584-8
Wageningen University, The Netherlands

© 2002 Rugege. D.



ITC Dissertation No. 87

The research presented in this thesis was conducted at the International Institute
for Aerospace Survey and Earth Sciences (ITC)

P.O.Box 6
7500 AA Enschede
The Netherlands

Regional Analysis of Maize-Based Land Use Systems for Early Warning Applications

Abstract

Conventional analytical crop growth models cannot handle *actual* Land Use Systems because of massive data needs, algorithm complexity and prohibitive error propagation. It is possible however to describe rigidly simplified 'Production Situations' representing Land Use Systems with annual row crops and minimal environmental constraints. The simplest Production Situation imaginable is a Land Use System in which all constraints that can be eliminated by a farmer are indeed (assumed to be) eliminated. Crop growth and yield are then entirely conditioned by crop physiology and weather conditions, notably by the temperature and radiation during the crop cycle. The calculated production level is not the actual production but the production potential.

In many countries, water availability to the crop is the main constraint to crop production. The biophysical production potential model has therefore been extended with a water budget routine that matches actual water use with the crop's requirement in order to calculate the "water-limited production potential". In this configuration, crop physiology, temperature, radiation *and* water availability condition the calculated level of crop (potential) production. This thesis discusses the use of satellite-derived rainfall data for regional analysis of water-limited yield potentials.

Monitoring and crop yield forecasting for early warning applications require insight in farmers' reality. Often, a score of environmental and socio-economic constraints reduce on-farm production to a level that lags far behind the theoretical production potential. This thesis explores farmers' insights, in an attempt to identify the causes and structure of the "yield gap" between potential (reference) production levels and production levels realized on-farm.

So far, actual production could only be established through field measurements. This thesis presents a methodology for estimating regional levels of actual crop production. The difference between remotely sensed canopy temperature and ambient temperature is used to estimate the degree of stomata closure of the crop. Introducing this Remote Sensing based degree of stomata closure in calculations of assimilatory activity permits to calculate the actual rate of crop growth over regions.

Repeated measurements during the crop cycle allow monitoring of the sufficiency of actual management practices. Introducing estimated or forecast weather data in crop growth calculations for the remainder of the crop cycle permits to make repeated estimates of anticipated crop production and to timely signal a need for remedial action.

Dedication

To my wife Lineo and daughters Naleli and Tsatsi for the energizing love.

Acknowledgements

I am deeply indebted to many individuals in the Netherlands, Zimbabwe and South Africa who supported me in the production of this thesis. It is impossible to mention all of them by name and their various supporting contexts. However, I wish to thank the following persons for their direct scientific contribution to research:

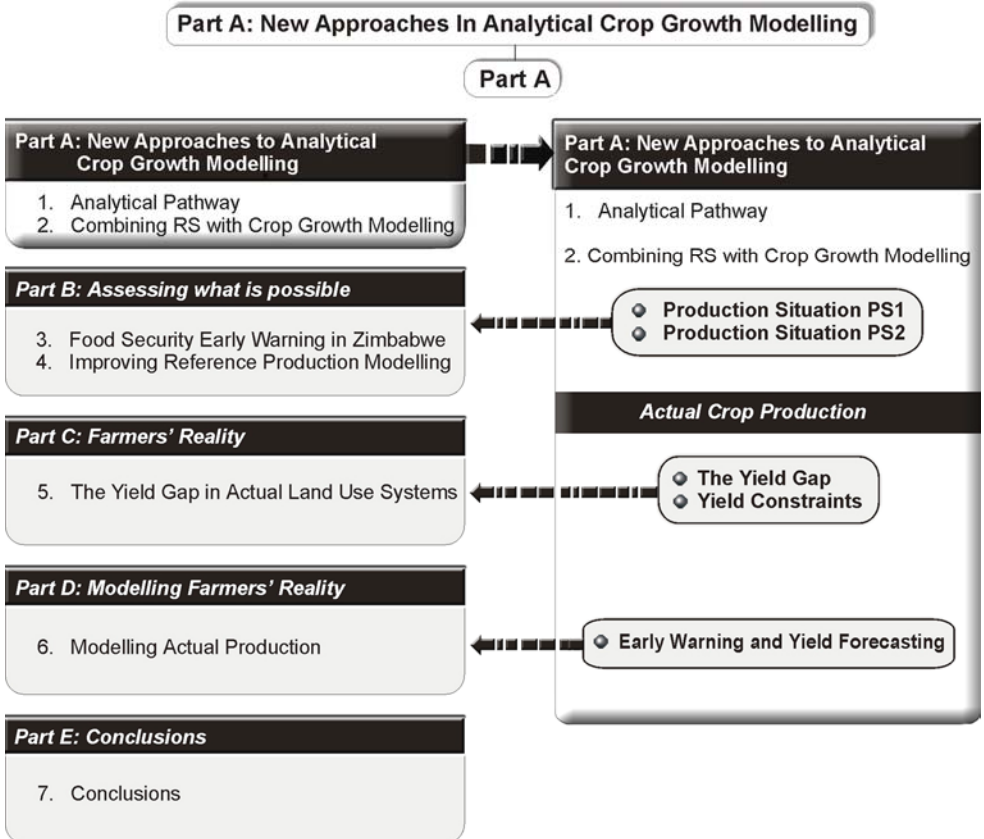
- Paul Driessen for his patient and ever reassuring supervision as co-promotor. I greatly benefited from his skill in simplifying difficult subjects with humour.
- Johan Bouma for his conscientious and critical guidance as my WU promotor.
- Andrew Skidmore for his critical as well as affirming comments as my ITC promotor.
- Rogerio Bonifacio for his assistance in the mathematical considerations in geostatistics and for his consistent friendship.
- Gabriel Parodi for his unreserved assistance in remotely sensed surface temperature retrieval methods.
- Kees de Bie for his assistance in the yield gap studies, thesis production and for his long-standing friendship.
- Marieke de Groen for her friendship, assistance in the field and for useful comments on the rainfall interpolation methodology.
- Philip Thornton and Peter Jones for making available the Marksim weather generation software and for friendly advice.
- Wuntah Wuni and Zook Muleya for collaboration in data collection during their MSc fieldwork.

Table of Contents

Part A. New Approaches in Analytical Crop Growth Modelling	9
1. Analytical Pathway: The Train of Thought	11
2. Combining Remote Sensing with Crop Growth Modelling for Reference and Actual Production Situations	13
2.1 Production Situations PS-1 and PS-2	13
2.2 Actual Crop Production - Production Situation PS-n	17
2.2.1 The energy balance equation	17
2.2.2 Net radiation intercepted by the canopy (INTER)	17
2.2.3 Total incoming radiation (CANRAD)	18
2.2.4 Net long-wave losses (LWLOSS)	19
2.2.5 Sensible heat flux (INRAD)	20
2.2.6 Aerodynamic resistance to heat transport (AERODR)	20
2.2.7 Latent heat flux (TRLOSS)	21
2.3 The Yield Gap	24
2.4 Early Warning and Crop Yield Forecasting	25
Part B. Assessing What is Possible	27
3. Case Study 1: Food Security Early Warning in Zimbabwe	29
3.1 General Background	29
3.1.1 Agro-ecology	30
3.1.2 Maize-based land use systems in communal lands	30
3.2 Food Security Early Warning Systems	31
3.2.1 Limitations of the WRSI model	33
3.2.2 Required and achievable improvements	33
3.2.3 Hypotheses	34
3.2.4 Assumptions	34
4. Improving Reference Production Modelling using Remotely Sensed Precipitation	35
4.1 Rain-Gauge related Limitations	35
4.2 Prospects for Satellite Derived Rainfall Estimates	37
4.3 The Cold Cloud Duration (CCD) Concept	37
4.4 Rainfall Estimation Methodology adopted in this Study	38
4.5 Comparison between Gauged Rainfall and Satellite-Derived Estimates	39
4.5.1 Deriving a semi-variogram model for North-Western Zimbabwe	41
4.5.2 Estimating area average rainfall using block-kriging	43
4.5.3 Results and validation of Meteosat-derived RFEs	45
4.6 Merits of Meteosat-Derived RFEs	48
4.7 Model Time-Step versus Available Data	49
4.7.1 Disaggregating dekadal rainfall estimates to daily values	49
4.7.2 Validation of the disaggregated rainfall estimates	51
4.8 PS-2 Simulations of Maize-Based Land-Use Systems using Meteosat	53

4.9 Discussion.....	58
Part C. Farmers' Reality	59
5. Case Study 2: The Yield Gap and Causative Constraints in Maize-Based Land Use Systems in Piriwiri and Mupfure Communal Lands, Zimbabwe	61
5.1 Study Area	61
5.2 The Weather during the 1996/97 Growing Season	62
5.3 Descriptive Statistics.....	63
5.3.1 Yield and context data.....	63
5.3.2 Management data.....	64
5.3.3 Data on yield reducing factors	69
5.3.4 Land data	70
5.4 Multiple Regression	73
5.5 Yield Gap by Yield Constraint.....	75
Part D. Modelling Farmers' Reality	77
6. Case Study 3: Using Remotely Sensed Canopy Temperatures in Modelling Actual Crop Production in Quzhou County, North China Plain	79
6.1 Crop Canopy Temperature Retrieval.....	79
6.2 Validating the Temperature-Difference Phenomenon	82
6.3 Updating the Temperature Difference Variable in the PS-n Model	84
6.3.1 Parallel processes feeding data into the PS-n model	84
6.3.2 Estimating day-equivalent canopy temperatures.....	85
6.4 Model Results and Validation	85
6.5 Discussion.....	88
Part E. Conclusions.....	89
7. Conclusions.....	91
8. References	93
9. Appendixes	97
A: Outline of the Structure of the PS-n Algorithm	97
B: Land surface Temperature Retrieval	103
C: 1998 Weather of Karoi from Interpolated Surfaces	106
D1: Land Mapping Units (LMUs) in Piriwiri/Mupfure	107
D2: Legend to Land Mapping Units.....	108
E1: Sample Checklist.....	109
E2: Sample Revelee Data Sheet	112
F: ITC PhD Dissertation List	114
Samenvatting	119
Curriculum Vitae	121

Part A. New Approaches in Analytical Crop Growth Modelling



Notice

Important publications, which shaped modern land evaluation, are discussed in their original form. Consequently, units, symbols and definitions do not always follow the guidelines of the International Organization for Standardization (ISO).

Equations in Part A of this text include some conventions of BASIC and are represented by multiple letters, as in computer programs and in Appendix A of this text.

1. Analytical Pathway: The Train of Thought

The success of a particular Land Use System, i.e. of a particular Land Use on a particular Land Unit, cannot be judged solely by the produce obtained. A rice farmer in Indonesia who harvests 5 tons of rice grain per hectare can look back on a commendable job. That same yield would not impress anyone in the Po Delta (Italy) where solar radiation is greater (longer day lengths and less clouds) and rice yields are accordingly higher. If crop yield is to be used as an indicator of the adequacy of management, the yield obtained must be judged in relation to a **reference** yield, i.e. the yield obtained in a comparable but constraint-free (ideally managed) Production Situation. This 'bio-physical yield potential' can be calculated and verified in field trials on an experiment station. It varies between years, even under perfect management, inter alia because weather conditions vary between years.

Actual yield, i.e. the yield realized by a farmer, is likely to be less than the bio-physical potential because it is generally not economical to fully remove *all* constraints to crop growth. The actual yield is affected by a score of constraints: sub-optimum availability of water and/or nutrients, weeds, pests, diseases, harvest losses, unforeseen biophysical events and the socio-economic setting (and interactions between these) all influence the final result. The analytical complexity of actual Land Use Systems precludes modelling actual crop yield as a dependent variable. In other words, actual crop performance cannot be calculated; it can only be observed.

Crop growth is a highly dynamic process. Calculations of reference production levels must therefore make use of **dynamic crop growth modelling** and actual crop performance must be repeatedly gauged. Recurrently surveying actual crop performance over large areas is prohibitively expensive. However, integrating **remotely sensed crop information** in crop growth modelling permits estimating actual crop growth in a region. Comparing this actual crop growth with the calculated reference growth level reveals the compounded effect of all constraints operative in a Land Use System up to the moment of the satellite pass.

The difference between the calculated and experimentally verified theoretical (reference) production potential and the observed actual yield is the **Yield Gap**. Yield gap analysis, founded on a statistical evaluation of farmers' perceptions of individual constraints, produces a weighted ranking of management priorities.

Canopy warming/cooling is one term in an energy budget relating incident solar radiation to long-wave losses, reflected energy, energy used in vaporization of water (crop transpiration), etc. The difference between the remotely sensed crop canopy temperature and the corresponding ambient temperature is co-determined by the actual rate of crop transpiration at the moment of the satellite pass. The transpiration term is isolated from the energy budget and divided by the theoretical

transpiration rate of a constraint-free reference crop. The resulting '**coefficient of water sufficiency** ($cf(water)$, 0-1) indicates the degree of stomata closure and therewith the degree to which photosynthetic activity is reduced by the compounded constraints to the actual crop. Recurrent reading at short intervals accounts for the dynamics of crop growth and produces successive, near real-time estimates of actual crop performance.

Regional applications of this technique produce regularly updated index maps of relative crop performance that are invaluable in **early warning** applications. Substituting estimated weather parameter values over the period between the last satellite pass and the foreseen date of crop maturity in the simulation procedure enables making repetitively updated regional crop yield forecasts.

2. Combining Remote Sensing with Crop Growth Modelling for Reference and Actual Production Situations

2.1 Production Situations PS-1 and PS-2

In the present context, 'biophysical production potential' is defined as the level of dry mass production that a farmer would achieve if all constraints to crop growth that can be eliminated were indeed fully remedied. This means that moisture availability to the crop is (assumed to be) exemplary throughout the growth cycle of the crop, that plant nutrients are present in sufficient and balanced amounts and that there are no weeds, pests, diseases or other removable constraints. Forcing variables that a 'normal' farmer cannot alter, notably the amount of incoming solar radiation and the temperature, will then condition crop growth, within the limits set by the plants' photosynthetic mechanism. (In glasshouse cultures, artificial lighting, heating and even additions of CO₂ are used to fully exploit the plants' photosynthetic potential. This possibility is not open to the 'normal' farmer referred to in this thesis.)

This minimum configuration, known as 'Production Situation 1' (PS-1), represents a simplified Land Use System in which production and yield are solely determined by the available light, the temperature and the photosynthetic mechanism of the crop:

$$\text{PS-1: } P, Y = f(\text{light, temperature, } C3/C4) \quad (\text{Eq.1})$$

The levels of crop production and yield calculated for PS-1 are not the actual production and yield but *potentials* that are normally only realized at experiment stations where even the last weed plant or bug is mercilessly eliminated, irrespective of cost.

Analytical models of the biophysical production potential of annual food and fiber crops have been built and tested in The Netherlands and elsewhere since the 1960's (De Wit and Penning de Vries, 1985). These models account for the dynamics of crop growth by dividing the crop cycle in successive (short) time intervals during which processes are assumed to take place at steady rates. 'State variables' such as leaf, root, stem and storage organ masses indicate the state of the system during a particular interval; their values are updated after each cycle of interval calculations.

A particular set of interval calculations first quantifies the actual gross rate of assimilation during the interval. The gross assimilate production is then assigned to leaf growth, stem growth, root growth and storage organ growth as a function of the momentary relative development stage of the plants. Next, maintenance respiration losses during the interval are calculated for each plant organ and subtracted from the gross assimilate allocations to obtain net assimilate quantities available for growth. These are subsequently multiplied by organ-specific

'conversion efficiency' coefficients to obtain the increments in dry organ masses during the interval that are used to adjust corresponding state variable values.

The complete procedure involves three characteristic phases illustrated by the relational diagram in **Figure 1**.

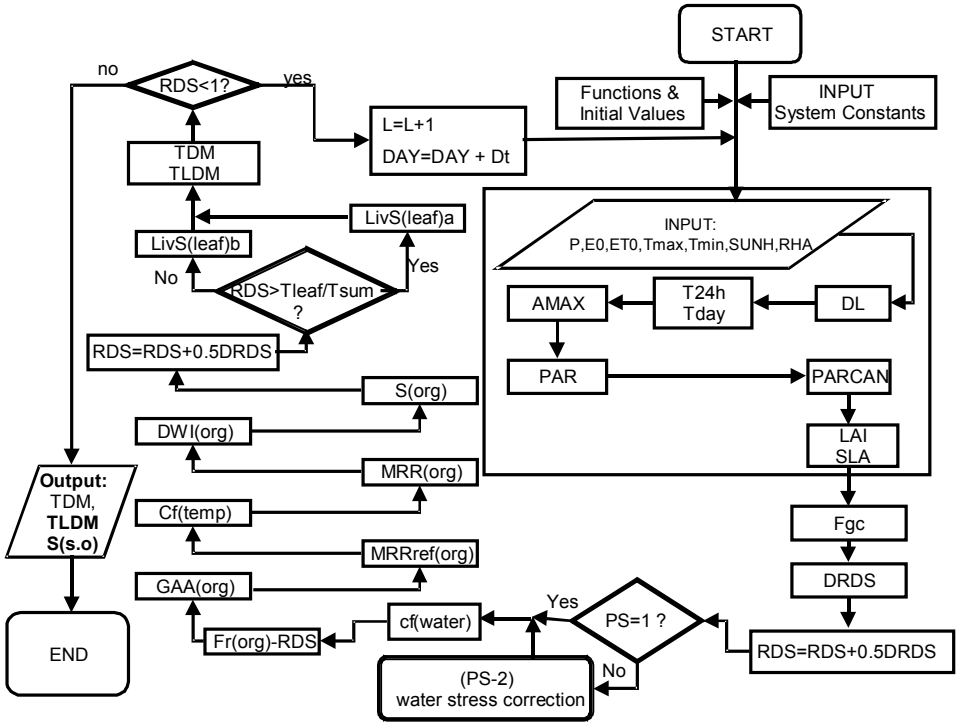


Figure 1. Relation diagram of the analysis of production situation PS-1, after Driessen & Konijn (1992).

a) *Initialisation*

- Input of system constants: management data, crop data and location and interval data,
- Initial state variable values: leaf, stem and root masses at crop emergence or planting

b) *Recurrent interval analyses*

- Input of interval-specific (i.e. daily) weather data: minimum and maximum temperatures (T_{max} , T_{min}) and number of sunshine hours/interval (SUNH) and relative air humidity (RHA),

- Calculation of gross rate of assimilate production (F_{gross}) as a function of 'photosynthetically active radiation' at top of canopy (PARCAN), day length (DL), momentary leaf area index (LAI), maximum assimilation rate at actual temperature (adjusted AMAX) and canopy properties, notably the extinction coefficient for visible light (k_e) and the light use efficiency at low light intensity (EFF),
- Apportioning of gross assimilates production to the various plant organs and calculation of Gross Assimilates Availability to each plant organ ($GAA(\text{org})$),
- Loss of assimilates in respiration to maintain living plant matter, by plant organ ($MRR(\text{org})$),
- Conversion of the remaining ('net') assimilates production into dry organ mass increments ($DWI(\text{org})$),
- Adding up all organ masses ($S(\text{org})$) to total dry mass (TDM) and/or total living dry mass (TLDM)

c) **Output of results**

Once physiological development is complete and all intervals in a growing cycle have been processed, the biophysical production potential (TDM) and the yield potential, usually the storage organ mass ($S(\text{so})$), are output.

The relative simplicity and low data needs of PS-1 analyses allow to accurately quantify reference yield (i.e. the harvested produce) and production (i.e. total dry plant mass) levels, provided that adequate basic data are available. This condition may be fulfilled in an experimental set-up but is seldom met in regional analyses. Therefore the analytical models have been re-worked to so-called 'policy support models' that make the most of routinely collected *daily* radiation and temperature data.

In many regions, water availability to the crop is the main constraint to crop growth. Water is needed in great quantity (in dry regions a maize crop may well transpire 1 cm of water on a clear sunny day, equivalent to $100,000 \text{ l ha}^{-1} \text{ d}^{-1}$). Irrigation (and/or drainage) requires expensive infrastructure and skilled labour to restrict losses to the minimum and prevent soil degradation, e.g. caused by accumulation of soluble salts in the root zone. It has therefore been tried to extend the model with a water budget routine that matches actual consumptive water use with the crop's water requirement, i.e. with the theoretical transpiration rate of a constraint-free crop. The so-defined 'Production Situation 2' (PS-2) calculates the 'water-limited production potential' of the crop as a function of available light, temperature, photosynthetic mechanism *and* available water:

$$\text{PS-2: } P, Y = f(\text{light, temperature, C3/C4, water}) \quad (\text{Eq.2})$$

In production environments where the crop's consumptive water needs are met at all times, the water-limited production potential is equal to the biophysical

production potential because actual crop transpiration is equal to the theoretical maximum rate. If water uptake by the roots is less than required to meet the maximum transpiration needs, actual transpiration is limited to the actual water uptake rate. In this case the water sufficiency coefficient ($cf(\text{water})$) assumes a value <1.0 and assimilation and growth are less than in Production Situation 1. The actual rate of water uptake (MUR, in cm/d) from the soil is a function of the crop's 'critical leaf water potential', the 'soil moisture potential' and the summed resistances to water flow through the root zone and the plant. For steady state conditions, MUR is approximated as:

$$\text{MUR} = (\text{PSI}_{\text{leaf}} - \text{PSI}_{\text{soil}}) / (r_{\text{plant}} + r_{\text{root}}) \quad (\text{Eq.3})$$

Where:

PSI_{leaf} is critical leaf water head (i.e. the maximum suction the plants can generate to compensate the forces with which the soil retains its water), in cm or hPa

PSI_{soil} is soil moisture potential (i.e. the combined matrix and osmotic potentials of the root zone), in cm or hPa

r_{plant} is resistance to water flow inside the plant over the distance of flow, in d

r_{root} is resistance to water flow from the root zone to the roots over the distance of flow, in d.

The *total* soil moisture potential (PSI_{soil}) is composed of a matrix component (calculated from the momentary soil water content – one term in the soil water budget equation - with the aid of the soil moisture retention curve) and an osmotic component. Appending a salt load to each term in the water budget equation extends the water balance module to a water-and-salt budget analysis. Assuming that every 0.6 grams of salt in the soil solution corresponds with 1 mS/cm electrical conductivity and with an equivalent osmotic potential of 450 hPa, the model quantifies the effect of electrolytes in the soil solution on water uptake, assimilation and growth. *Note that* effects of electrolytes imbalance on growth are not accounted for as the definition of Production Situation 2 stipulates that nutrients are optimally available to the crop. *Note further that* generic tables relating the electrical conductivity of saturated soil pastes to yield depression ignore that the actual soil moisture content influences the salt concentration of the soil solution. Such tables are to be used with great caution!

In **Figure 1** it is shown that the routine of the PS-1 calculations is fully maintained in calculations at the PS-2 level; the only difference is that a water budget analysis determines the value of $cf(\text{water})$, whereas $cf(\text{water})$ assumes the value of 1.0 in calculations under constraint-free PS-1.

Calculations of potential crop production under Production Situation 2 permit evaluating alternative irrigation and drainage scenarios, with attention for the effects of the mode and timing of irrigation(s) and of the salt contents of the soil and of irrigation and groundwater. In the North China Plain where secondary soil

salinity is a pressing problem, the calculated electrical conductivity of the rooted surface soil is used as an indicator of the sustainability of land management.

2.2 Actual Crop Production - Production Situation PS-n

Incident radiation heats the canopy whereas transpiration cools it (Barros 1997; Kalluri and Townshed 1998). The fraction of the incoming radiation that is available for heating the canopy is set equal to the net intercepted radiation minus the energy needed for assimilation and for the vaporization of water lost in actual transpiration. The instantaneous temperature difference between air temperature and canopy temperature of a crop surface is approximated from the sensible heat component of the energy balance equation.

2.2.1 The energy balance equation

$$\text{INTER} = \text{INRAD} + \text{TRLOSS} + \text{MISCLOSS} \quad (\text{Eq.4})$$

Where:

INTER is net radiation intercepted by the canopy,
 INRAD is sensible heat exchangeable between crop canopy and air,
 TRLOSS is latent heat flux to the air due to canopy transpiration,
 MISCLOSS represents miscellaneous energy transfer components.

The components represented by MISCLOSS are comparatively small and usually ignored from the equation (Rosenberg 1983; Driessen and Konijn, 1992). Hence the energy budget can be approximated as:

$$\text{INTER} = \text{INRAD} + \text{TRLOSS} \quad (\text{Eq.5})$$

2.2.2 Net radiation intercepted by the canopy (INTER)

The intercepted radiation equals the fraction of total incoming radiation at canopy level (CANRAD) minus long-wave losses, and corrected for reflection and possibly for less than complete crop coverage. The net long-wave radiation (LWLOSS) represents the difference between incoming radiation emitted by atmospheric gases that reaches the earth's surface and outgoing radiation emitted from the ground back to the atmosphere. Outgoing short-wave and long-wave radiation components are accounted for by a daily average broadband surface albedo factor (REFLCROP) as in equation 6 below (Driessen and Konijn, 1992; Jackson, 1982; Soer, 1980).

$$\text{INTER} = (\text{CANRAD} - \text{LWLOSS}) * (1 - \text{REFLCROP}) * \text{CFLEAF} \quad (\text{Eq.6})$$

Where:

CANRAD is total incoming radiation at canopy level [$J m^{-2} d^{-1}$]
 LWLOSS is net long-wave losses [$J m^{-2} d^{-1}$]
 REFLCROP is reflection coefficient (broadband albedo converted to a daily average value) from crop canopy [$= 0.27$ (Driessen and Konijn, 1992; Parodi, 2000)]

CFLEAF is ground cover fraction of the actual canopy

With:

$$\text{CFLEAF} = 1 - \text{EXP}(-k_e * \text{LAI}) \quad (\text{Eq.7})$$

Where:

k_e is extinction coefficient for visible light [0-1],

LAI is Leaf Area Index [$m^2 m^{-2}$],

2.2.3 Total incoming radiation (CANRAD)

Solar radiation reaching the top of the atmosphere is referred to as 'extraterrestrial radiation' (EXTRA) and is a function of day of year (time in case of instantaneous considerations) and latitude of the site. Atmospheric components that include ozone, water vapour, aerosols, and carbon dioxide absorb, re-emit and scatter some of the incoming radiation as it proceeds towards earth. Iqbal (1983) and Parodi (2000) explain atmospheric attenuation effects in some detail. In the present text, these radiation losses are accounted for by an atmospheric transmissivity term (TRANS) that represents the fraction of EXTRA that makes it through the atmosphere (equation 10; Driessen and Konijn, 1992).

$$\text{CANRAD} = \text{EXTRA} * \text{TRANS} \quad (\text{Eq.8})$$

With:

$$\text{EXTRA} = \text{SC} * \text{RDN} * 3600 * \text{DL} \quad (\text{Eq.9})$$

$$\text{TRANS} = 0.29 * \text{COS}(\text{LAT} * \text{RAD}) + 0.52 * \text{SUNH}(\text{DAY}) / \text{DL} \quad (\text{Eq.10})$$

Where:

CANRAD is total incoming radiation at canopy level [$J m^{-2} d^{-1}$]

EXTRA is total extraterrestrial radiation [$J m^{-2} d^{-1}$]

TRANS is fraction of EXTRA that passes through the atmosphere [-]

SC is Solar Constant [$J m^{-2} sec^{-1}$]

DAY is Julian day number on Northern Hemisphere or Julian day number plus or minus 182 on Southern Hemisphere

RDN is fraction of Solar Constant at given latitude (LAT) and DAY [-]

LAT is site latitude [radians]

DL is day length [$h d^{-1}$]

SUNH(DAY) is number of sunshine hours on day nr DAY [$h d^{-1}$]

PI is a constant (3.1416)

RAD is degree to radian conversion factor

DEC is solar declination [radians]

With:

$$\text{SC} = 1353 * (1 + 0.33 * \text{COS}(2 * \text{PI} * \text{DAY} / 365))$$

$$\text{RDN} = (\text{SSIN} + 24 * \text{CCOS} * \text{SQR}(1 - \text{SSCC} * \text{SSCC})) / (\text{PI} * \text{DL})$$

$$\text{SSIN} = \text{SIN}(\text{LAT} * \text{RAD}) * \text{SIN}(\text{DEC} * \text{RAD})$$

$$\text{CCOS} = \text{COS}(\text{LAT} * \text{RAD}) * \text{COS}(\text{DEC} * \text{RAD})$$

$$\text{SSCC} = \text{SSIN} / \text{CCOS}$$

$$\begin{aligned} \text{RAD} &= \text{PI} / 180 \\ \text{DL} &= 12 * (\text{PI} + 2 * \text{ARCSIN}(\text{SSCC})) / \text{PI} \\ \text{DEC} &= -23.45 * \text{COS}(2 * \text{PI} * (\text{DAY} + 10) / 365) \end{aligned}$$

2.2.4 Net long-wave losses (LWLOSS)

The earth's surface exchanges thermal radiant energy with the atmosphere at the 3-100 μm wavelength region of the electromagnetic spectrum (Parodi 2000). Since the surface is warmer than the atmosphere on average, the net emission is outgoing hence the term "long-wave losses".

Daily long-wave radiation can be directly measured by a "net long-wave radiometer" at a meteorological station. However, in cases where such a radiometer is not available, an indirect method that relates net long-wave radiation with daily surface temperature, actual vapour pressure and cloudiness can be applied according to Planck's law.

The net long-wave emission can be expressed as:

$$\text{LWLOSS} = \text{BOLTZ} * (\text{TDAY}(\text{DAY}) + 273)^4 * (0.56 - \text{SQR}(\text{VPA}) * 0.079) * (0.1 + 0.9 * \text{SUNH}(\text{DAY}) / \text{DL}) \quad (\text{Eq.11})$$

Where:

LWLOSS is 24 hours net long-wave exchange between the atmosphere and canopy [$\text{Jm}^{-2}\text{d}^{-1}$],
 BOLTZ is Stephan-Boltzman constant [$0.0049 \text{ J m}^{-2} \text{ d}^{-1} \text{ K}^4$],
 TDAY(DAY) is daytime air temperature on day nr DAY [$^{\circ}\text{C}$],
 VPA is estimated actual vapour pressure [millibar],
 SUNH(DAY) is number of sunshine hours on day nr DAY [h d^{-1}],
 DL is day length [h d^{-1}]

With:

$\text{TDAY} = \text{TAV} + (\text{SUNSET} - 14) * \text{AMPL} * \text{SIN}(\text{AUX}) / (\text{DL} * \text{AUX})$,
 $\text{TAV} = (\text{Tmax}(\text{DAY}) + \text{Tmin}(\text{DAY})) / 2$,
 $\text{AMPL} = (\text{Tmax}(\text{DAY}) - \text{Tmin}(\text{DAY})) / 2$,
 $\text{AUX} = \text{PI} * (\text{SUNSET} - 14) / (\text{SUNRISE} + 10)$,
 $\text{VPA} = \text{SVAPEST} * \text{RHA}(\text{DAY})$ and
 $\text{SVAPEST} = 6.11 * \text{EXP}(17.4 * \text{TDAY}(\text{DAY}) / (\text{TDAY}(\text{DAY}) + 239))$

Where:

TAV is mean daily air temperature on day nr DAY [$^{\circ}\text{C}$],
 Tmax (DAY) is maximum air temperature on day nr DAY [$^{\circ}\text{C}$],
 Tmin (DAY) is minimum air temperature on day nr DAY [$^{\circ}\text{C}$],
 AMPL is air temperature amplitude on day nr DAY [$^{\circ}\text{C}$],
 SUNSET is hour of sunset on day nr DAY [-],
 SUNRISE is hour of sunrise on day nr DAY [-],
 SVAPEST is estimated saturated vapour pressure on day nr DAY [millibar],
 RHA(DAY) is relative air humidity on day nr DAY [0-1],

2.2.5 Sensible heat flux (INRAD)

Sensible heat flux denotes the transfer of energy from objects that are warmer than their surroundings to the air, or from the air to cooler objects. Heat transfer processes can be laminar, as conduction or convection according to Fourier's law, or turbulent. Turbulent heat transfer is expressed using the Ohm's law analogy whereby the rate of heat transfer is determined by a difference in temperature and the resistance to the movement of heat.

$$INRAD = \frac{\Delta T * VHEATCAP}{AERODR} \quad (\text{Eq.12})$$

Where:

- INRAD is sensible heat transfer from the canopy to the air [$J m^{-2} s^{-1}$],
- ΔT is temperature difference between canopy temperature and air temperature [K],
- VHEATCAP is volumetric heat capacity [$J m^{-3} K^{-1}$]
- AERODR is aerodynamic resistance to heat transfer [$s m^{-1}$].

2.2.6 Aerodynamic resistance to heat transport (AERODR)

Quantifying aerodynamic resistance to heat transport is far from easy. In theory, aerodynamic resistance to heat transport can be presented as a function of wind speed and surface roughness. For situations where surface temperature is close to air temperature, Jackson et al (1988) suggest:

$$AERODR = \{ \ln[(z-d)/z_0] / k \}^2 / U \quad (\text{Eq.13})$$

Where:

- z is height of wind speed measurement [m],
- d is displacement height of canopy [m] (i.e. the height at which wind speed becomes zero in the plant canopy),
- z_0 is roughness length [m] (i.e. area of the canopy that contributes to turbulent mixing),
- k is von Karman constant (~ 0.4) [-],
- U is wind speed over 1 day [$m sec^{-1}$].

For full cover crop canopies z_0 and d can be chosen as a function of crop height h (m) whereby $z_0 \sim 0.13h$ and $d \sim 0.63h$.

Equation 13 is further constrained by assumptions that heat and momentum transport are transferred at the same locations in the canopy and that wind speed is sufficient to create turbulent transfer processes. For full cover crop canopies, assumptions regarding neutral condition (i.e. 'small ΔT ') and transfer locations may not introduce much error but assumed wind speed values can create significant errors. Equation 13 suggests infinitely large resistance to heat transfer as the wind speed approaches zero, which seems unrealistic. A semi-empirical equation that maintains its integrity at low wind speed (Jackson et al 1988) is:

$$\text{AERODR} = 4.72\{\ln[z-d]/z_0\}k^2 / (1 + 0.54U) \quad (\text{Eq.14})$$

For non-neutral conditions (i.e. 'measurable ΔT '), AERODR varies non-linearly with temperature; approximate values are obtained with iterative methods. More rigorous considerations of the momentum flux theory are provided by, inter alia, Bastiaanssen (1998) and Parodi (2000).

2.2.7 Latent heat flux (TRLOSS)

Latent heat flux can be isolated from the energy balance equation using a similar formulation as used by Soer (1980):

$$\text{TRLOSS} = (\text{INTER}) - \left[\frac{\Delta T * \text{VHEATCAP}}{\text{AERODR}} \right] \quad (\text{Eq.15})$$

TRLOSS represents the energy needed to vaporize the water lost in actual transpiration by the crop:

$$\text{TRLOSS} = \text{TR}_{\text{act}} * \text{LATHEAT} \quad (\text{Eq.16})$$

Where:

TR_{act} is actual transpiration rate [$\text{kg m}^{-2}\text{s}^{-1}$]

LATHEAT is latent heat of vaporisation [$2.46 * 10^6 \text{ J kg}^{-1}$]

Isolating TR_{act} as a function of ΔT yields:

$$\text{TR}_{\text{act}} = \frac{\text{INTER} - \left(\frac{\Delta T * \text{VHEATCAP}}{\text{AERODR}} \right)}{\text{LATHEAT}} \quad (\text{Eq.17})$$

Introducing Equation 17 in crop growth simulation is only possible if parameter values are commensurate with the minimum temporal resolution of the simulation. The actual transpiration rate, TR_{act} , must be presented as a daily value, which implies that ΔT cannot be the instantaneous value measured at the time of the satellite pass but must be converted to an equivalent *daily* value. Another complication is that ΔT is not available for all days in the crop cycle because it can only be measured if the pixel is entirely cloud-free at the moment of the satellite pass.

The following procedure was adopted to obtain equivalent canopy temperature values for whole days (satellite pass at 14.00 h; an outline of the PS-n model program is given in Appendix A):

- Calculate the equivalent AVHRR-derived instantaneous canopy temperature for days in-between measurements as a function of the daily rate of change over the interval between two successive AVHRR passes in a linear interpolation procedure.

- Convert obtained instantaneous canopy temperatures to equivalent daily values by accounting for actual conditions during the day. To this end, the instantaneous canopy temperature values are multiplied by the fraction of sunshine hours for the day of year plus 20% of the clouded fraction. (It is assumed that there is still 20% radiation under an overcast sky.)

In the crop growth model, the equivalent daily canopy temperature for each day in the crop cycle is approximated with:

$$\text{INTERTcan(adjusted)} = \text{INTERTcan} * \text{CONVFAC} \quad (\text{Eq.18})$$

Where:

INTERTcan is interpolated AVHRR-derived temperature value [$^{\circ}\text{C}$]
 CONVFAC is conversion factor for actual daytime conditions.

With:

$$\text{CONVFAC} = (\text{SUNH} + 0.2 * (\text{DL} - \text{SUNH})) / \text{DL} \quad (\text{Eq.19})$$

Equation 19 is applied to days with measurements as well as to days between measurements.

The maximum transpiration rate (TRmax)

The *maximum* transpiration rate (TRmax) is a reference value conditioned by the evaporative demand of the atmosphere (represented by the potential water use from a Penman-type reference canopy) and the properties of the actual crop canopy, notably its exposure to the atmosphere:

$$\text{TR}_{\text{max}} = \text{TR}_0 * \text{CFLEAF} * \text{TC} \quad (\text{Eq.20})$$

Where:

TR_{max} is maximum transpiration rate [$\text{kg m}^{-2} \text{s}^{-1}$]
 TR₀ is potential transpiration rate from Penman-type canopy [$\text{kg m}^{-2} \text{s}^{-1}$]
 CFLEAF is ground cover fraction of the actual canopy [0-1]
 TC is 'actual turbulence coefficient' [-]

The potential transpiration rate from a Penman-type canopy equals the potential evapotranspiration rate (ET₀) minus the evaporation component (E_{max}). The Penman-type reference canopy is defined as a short, green, closed, well-watered canopy with standard properties. The LAI of this canopy will be close to LAI = 6 and the extinction coefficient is of the order of 0.5. It follows that the maximum rate of evaporation from underneath this reference canopy is approximated by E_{max} = E₀ * exp (-ke * LAI) = E₀ * exp (-3) = 0.05 * E₀. Consequently, potential transpiration from the reference canopy amounts to:

$$\text{TR}_0 = \text{ET}_0 - 0.05 * \text{E}_0 \quad (\text{Eq.21a})$$

Where:

ET_0 is potential evapotranspiration rate from reference canopy [$kg\ m^{-2}\ s^{-1}$]
 E_0 is potential evaporation rate [$kg\ m^{-2}\ s^{-1}$]

If it is assumed that the difference between ET_0 and E_0 is small, i.e. within the error margin of NOAA-derived ET_0 -estimates, TR_0 can be approximated by:

$$TR_0 = 0.95 * ET_0 \quad (\text{Eq.21b})$$

The ground cover fraction of the actual crop canopy was described by equation 7. The effects of turbulence on the theoretical maximum transpiration rate are variable and complex; they depend on such diverse factors as wind speed, ET_0 , canopy height, canopy roughness and parcel size. Driessen and Konijn (1992) propose a turbulence coefficient with values between 1.0 and a maximum coefficient value TCM. The value of TCM is set equal to the maximum value of the crop coefficient, kc , as defined by Doorenbos et al (1979). Driessen and Konijn (1992) suggest the following relationship:

$$TC = 1 + (TCM - 1) * CFLEAF \quad (\text{Eq.22})$$

With the sufficiency coefficient $cf(\text{water})$ equal to TR_{act} / TR_{max} , $cf(\text{water})$ can thus be described as a function of the difference in temperature between the canopy and the surrounding air:

$$cf(\text{water}) = \left[\frac{INTER - \left(\frac{\Delta T * VHEATCAP}{AERODR} \right)}{LATHEAT * TRO * CFLEAF * TC} \right] \quad (\text{Eq.23})$$

On this basis, it becomes possible to adjust assimilation and calculated actual crop growth from instantaneous measurements or derivations of canopy and ambient temperatures. Note that the so obtained value of $cf(\text{water})$ takes the analysis beyond the water-limited production potential (PS-2 level) to the level of an actual-farmer (PS-n) without the necessity of accounting for all yield-limiting and yield-reducing factors (stress due to water scarcity, water logging, nutrient shortage or excesses, pests, diseases, pollutants etc). The algorithm and the associated computational steps for the estimation of $cf(\text{water})$ based on crop canopy-ambient air temperature difference are outlined in Appendix A.

Stomatal closure due to water shortage is a well-documented and understood phenomenon. However, also pest and disease attacks on crops, depending on severity of the damage inflicted, reduce the numbers and/or the efficient functioning of stomata leading to reduced transpiration hence assimilation. The crop's natural, bred or selected resistance and/or tolerance may influence severity of damage due to pests and disease attacks. Resistance or tolerance to pathogens and pest damage has also been related to the crop's nutritional status (Marschner, 1996).

Direct responses of stomata to the various stresses other than water are not straightforward. For example, restricted oxygen movement due to water-logging may cause NO_3^- deficiency while other nutrients (Mn^{2+} , Fe^{2+} , Al^{3+} , H_2S) rise to toxic levels, both conditions leading to stomatal closure (Goss, 2001). Stomatal disfunction and eventual crop wilting has also been found to be caused by potassium deficiency (NSW Agriculture, 1998). Potassium deficiency is known to affect cell turgor in stomata guard cells responsible for opening and closing mechanisms. Marschner (1996) reported that the multiplication of bacterial diseases whose pathogens usually enter through the stomata, are enhanced when potassium and calcium are deficient and often but not always when nitrogen is deficient. In Part D a case study demonstrates the direct relation between cf(water), production and yield.

2.3 The Yield Gap

The difference between the biophysical production potential (PS-1) and actual, on-farm production (PS-n) is caused by the compounded constraints that confront a real-world farmer but are (assumed to be) eliminated in Production Situation 1. It is an illusion to think that modelling the effects of individual constraints to crop performance can ever accurately disclose the structure of the Yield Gap. The dynamics and complexity of actual Land Use Systems, with interactions between individual constraints and with management affected by e.g. the social-economic situation, are prohibitive.

The difference between the biophysical production potential (PS-1) and the water-limited production potential (PS-2) is caused by sub-optimal water availability but does not constitute the 'water-related part' of the Yield Gap. In *actual* Land Use Systems, less dry mass production under conditions of water stress means also greater chances for weeds, different exposure to pests and diseases. **Figure 2** shows repetitive 10-day simulations time-series of reference yield in comparison with on-farm PS-n simulation.

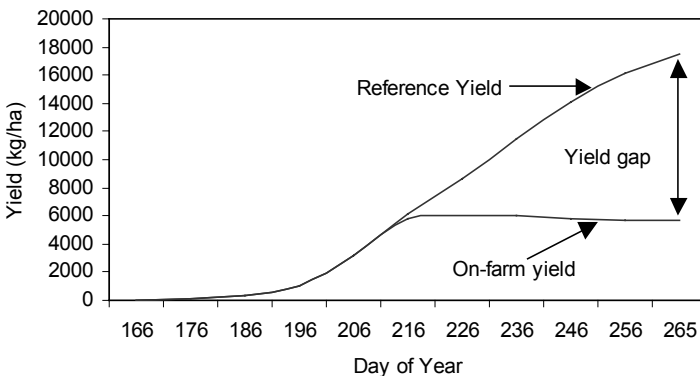


Figure 2. Reference yield and actual (on-farm) yield time-series illustrating the development of a yield gap during crop growth.

Modelling the effects of individual constraints on actual crop production and yield is far from easy. Describing the availability of just one nutrient element -say nitrogen- and the effect that it has on crop performance is already prohibitively complex. One would have to describe *supply* of nitrogen from (1) decomposing soil organic matter, (2) binding of nitrogen by symbiotic and autotrophic binders, (3) atmospheric deposition ($10\text{-}40 \text{ kg ha}^{-1}\text{yr}^{-1}$), and (4) applied fertilizers and manure. *Losses* would have to be quantified: (5) the leaching of nitrates and volatilisation of ammoniacal nitrogen, and also (6) *inactivation* of nitrogen in complexes and otherwise. Last but not least, one would have to account for all *interactions* between these dynamic processes as well as interactions with other plant nutrients in the soil. The result, if one would ever succeed in collecting the needed basic data and constructing a realistic algorithm, would probably be rather inaccurate and it would come too late to be of much practical value.

Consequently farmers tend to rely on their experience; they apply 'sufficient', i.e. usually too much, nitrogen fertilizer and assume that the environment 'can take it'. The same holds for weeds, pests and diseases: if one bin of herbicide or pesticide will cure the problem at affordable cost, one is not inclined to rely on models of population dynamics. For all these reasons yield gap analyses are best done by statistical analysis of observed biophysical and infrastructure data as well as management data (field operations), notably of farmers' perceptions of the relative severity of individual constraints for geo-referenced fields (Bie, 2000).

2.4 Early Warning and Crop Yield Forecasting

A normalized index value of Land Use System performance (0-1) can be obtained - at any moment in the crop cycle - by dividing the calculated or observed PS-n production by the corresponding PS-1 reference production potential. The index value indicates the overall sufficiency of management until that moment; low values signal upcoming problems and a need for remedial action.

Predicting the eventual crop yield, i.e. the harvested produce (usually storage organ mass) at the *end* of the crop cycle involves the following steps:

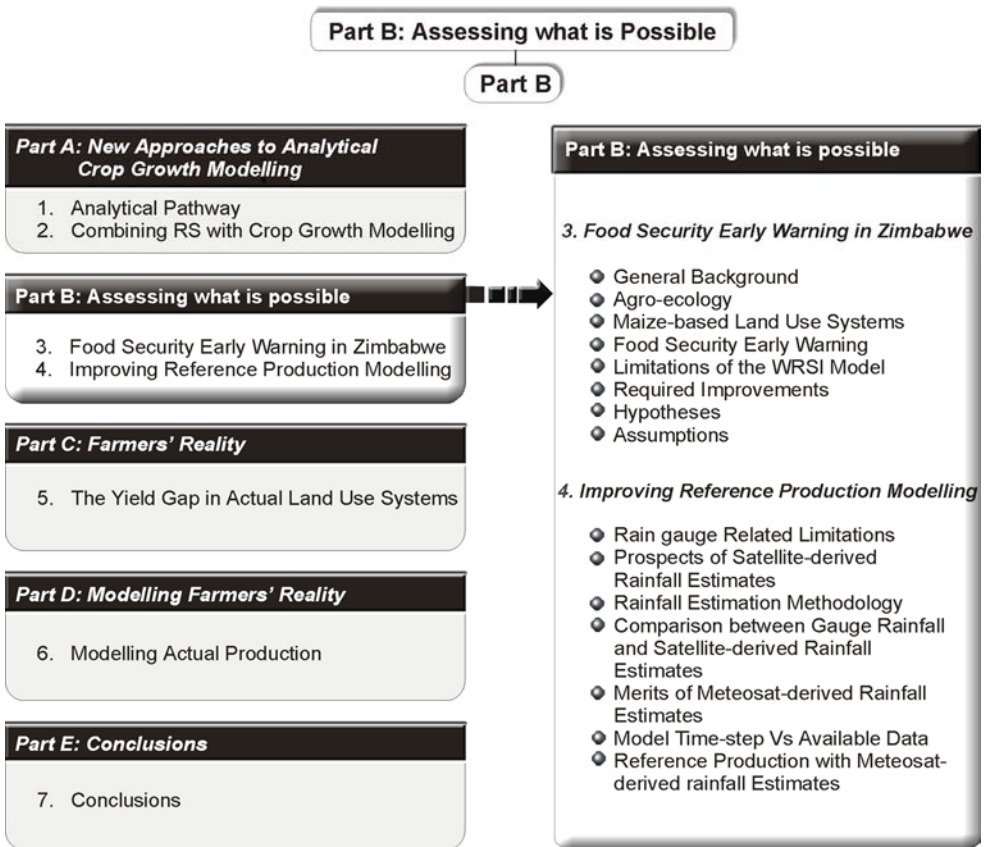
- First, one calculates the anticipated (*reference*) *production* potential at the end of the crop cycle. To this end, estimated weather parameter values for the period between the last (PS-n / PS-1)-analysis and the end of the crop cycle are entered in the weather file used in the PS-1 and PS-n calculations.
- Next, one multiplies the anticipated reference production by the index value obtained at the last (PS-n / PS-1) - analysis. This produces an estimate of the *anticipated actual production* at the end of the crop cycle.
- This production estimate is then multiplied by a crop-specific harvest index value to obtain the *anticipated crop yield*.

Repetitive analyses at e.g. 10-days intervals (assuming that satisfactory, cloud-free satellite imagery can be obtained) produce successive crop yield forecasts that become ever more accurate towards the end of the crop cycle as less

radiation and temperature estimates (and more measured values) are used in the calculations. Evidently, crop yield forecasts that are generated only a few days before crop maturity have lost their early warning function; as crop yield estimates they may still be of value for regional reconnaissance inventories.

This may be the proper moment to emphasize that the approach outlined here is (merely) an interpretation procedure. No interpretation procedure generates 'new' information; at best it reveals information that was hidden in the (collected and/or estimated) basic data and does so with acceptable error. At present, efforts are being made to improve the quality of basic data collection and data interpolation. Venus (1999) made a study of 100-years weather records of southern Africa. He found that the accuracy of substitute weather data as used in crop yield forecasting improves markedly if – rather than averaging all years on record – only those years are used that had a similar pattern as the year for which yield forecasts are made. In this thesis, the use of remotely sensed data is investigated to quantify regional weather data patterns in areas with a sparse distribution of synoptic weather stations.

Part B. Assessing What is Possible



3. Case Study 1: Food Security Early Warning in Zimbabwe

3.1 General Background

Agriculture in Zimbabwe is comprised of two main sectors, viz small-scale mainly communal farming and large-scale commercial farming. **Figure 3** shows the land distribution between the small-scale, mainly communal sector and the large-scale commercial sector. In 1992 (Rukuni and Eicher, 1994; Whingwiri et al, 1992), the small-scale sector was estimated to include 1 million households utilizing 16 million hectares (42% of pre-independence communally owned land); 52,000 households utilizing 3.3 million hectares under post-independence resettlement schemes and 8,650 households were found on 1.2 million hectares of privately owned land. In contrast, only 4,500 commercial farms held 11 million hectares of prime agricultural land under private ownership.

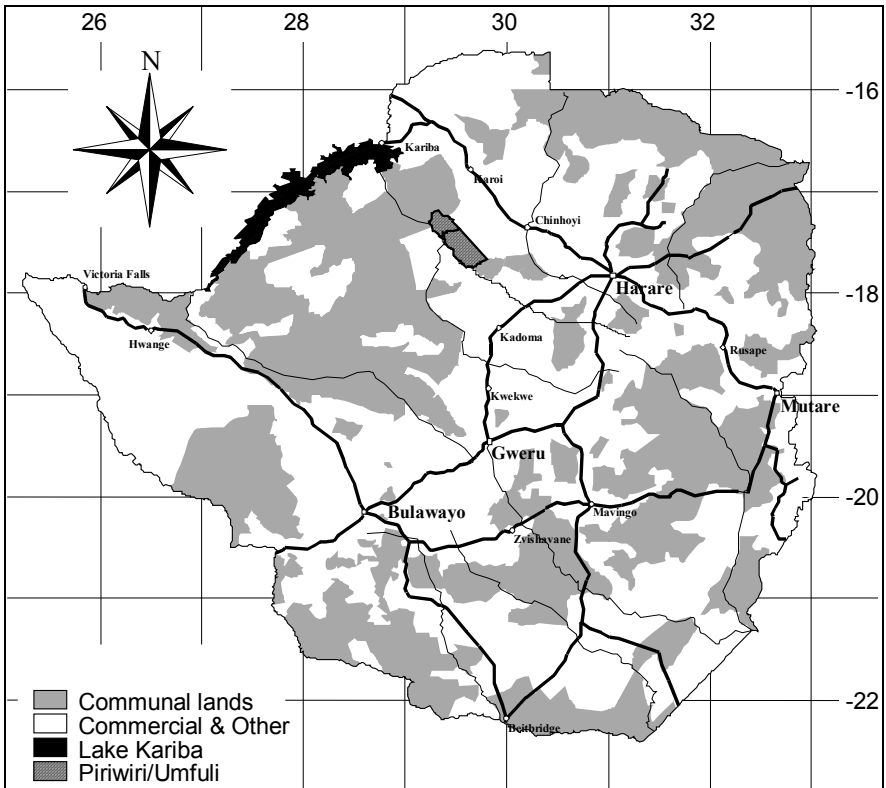


Figure 3. Map of Zimbabwe showing the location of communal lands and the areas of Piriwiri and Umfuli that were surveyed for the study of yield constraints of maize-based land use systems.

Developed under the previous Rhodesian regime, the largely whites-owned large-scale farming sector is/was relatively successful by international standards with adequately invested modern technology. Small-scale production is also hampered by a backlog of institutional and infrastructural development from colonial neglect evidenced by the exclusion of the main road network and urban areas from the communal lands.

3.1.1 Agro-ecology

Zimbabwe was first delineated into five agro-ecological zones (known locally as Natural Regions I to V) by Vincent and Thomas (1960; described in Anderson, 1993). Whingwiri et al (1992) and Rukuni and Eicher (1994) also used “effective rainfall” as the main differentiating criterion. Later, modifications of the zone boundaries were based on the so-called rainy pentad defined as “the centre one of the three pentads (consecutive five days of rain) that together receive more than 40mm of rain and not more than one of the three having less than 8mm”. Over 90% of communal farming areas are located in Regions III, IV and V where cropping is done under severe biophysical constraints; see **Table 1**. Various researchers have suggested that rainfall deficits of 13 to 19 years periodic cycles in Southern Africa are related with the El Nino effect (Scoones et al, 1996; Eastman, 1996) rendering drought a regular occurrence.

Table 1. Distribution of communal lands including resettlement areas by Natural Regions (after Rukuni and Eicher, 1994; Whingwiri et al, 1992)

Natural Region	Mean Annual Rainfall (mm)	% Total	% Communal Land	Production Reliability	Farming Practice
I	>1000	1.8	0.8	Reliable	Tea; coffee
II	750-1000	15.0	7.8	Reliable	Crop & animal production
III	650-800	18.6	17.2	Unreliable	Crop & animal production
IV	450-650	37.8	44.9	Unreliable	Crop & animal production with high drought risk
V	<450	26.7	29.3	Erratic & very low	Crop & animal production with high drought risk

3.1.2 Maize-based land use systems in communal lands

Maize plays a dominant role in the food economy of Zimbabwe, accounting for 88% of the national coarse grain production. The crop provides about half of the calorie intake of the average Zimbabwean (Rukuni and Eicher, 1994). Maize is the main crop grown in the communal lands in all Natural Regions except Natural

Region-V. The maize crop is usually intercropped with smaller proportions of sorghum, pumpkin and sunflower. The fields are typically small (0.2-0.5 ha) and irregularly shaped. Communal farmers grow maize for subsistence as the staple food, but also for cash when there is surplus. Early maturing hybrid seeds suitable for areas with little and erratic rainfall have been adopted. Farm operations in communal lands largely rely on livestock for power. Cattle and donkeys provide draught power for ploughing, planting, weeding and for transportation of inputs to the fields and of harvested products to the homestead and to the markets. Manure from the animals is a valued supplement to soil fertility.

About two-thirds of Zimbabwe is covered with sandy soils that are derived mainly from granites. Like most of the heavier textured soils, these sandy soils are inherently deficient in nitrogen, phosphorous and sulphur (and in many cases in potassium as well). The sandy soils have low buffering capacity, low nutrient reserves and are relatively acidic. Compaction, capping and low water holding capacity are common. Management inputs for fertility maintenance and for crop protection against pests and diseases are low, largely imposed by lack of capital or credit facilities.

3.2 Food Security Early Warning Systems

Zimbabwe has had to import maize in increasing amounts since the early 1980s, with imports reaching a crisis level during the 1991/92 drought when lack of timely action cost the country an estimated US\$ 340 million or 11% of the (then) gross domestic product.

Events and actions during this period provide an opportunity to evaluate the effectiveness of the early warning system. Rukuni and Eicher (1994) argue that the devastating maize shortage of 1992 reflected failure on the part of senior decision-makers to initiate import procedures once impending shortages were anticipated and reported by the Grain Marketing Board and the National Early Warning Unit. This failure to act resulted in a fourfold increase of the cost of maize-meal as the Government embarked on emergency and naturally much more expensive means of processing and distribution.

Questions then arose as to why the authorities failed to heed the warning. Walker (1989) compiled the following attributes that contribute to an information system's value and by which its usefulness can be judged:

- **Clarity:** The information must be unambiguous i.e. quantitative when describing quantities.
- **Accuracy:** The information might be quantitative and clear but of no value if inaccurate.
- **Significance:** The actual implications of the information must be clearly put across to the intended recipient.
- **Timeliness:** Crop yield predictions tend to gain accuracy closer to crop maturity but lose in timeliness.

- **Adequacy:** An information system should aim at providing all the facts necessary to make a decision. The fewer the facts it provides, the less adequate it is.
- **Validity:** Validity of information is illustrated by the example that economic surveys may gather high-grade data on the price and availability of food in the market but if most of the poor and those likely to suffer operate outside the market, the information is of little use.

Any combination of deficiencies in the above mentioned attributes could have impacted on the decision making process that led to the food security crisis in Zimbabwe in 1992. Surely, the decision-makers would have known that the accuracy of crop yield predictions presented by NEWU was not established. Although there is no guarantee that decision-makers would be prompted to take appropriate action, an improved early warning system would provide information, within its affordability, that combines maximum clarity, accuracy, significance, adequacy and validity. This case study considers the accuracy attribute in the early warning system employed by NEWU.

Monitoring and accurate forecasting of maize production and yield puts Zimbabwe in a better position to timely procure needed supplies at least cost when production falls short and to profitably dispose of surpluses in times of plenty. An effective early warning system is clearly of great value for identifying emerging trends, while a mechanism to translate this information into timely action should be in place. The accuracy with which crop yield estimates are carried out is vital to the management and planning of a country's food security system. This is becoming even more important now that the maize industry of the region is increasingly confronted with free market mechanisms (Brink, 1996).

Food Security Early Warning in Zimbabwe is the responsibility of the National Early Warning Unit (NEWU) of the Department of Agricultural Technical and Extension Services (AGRITEX) under the auspices of the Southern Africa Development Community (SADC) Regional Early Warning Unit (REWU). REWU is composed of National Early Warning Units (NEWUs) from each of the SADC member-countries. In Zimbabwe, the National Early Warning Unit is composed of experts from the Department of Agricultural Technical and Extension Services (AGRITEX), the Department of Meteorological Services and the Central Statistics Office. NEWU provides early warning information to Government and other decision-making agencies on expected grain and other agricultural products.

NEWU employs the FAO Soil-Water Balance Model adapted for Zimbabwe in its crop production forecasting. The model evaluates weather, soils and crop data and calculates a crop 'Water Satisfaction Requirement Index (WRSI)', in order to estimate yield potentials while the crop is still on the field. A WRSI value of 100% is interpreted as 'no yield reduction due to water stress' whereas less than 50% is taken as an indication of crop failures. The concept is adopted from an empirical linear yield-reduction relation (Saney et al, 2001).

The Famine Early Warning System (FEWS), a REWU collaborator, developed a grid-based WRSI model for Southern Africa that estimates the water-limited yield potential based on start and end of crop season, precipitation and potential evapotranspiration according to the Penman-Monteith equation (Saney et al, 2001). In the monitoring mode, the WRSI is produced till the most recent dekad using observed data in the growing season. The alternative forecasting mode continues the WRSI calculation until the end of the growing season using long-term potential evapotranspiration and rainfall data. A linear correction factor was added to the model to account for yield reduction caused by water logging.

The model has been in use for a number of years notably for forecasting expected national productions of maize, sorghum, millet, groundnut and sunflower. However, although the model is tuned with observed yield data, the accuracy of predictions is as yet unclear. Forecasts of planted areas and production are made by agro-statisticians, using statistical surveys based on a combination of subjective and objective crop area and yield assessments and measurements.

3.2.1 Limitations of the WRSI model

Crop yield estimation based on the 'Water Requirements Satisfaction Index (WRSI) model' as employed by NEWU has its limitations:

- WRSI applies index values quantified with empirical relationships that link rainfall and vegetation index data with (observed) yields. Significant limitations emerge from neglecting vital physiological and environmental mechanisms that control crop growth. Empirical relationships are not universally valid and hence results may location-specific and not transportable.
- It is assumed that rain is the main factor determining yields; other yield constraints are not taken into consideration,
- The accuracy of crop area estimates is not known,
- It is assumed that rain gauge (point) data represent the area for which the estimate is made. In areas with sparse distribution of rainfall gauging stations such as the communal lands this is questionable,
- Where applied, the accuracy of satellite-derived rainfall estimates is unknown.

3.2.2 Required and achievable improvements

NEWU can improve the quality of crop yield estimates through the following:

- Assessment of the accuracy level of satellite-derived rainfall estimates that are applied in modelling the water-limited production potential,
- Deployments of mechanistic models in the establishment of reference production that take into account the physiological and environmental processes that control crop growth. Production situation models (PS-1, PS-2) calculate the biophysical and the water-limited production potentials in order

to assess production levels that are possible under respective constraint-free and rain-fed conditions,

- Understanding of actual farmer's production and yield levels in order to determine yield-gap and the constraints that cause it,
- Application of the actual farmer's production situation model (PS-n) that estimates actual production and yields using the crop canopy-ambient air temperature difference concept.

3.2.3 Hypotheses

The accuracy of current crop yield estimation in Zimbabwe is impaired by:

- Using the empirical Water Requirement Satisfaction Index (WRSI) model in the current crop yield monitoring and forecasting; WRSI solely considers a soil-water balance, ignoring other yield limiting and yield reducing factors,
- The sparse network of meteorological and rain gauge stations,
- The unknown accuracy of crop area estimates,
- The unknown accuracy of satellite-derived rainfall estimates applied in the WRSI model,
- The lack of understanding of constraints, which cause the gap between theoretical yield potentials and the actual farmers' yields.

The accuracy of crop yield estimation can be improved by:

- Determining what is possible in terms of production levels under rain-fed conditions using the production-situation-based analytical approach instead of empirical methods,
- Understanding yield-limiting and yield-reducing factors that prevail under actual farmers conditions,
- Estimating actual production analytically by directly linking crop production to the difference between ambient air and remotely sensed canopy temperature (PS-n).

3.2.4 Assumptions

- Actual yield data can be obtained with good reliability from interviews with farmers,
- Water-limited potential production can be linked to rainfall data predicted from Meteosat satellite data and interpolation techniques,
- Actual crop yield can be linked to crop canopy parameters derived from NOAA AVHRR satellite data.

4. Improving Reference Production Modelling using Remotely Sensed Precipitation

Regional crop yield forecasting makes use of area-specific crop state variables derived from satellite remote sensing. Available methods apply index values quantified with empirical relationships that link satellite data with (observed) yields. Furthermore, the accuracy of the satellite-derived variable values is often not well established. Significant limitations emerge from neglecting vital physiological and environmental mechanisms that control crop growth. Mechanistic models including PS-1, PS-2 and PS-n, dynamically describe and apply these mechanisms but are applicable only at field scale. The solution proposed here builds on the possibility to derive crop state information from satellite data and adopt appropriate strategies for its use as substitute field-level variables. In this case study, the derivation methodology and accuracy of the Meteosat-derived Rainfall Estimates (RFEs) are assessed. Trial PS-2 model runs using Meteosat-derived RFEs are presented later on in the proceeding section.

4.1 Rain-Gauge related Limitations

Rainfall values measured with rain gauges have limitations that negatively affect their application in regional crop growth analyses. The most disturbing of these limitations are:

Point measurements. Rain gauges provide point measurements. Areal values are required for regional analyses. However, convective effects tend to be localized. A single gauge may be representative of only a very small area. **Figure 4** (Flitcroft et al, 1989) presents the variation of rainfall over a 10km square on 20th July 1985 in Niger, West Africa. Although the average rainfall over this square is 50mm, there is wide variation in values over very short distances.

If only one of the gauges was chosen to represent the 10km square, any value between 30mm and 78mm could be obtained. Nonetheless, rain gauge values are often taken to be representative of very large areas or used in simple interpolation procedures to construct isohyetal maps.

Thin plate spline has been used to incorporate elevation as an independent variable in addition to latitude and longitude to interpolate monthly mean precipitation within a standard error of 10% (Hutchinson and Corbett, 1993). However, precipitation error of interpolated surfaces is strongly related to gauge network density (Lebel et al, 1997; Hutchinson and Corbett, 1993; Flitcroft et al, 1989). Large interpolation errors would be expected in such areas of sparse gauge network density as the communal lands of Northwestern Zimbabwe.

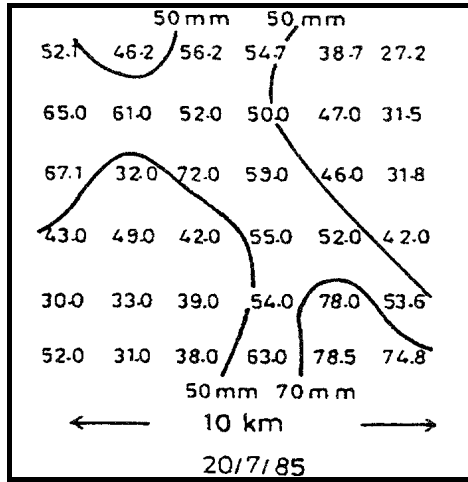


Figure 4. Rainfall variability within a 10km square on 20 July 1985 in Niger, West Africa (source: Flitcroft et al, 1989).

- Rain gauge distribution.** Rain gauge distribution is often corrupted by such deliberations as 'ease of access' because recordings are made daily. This means that fewer gauges are placed in uninhabited areas and more are located along communication lines such as roads, railways and rivers. **Figure 5** shows the distribution of meteorological and synoptic stations in Zimbabwe. Note the relative density of gauging stations along the major road network and the almost total absence in the communal areas.

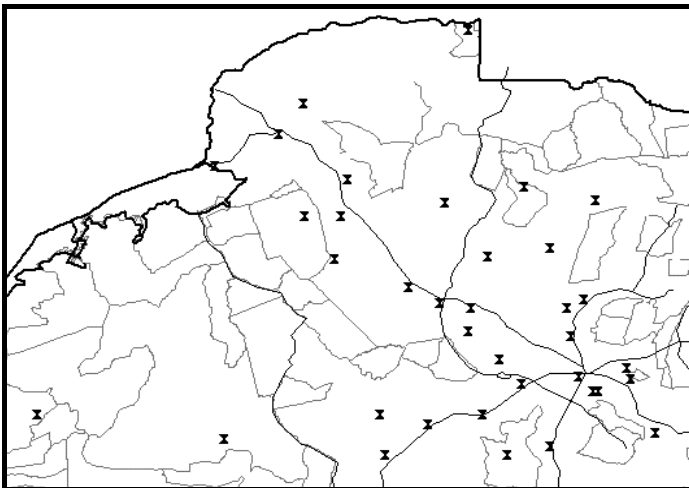


Figure 5. Rain gauge distribution in northwestern Zimbabwe is denser along major roads.

- **Measurement errors.** Rainfall measured in strong winds may only be 60% of the actual rainfall because of turbulence created by the gauge itself (Grimes et al, 1998; Seed and Austin, 1990). Other measurement errors include human errors such as omission of decimal points and assigning rainfall to the wrong day during the repetitive transcription of measurements before central archiving.
- **Time delay.** From the time of recording, rainfall data may take several weeks to months before becoming available for use.

4.2 Prospects for Satellite Derived Rainfall Estimates

Meteorological satellites provide data, which can be used to make empirical estimates of rainfall based on cloud top temperatures. Data from meteorological satellites are available free of charge for non-commercial use. Initial costs incurred in the installation of data reception equipment and computer facilities for data processing are normally affordable. The data are received in near real-time by a relaying process from the satellite sensor through a receiver to the processing computer.

However, satellite-based rainfall estimates also have limitations. Sources of error in satellite-based rainfall estimation are discussed by Flitcroft et al. (1989) and by Grimes (1998). Errors stem mainly from the fact that data from geostationary satellites are only indirectly related to rainfall (e.g. cloud top temperature).

Sources of error include:

- Inability to monitor local variations in rain storm intensity
- Error commission on account of non-rain bearing cirrus clouds
- Error due to mismatch between gauge position and centre of pixel (co-location error)

Published research on quantification of the above mentioned errors is not available yet.

4.3 The Cold Cloud Duration (CCD) Concept

Rainfall in the tropics can be related to clouds whose temperatures are colder than 235K (-38°C). The GOES Precipitation Index (GPI) was subsequently introduced to convert hours of persistence of a cloud pixel at threshold temperature (235K) into an estimated rainfall value. This is the so-called Cold Cloud Duration (CCD) concept. A detailed description of various techniques for rainfall estimation from Meteosat satellite data is given by Snijders (1991); Grimes, (1993); Bonifacio et al (1993) and Milford et al. (1994).

Two methods that are based on the CCD concept are in operation in southern Africa. The SADC Regional Remote Sensing Project (RRSP) applies a method developed by the NOAA Climate Analysis Centre (CAC). The CAC technique uses

daily rainfall data from the Global Telecommunication System (GTS), mainly oceanic floating buoys, to model a relationship with the CCD through statistical regression (SADC-RRSP, 1998). The regression equation is then used to tune the GPI estimate. This approach works well over oceans but under-estimation is reported for land areas mainly on account of (ignored) land surface characteristics such as topography. A second method, developed by the TAMSAT group, University of Reading, is also based on the GEOS Precipitation Index. Grimes et al (1998) and Flitcroft et al (1989) provide a detailed description. This method was adopted in this study, to derive rainfall estimates for use in crop production simulations at PS-2 level.

4.4 Rainfall Estimation Methodology adopted in this Study

Half-hourly Thermal Infrared (TIR) image data at a (coarse) resolution of 5.5 to 7 km (smallest picture element, or pixel, 30 to 50 km²) are captured by a Meteosat Primary Data User Station (PDUS) located at the Institute of Natural Resources, University of Natal, South Africa. The images are automatically processed using TAMSAT Rainfall Estimation Software (TRES). CCDs are derived at several temperature thresholds (usually 5 thresholds from -30°C to -70°C in steps of 10°) in the following way:

As TIR images come in every half-hour, new sets of cold cloud detections are added to the CCD images until a day is complete (24hrs). This image shows, for each pixel, the total number of time slots when cold cloud is detected. This is subsequently converted to hours and shows the relative persistence of cold cloud for each area. The process is also run for meteorological dekads to produce dekadal CCD images. From these dekadal CCD images, the software creates a dekadal rainfall estimate (RFE) image based on historical calibration rules pre-loaded into the system. The calibration rules are based on a number of past seasons of data and hence the quality of the rainfall estimate is influenced by the amount of data used in the calibration.

The calibrations are carried out by first determining which CCD threshold best discriminates rainfall occurrence. CCD data at this threshold is then used; pixel CCD values at gauged pixels are paired with corresponding gauge values and used in a robust regression scheme. Weighted least squares regression between median gauge rainfall within CCD classes (as narrow as data allows) and mid-class CCD, where the weights are proportional to the number of data pairs in each CCD class is then done. The final model is:

$$\begin{aligned} \text{RFE} &= a * \text{CCD} + b && \text{if CCD} > 0 \\ \text{RFE} &= 0 && \text{if CCD} = 0 \end{aligned} \quad (\text{Eq.24})$$

Where:

a and b are coefficients and CCD is at the determined temperature threshold.

The regression coefficients are derived on a spatially and temporally varying basis (Milford, (1994)). These "TAMSAT method" calibrations and threshold temperatures

for each month were developed in the mid-90s for (most) SADC countries, in workshops funded by FAO and USAID and are currently in use.

4.5 Comparison between Gauged Rainfall and Satellite-Derived Estimates

To make proper comparison between rainfall measured at a particular rain gauge and Meteosat-derived RFEs, it is necessary to determine the average rainfall in an area around the rain gauge that corresponds with the satellite pixel. Meteosat pixels are close to 36 km² in the situation discussed here.

The calculation of a pixel average rainfall value for the area around a rain gauge can be carried out using block-kriging procedures (Lebel et al, 1997). The procedure generates an estimate of rainfall over a predefined pixel size and an estimate of the error from a linear combination of gauge rainfall measurements.

The following equation describes the estimation of area average rainfall as a weighted mean of point values:

$$P_A = \sum_{j=1}^n \lambda_j p(\mathbf{x}_j) \tag{Eq.25}$$

Where:

- P_A is area average rainfall,
- A is pixel-sized area around a gauge
- $p(x_j)$ is observed rainfall for gauge j at position x_j ,
- λ is weight dependent on the degree of spatial variability of the data. The weights of these measurements are derived so as to give unbiased estimates of minimum variance (Curran, 1988).

Applying “ordinary block-kriging” of point estimates can produce estimates over finite areas (equivalent to satellite pixels). The derivation of the block-kriging system used in this study is provided hereafter. The method is used to generate estimates of pixel-size rainfall, but **only** for pixels that contain a gauge.

The semi-variance $\gamma(\mathbf{h})$ is calculated as half the average squared difference between gauge values separated by a distance \mathbf{h} according to the following equation:

$$\gamma(\mathbf{x}_1, \mathbf{x}_2) = \gamma(\mathbf{h}) = \frac{1}{2} \frac{\sum_N (p(\mathbf{x}_1) - p(\mathbf{x}_2))^2}{N} \tag{Eq.26}$$

Where:

- N is number of gauge pairs at locations x_1 and x_2 separated by distance \mathbf{h} .

The set of values of $\gamma(\mathbf{h})$ as a function of \mathbf{h} is known as the experimental variogram.

Block-kriging requires that a model be fitted to this empirical semi-variogram; only a few are suitable for continuous variables. Basic types of variogram model are described in Journel and Huijbregts (1978). The three most commonly used are the spherical, exponential and linear models (Bogert et al, 1995, Journel and Huijbregts 1978, Curran 1988). The spherical and exponential models show a linear decline of spatial dependency of the variable with increasing distance until a sill value where it disappears. The linear model applies if spatial variability perpetually increases with increasing distance, never reaching the sill. The spherical model reaches the sill at a finite distance while the exponential model reaches its sill asymptotically according to the following mathematical formulations:

- Spherical:

$$\gamma(h) = \begin{cases} C_0 + C_1 \left[1.5 \cdot \left(\frac{h}{a} \right) - 0.5 \cdot \left(\frac{h}{a} \right)^3 \right], & h < a \\ C_0 + C_1, & h \geq a \end{cases} \quad (\text{Eq.27})$$

- Exponential:

$$\gamma(h) = C_0 + C_1 \left[1 - \exp\left(-\frac{h}{a}\right) \right] \quad (\text{Eq.28})$$

The exact shape is determined by the values of the coefficients C_0 , a and b , which characterise the spatial variability of a field. The coefficients are the theoretical nugget C_0 , sill C_1 and range a . Model fitting can be done by simple visual adjustment, statistical methods of varying degrees of complexity (weighted least squares, maximum likelihood).

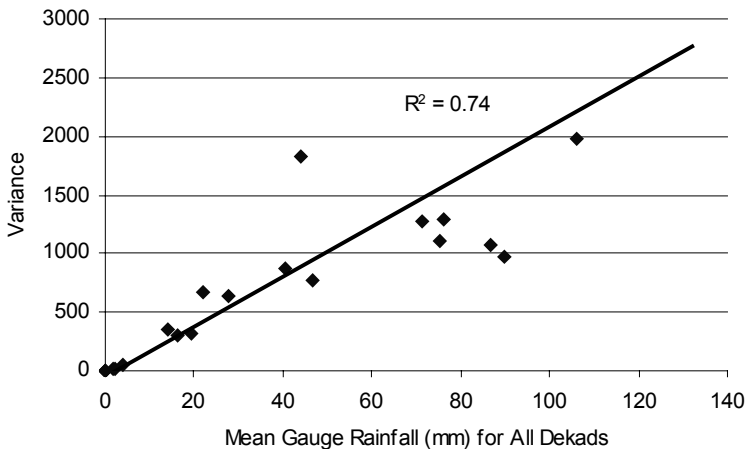


Figure 6. Increase of variance with increase in mean gauge rainfall indicating a seasonal effect.

4.5.1 Deriving a semi-variogram model for North-Western Zimbabwe

The usual practice in block-kriging interpolation would be to apply a variogram model from a single dataset. However, rainfall data are often characterized with several time steps with only a small number of data points in each step. The following limitations of the variogram model fitting are encountered:

- the work involved in fitting dozens of variogram models is enormous,
- often the rainfall field is sparsely sampled and the estimates of the variogram parameters may be poorly estimated,
- when many rainfall fields are available, treating each one separately makes only partial use of the global information contained in the whole data set.

Nevertheless, a single variogram would not be appropriate, as it would neglect seasonal and meteorological effects. **Figure 6** shows increasing variance with increasing mean dekadal gauge rainfall. The high correlation shows the time variation in the mean rainfall confirming the seasonal effect. In Zimbabwe, the rains begin in October and fall until April with peak downfall in December and January. A practical solution suggested by Lebel et al (1997) is to introduce a scale factor to the variogram as in the following:

$$\gamma(\mathbf{h}, t) = \alpha(t) \cdot \gamma^*(\mathbf{h}) \quad (\text{Eq.29})$$

Where:

- $\alpha(t)$ is a scale factor derived as the sample variance at each time step t
- $\gamma^*(\mathbf{h})$ is a time-invariant scaled variogram

Ideally, a scaled variogram is required for each localised rainfall generating process. However, for practical applicability, one scaled variogram is derived for each calendar month. All dekadal rainfall data in a month are grouped together so as to have T fields of N data points each. A climatological variogram is the derived using all $T \cdot N$ data points in the following expression:

$$\gamma^*(\mathbf{h}) = \frac{1}{2} \frac{\sum_T \sum_N (p^*(\mathbf{x}_1, t) - p^*(\mathbf{x}_2, t))^2}{N \cdot T} \quad (\text{Eq.30})$$

Note that in the climatological variogram formulation, rainfall data are standardised by their mean and variance by replacing p with p^* :

$$p^* = \frac{(p - \bar{p})}{\sigma_p} \quad (\text{Eq.31})$$

Where:

- σ_p is dekadal rainfall data variance
- p is observed rainfall
- \bar{p} is mean pixel area rainfall

This means using a variogram of fixed shape whose sill is 1.0 after variance normalization (Journel and Huijbregts, 1978) and scaling it by the variance at each time step. The climatological variogram used for each time step t (dekad) takes the form:

$$\gamma(\mathbf{h}, t) = \sigma^2(t) \cdot \gamma^*(\mathbf{h}) \tag{Eq.32}$$

Note that this leaves the range unchanged, it simply scales the nugget and sill, so that the value at the sill becomes the sample variance. The climatological variogram achieves a higher accuracy by using a lot more data in its estimation. Another advantage is that the operators do not have to derive a variogram for each new time step. The fixed scaled variogram is simply scaled-up by the sample variance of the new incoming dataset. However, due consideration should be given to the possibility that the sample variance is poorly estimated by the available data.

A climatological rainfall variogram for the season 1997/98 was obtained from the dekadal rainfall data set of 37 stations in and around the study area bounded by the coordinates (27.7, -15.5) and (31.5, -18.5), Northwestern Zimbabwe. The derived variogram model in **Figure 7** shows a high nugget indicating very significant short-range variability. The sill is reached at about 100km.

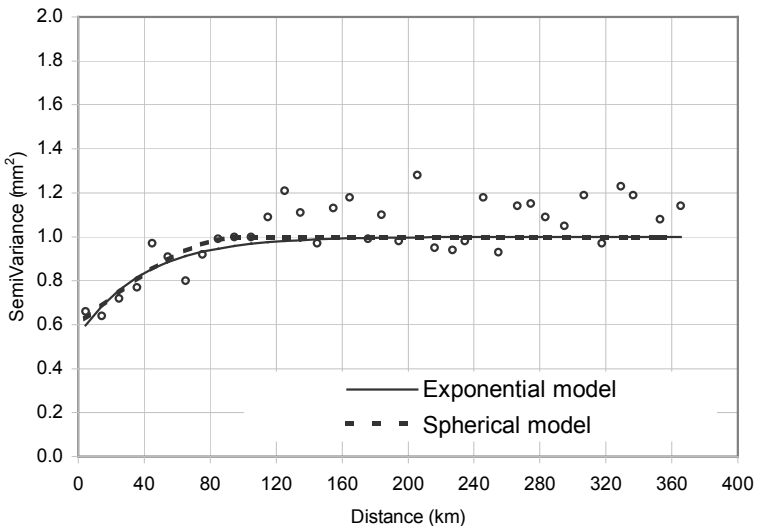


Figure 7. Mean seasonal rainfall variogram (1997-98) model for North-western Zimbabwe.

4.5.2 Estimating area average rainfall using block-kriging

Block-kriging assumes that an estimate (point or area) can be obtained from a linear combination of point measurements, i.e. the estimate (e.g. pixel average rainfall) is obtained as a *weighted mean* of point values (e.g. gauges in and around the pixel).

The block-kriging weights depend on the degree of spatial variability of the data as defined by means of the model semivariogram. Block-kriging weights are functions of the variogram model and depend on its type and on the value of its parameters. Expressing the areal rainfall P_A as a linear combination of point values:

$$P_A = \sum_{j=1}^n \lambda_j p(\mathbf{x}_j) \quad (\text{Eq.33})$$

The two basic conditions leading to the derivation of the block-kriging system are:

- the estimate is unbiased
- the estimate has minimum error (estimation variance)

These two conditions lead to the weights being calculated from a system of linear equations outlined below. The final result is:

$$\sum_{j=1}^n \lambda_j \gamma_p(\mathbf{x}_i, \mathbf{x}_j) + \mu = \bar{\gamma}_p(\mathbf{x}_i, A) \quad i = 1, \dots, n \quad (\text{Eq.34})$$

With:

$$\sum_{j=1}^n \lambda_j = 1$$

The sets of equations above constitute the *block-kriging system*. The estimation variance is given by:

$$\sigma_A^2 = \sum_{i=1}^n \lambda_i \cdot \bar{\gamma}_p(\mathbf{x}_i, A) + \mu + \bar{\gamma}_p(A, A) \quad (\text{Eq.35})$$

σ_A^2 is an estimate of the mean square error associated with P_A . Its square root will give an estimate of the uncertainty associated with the pixel rainfall estimate. In the above system of equations:

- μ is a dummy variable (Lagrange multiplier).
- $\gamma_p(\mathbf{x}_i, \mathbf{x}_j)$ is the rainfall variogram function between points \mathbf{x}_j and \mathbf{x}_i .

- $\bar{\gamma}_p(\mathbf{x}_i, A)$ is the mean rainfall variogram function between point \mathbf{x}_i and pixel A
- $\bar{\gamma}_p(A, A)$ is the mean rainfall variogram function within pixel A

For point block-kriging, to obtain estimates at a point location \mathbf{x}_0 (rather than pixel A), the system is similar, only $\bar{\gamma}_p(\mathbf{x}_i, A)$ is replaced by $\gamma_p(\mathbf{x}_i, \mathbf{x}_0)$, the variogram function at the distance between a data point, i , and the estimate location. Also the term $\bar{\gamma}_p(A, A)$ in the estimation variance vanishes as a point has infinitesimally small area.

The above system can be expressed more concisely in matrix form as:

$$K.\lambda = k \quad (\text{Eq.36})$$

To solve this equation for the weights λ , the k vector of point to pixel semivariances is multiplied by the inverse of matrix K , i.e. $\lambda = K^{-1}.k$. The error variance in matrix form is:

$$\sigma^2 = \lambda^T .D + \lambda(A, A) \quad (\text{Eq.37})$$

Given a set of point data, the above system can be solved for the weights and hence suggest estimates of the areal average (or point value in the case of point block-kriging) and its estimation variance. The block-kriging system discussed above is solved with standard methods of matrix algebra. In the case of point estimation that is where the complexities end.

However, for areal (pixel) estimation there are areal mean variogram function terms in the system: $\bar{\gamma}_p(\mathbf{x}_i, A)$ - climatological rainfall variogram function between point \mathbf{x}_i and area/pixel A and $\bar{\gamma}_p(A, A)$ - climatological rainfall variogram function within the area/pixel A . These terms are given by:

$$\bar{\gamma}_p(x_i, A) = \frac{1}{A} \int_A \gamma_p(\mathbf{x}_i - \mathbf{u}) d\mathbf{u} \quad (\text{Eq.38})$$

$$\bar{\gamma}_p(A, A) = \frac{1}{A^2} \int_A \int_A \gamma_p(\mathbf{u} - \mathbf{v}) d\mathbf{u} d\mathbf{v} \quad (\text{Eq.39})$$

For rectangular areas (e.g. satellite pixels) these integrals can be derived by reduction to lower order integrals, to be solved by numerical integration (e.g. Gaussian quadrature). They can also be derived by simple summation over the discretized pixel. For irregular areas such as river catchments, discretization is the convenient approach.

4.5.3 Results and validation of Meteosat-derived RFEs

Figure 8 shows, for 524 dekads from 37 stations, Meteosat-derived RFEs against gauged rainfall (left scatter-plot) and Meteosat-derived RFEs against the block-kriged pixel average of gauged rainfall (right scatter-plot). Less scatter and stronger agreement between pixel-average rainfall and satellite estimates are apparent, with a 20% increase in R^2 . However, notice the considerable reduction of gauge values of up to 100mm when averaged over a pixel-sized area in a block-kriging process. Global bias is illustrated by **Figure 9**; **Table 2** shows Meteosat RFEs-gauge rainfall residuals versus Meteosat-derived RFEs and Meteosat RFEs-kriged pixel averages of gauged rainfall residuals versus Meteosat RFEs. Reduction in scatter (-1.3 to -0.9) is again evident in the residuals from kriged pixel averages of gauged rainfall.

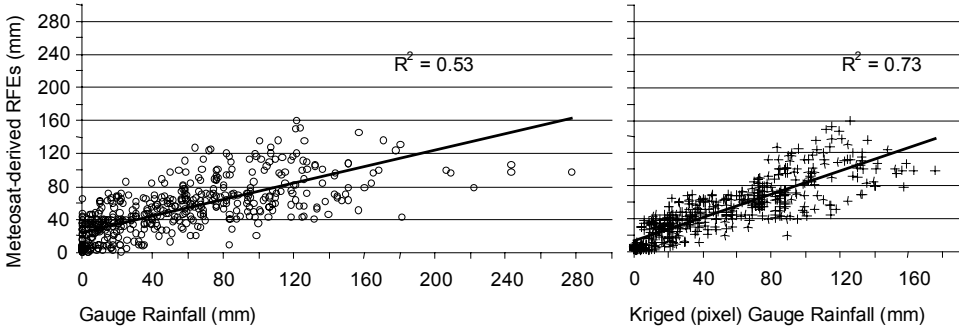


Figure 8. Scatter plots of gauge rainfall versus Meteosat-derived RFEs (left) and block-kriged (pixel) area mean rainfall versus Meteosat-derived RFEs (right). Note the 20% improvement in R^2 in the latter scatter plot due to reduced gauge rainfall variability brought about by block-kriging.

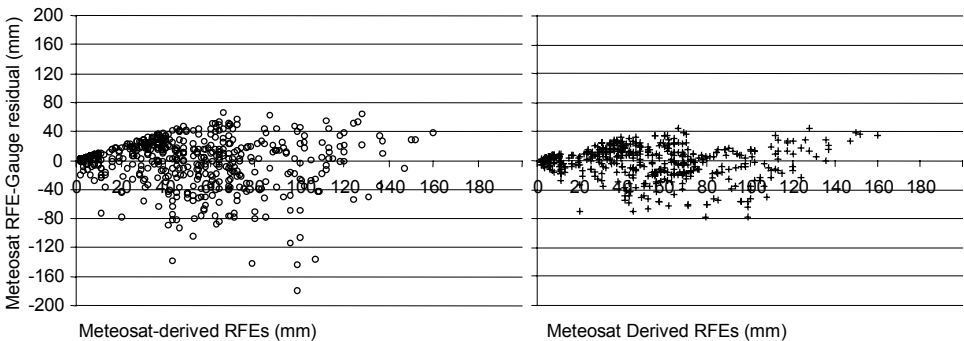


Figure 9. Scatter plots of Meteosat RFEs-gauge rainfall residuals versus Meteosat RFEs (left; bias = -1.3) and Meteosat RFEs-block-kriged gauge rainfall (pixel mean) residuals versus Meteosat RFEs (right; bias = -0.9). Note the reduced scatter and reduced tendency of residuals to increase with increase in RFE values.

Table 2. Global bias illustrated by Meteosat RFEs versus gauge rainfall (-1.3) compared with Meteosat RFEs versus block-kriged (pixel mean) rainfall (-0.9) and their respective *rmse* values

	Gauge (mm)	Meteosat-derived RFE (mm)
Bias	-1.3	-0.9
<i>rmse</i>	30.7	19.3

NE = 1.66

To better evaluate these differences, some simple statistical relations are used in both the satellite-point gauge and satellite-kriged gauge pixel comparisons. The statistics were:

$$bias = \frac{1}{N} \sum_{i=1}^N \delta_i \quad (\text{Eq.40})$$

$$rmse = \sqrt{\frac{1}{N} \sum_{i=1}^N \delta_i^2} \quad (\text{Eq.41})$$

Where:

$\delta_i = s_i - r_i$ is the residual of the satellite estimate and the gauge/pixel rainfall.

For satellite-pixel comparison a further parameter (normalised error) is of interest:

$$NE = \sqrt{\frac{1}{N} \sum_{i=1}^N \left(\frac{\delta_i}{\sigma_i} \right)^2} \quad (\text{Eq.42})$$

Where:

σ_i is block-kriging error estimate.

This parameter permits to evaluate how the satellite-pixel residual compares with the pixel error estimate. If the satellite-pixel residual is comparable to the gauge pixel block-kriging error, then NE tends to 1 and the satellite residual is on average of the same magnitude as the block-kriging standard deviation. The results show that both biases are close to 0, but as already obvious from the scatter plots using the pixel values leads to a much smaller *rmse* for the satellite data.

Finally some examples of comparisons for specific locations within the study area are presented. Two gauging sites, Karoi with a good agreement between the gauge rainfall and satellite derived estimates and Tengwe with a poor agreement are selected to illustrate the localised nature of convective rainfall as found in the study area. **Figure 10** shows that both gauge rainfall and block-kriged pixel mean rainfall values are well correlated with Meteosat-derived RFEs.

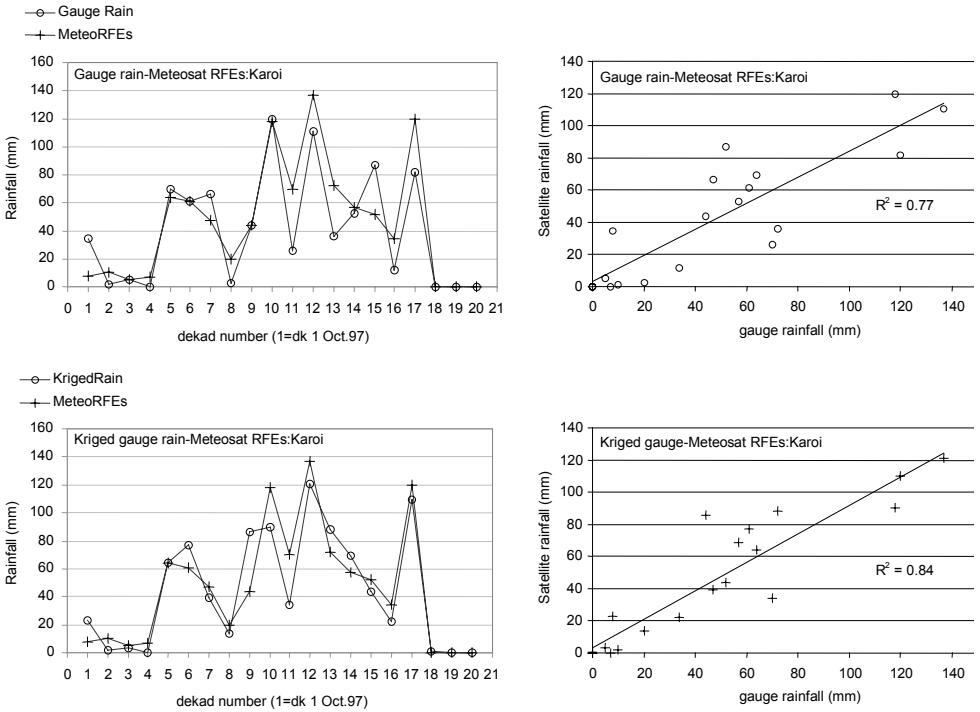


Figure 10. Karoi: Time-series comparison and R^2 of Meteosat-derived RFEs versus gauge rainfall (top) and Meteosat-derived RFEs versus block-kriged (pixel mean) rainfall (bottom). Although the R^2 improvement was only 7% for this site, a better match between Meteosat-derived RFEs and block-kriged pixel means is evident throughout the time-series.

However, a sharp contrast was observed between the correlations of gauge rainfall and block-kriged pixel mean rainfall with Meteosat-derived RFEs for the Tengwe site. Block-kriging of gauge rainfall improved the R^2 from 43% to 74%.

Figure 11 shows inter-comparison time-series plots of gauge rainfall, kriged gauge pixel rainfall and satellite derived rainfall estimates for Tengwe synoptic station.

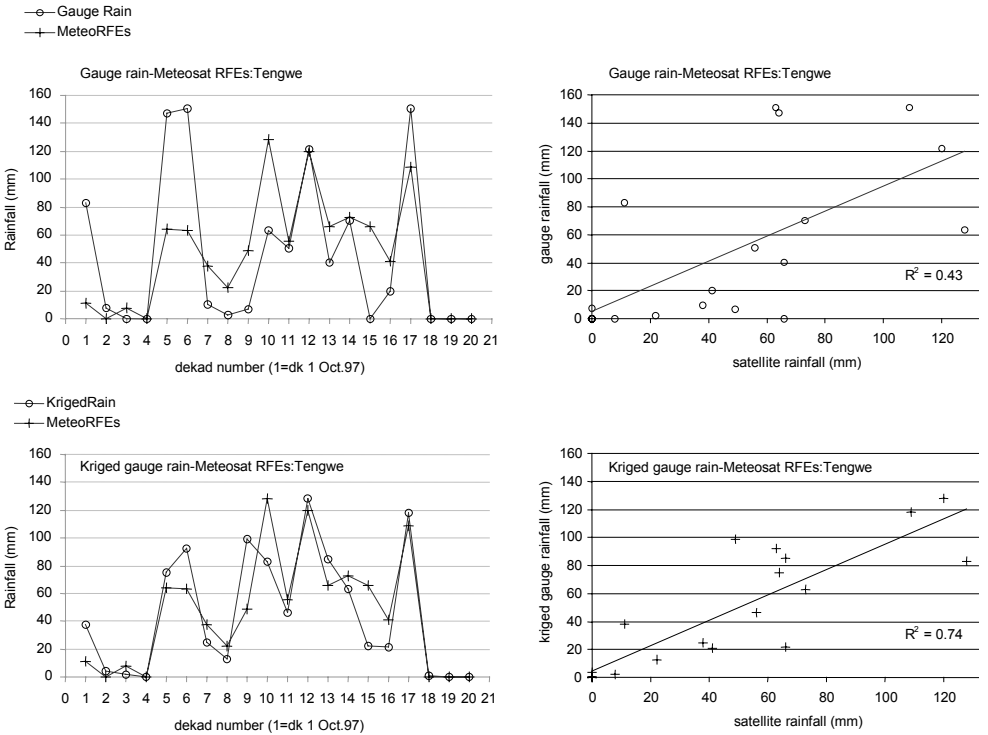


Figure 11. Tengwe: Time-series comparison and R^2 of Meteosat-derived RFEs versus gauge rainfall (top) and Meteosat-derived RFEs versus block-kriged (pixel mean) rainfall (bottom). Note the marked improvement in R^2 from 43% to 74% when RFEs are plotted against block-kriged pixel mean rainfall.

4.6 Merits of Meteosat-Derived RFEs

The foregoing has shown that Meteosat-derived rainfall estimates are well correlated with area average (pixel) gauge rainfall. It is an additional merit of Meteosat-derived rainfall estimates based on CCD that they are spatially “consistent” whereas geostatistical analysis suggests that gauge-based area rainfall estimates degrade away from the gauge at distances shorter than the shortest inter-gauge distance. For areas with sparse rain gauge networks as found in the study area, Meteosat-derived rainfall provides an indication of rainfall distribution.

It is a further advantage of Meteosat-derived RFEs that the estimation procedure is automated and operational in the Southern African region and that such estimates are therefore easier and quicker to obtain. In the next chapter, the integration of Meteosat-derived RFEs in the modelling of water-limited production potentials is discussed.

4.7 Model Time-Step versus Available Data

Meteosat geo-stationary satellites provide meaningful rainfall estimates at best over 10 days and more reliably over a month (Dugdale et al, 1991 in Lebel et al, 1997). Available algorithms derive RFEs as dekadal values from Meteosat CCD data. However, dynamic crop models require daily precipitation values.

Disaggregation of 10-day rainfall estimates to daily values has been achieved using the third-order Markov rainfall generator. Disaggregated daily values showed no significant difference to the independent gauged daily rainfall values ($p=0.51$ for the 1997 rainy season and $p=0.53$ for the 1998 rainy season). Disaggregated Meteosat-derived rainfall values were used to update the value of the precipitation variable in simulations of the water-limited production potential (PS-2) of maize.

4.7.1 Disaggregating dekadal rainfall estimates to daily values

Methods for probabilistic disaggregation of *monthly* rainfall totals into *daily* time-series are commonly based on the notion that the probability of observing an event depends on the occurrence of previous events. **Figure 12** presents a relational diagram of the final procedure followed in disaggregating RFEs events. Algorithms have been developed based on the Markov Chains (Groen, 2001; Jones and Thornton, 2000, 1999, 1997). The theoretical background and mathematical considerations involved are well explained and documented in Groen (2001), Jones and Thornton (1999) and Jones and Thornton (1997). In this study the software package MARKSIM (Jones and Thornton 2000) implementing the third order Markov weather generator was used to disaggregate Meteosat-derived dekadal RFE into daily values that are statistically similar to the observed values.

Climate normals derived from 9200 stations worldwide were grouped into 664 clusters. Rainfall model parameters for each of these clusters are derived from input monthly climate normals of rainfall, maximum and minimum air temperature, diurnal temperature range and station elevation and latitude. The program then assigns a cluster to a specified location using interpolated climate surfaces at a resolution of 10 minutes of arc (18km x 18km) and evaluates the parameter values for that point. The climate surfaces are derived from the NOAA dataset TGOP006 (Jones and Thornton, 2000) by spatial interpolation using a lapse rate to correct temperature for elevation effects.

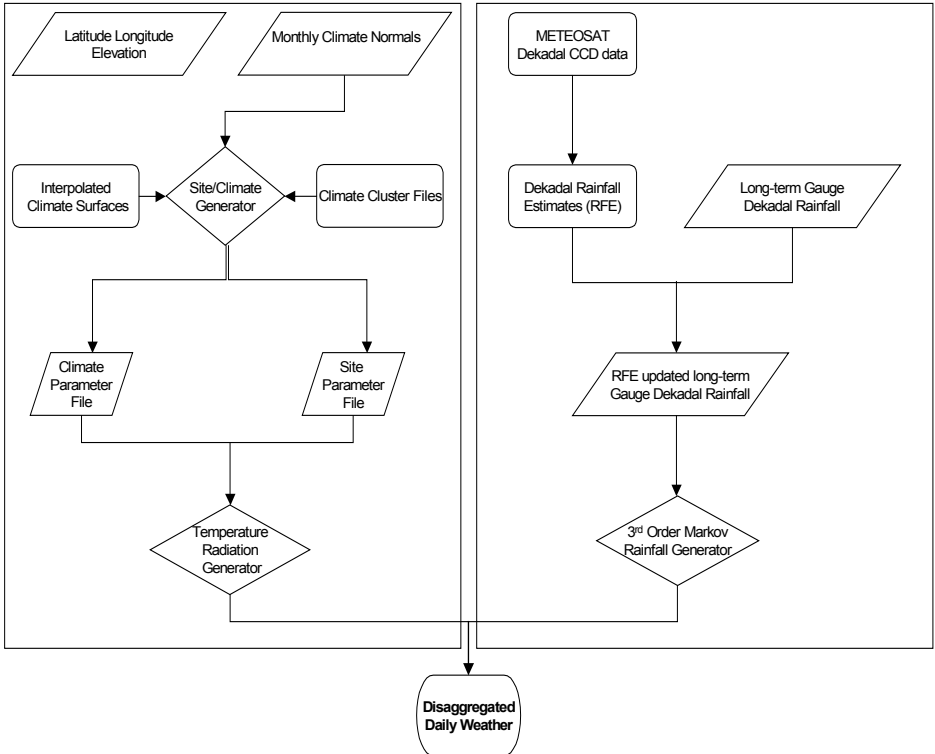


Figure 12. Relational diagram showing the disaggregation procedure of dekadal Meteosat-derived RFEs using the third order Markov weather generator after Jones and Thornton (2000).

The output weather file contains stochastically generated daily values of rainfall, solar radiation and extreme temperatures for a specified year and location (18km x 18km pixel centred around a specified latitude and longitude). Jones and Thornton (2000) acknowledge that inherent errors exist including wrongly interpolated surfaces caused by data gaps and interpolation method. Another error type described is due to local elevation changes within the 10 arc-minutes pixel resolution. This error could be minimised by applying an underlying, higher spatial resolution Digital Elevation Model (DEM) in the interpolation process (Jones and Thornton, 2000). Higher quality DEMs can be generated using the method developed by Hutchinson (2000). Another serious source of error is the incorrect assignment of pixels to a particular climate cluster, e.g. because of gaps in the calibration dataset. A fourth error type is associated with the inaccurate estimation of parameter values within the climate cluster.

4.7.2 Validation of the disaggregated rainfall estimates

The third-order Markov model was applied to Meteosat-derived dekadal RFEs over the pixel containing Karoi, the meteorological station nearest to the study area. **Figure 13** shows a time-series comparison between gauged rainfall values and values obtained from stochastic disaggregation of Meteosat-derived RFEs for the 1997-98 rainy season at Karoi. The spikes visible on the disaggregated time series around day-of-year 21 and day-of year 70 reflect random error in disaggregation. MARKSIM is a prototype software that is still being refined. It is hoped that the interpolator will improve to acceptable output random error levels.

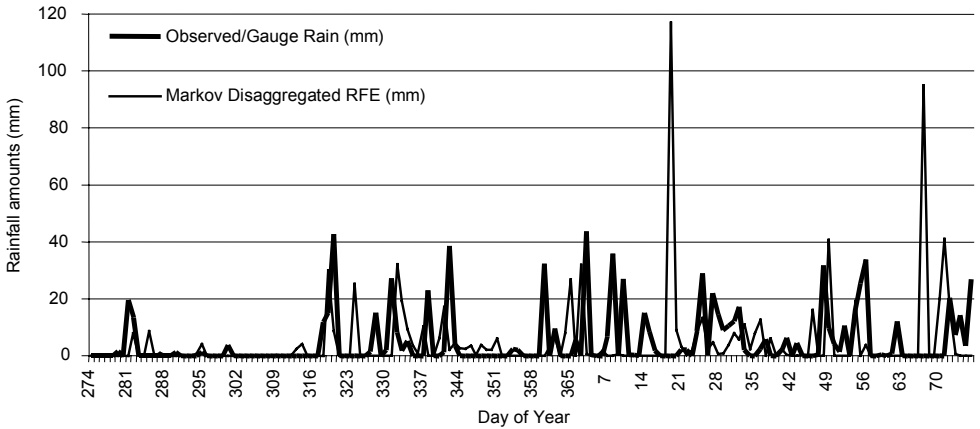


Figure 13. Time-series comparison of observed (gauged) rainfall versus disaggregated METEOSAT RFEs based on the third-order Markov rainfall generator (after Jones and Thornton 2000).

In order to show that the gauge rainfall values are statistically equivalent to disaggregated RFEs, the null hypothesis H_0 of no difference was tested. Denoting gauge rainfall as independent sample z and disaggregated RFEs as independent sample y , of sizes m and n , from possibly different probability distributions F and G respectively, the null hypothesis $H_0: F = G$ was tested. The test was based on the difference of means as a test statistic denoted by $t(\mathbf{x}) = \bar{z} - \bar{y}$, observed at 0.17 mm for the 1997/98 rainy season.

Neither the observed rain nor the generated rain showed normal distribution, symmetric distribution or similarity of shape of the data. Conventional hypothesis testing could therefore not be applied. The bootstrap hypothesis test based on the method developed by Efron and Tibshirani (1993) was deemed more appropriate. The bootstrap re-sampling technique has the capability to randomly replicate a sample with replacement to create a proxy population from which it was spawned.

The theoretical background of this re-sampling technique is explained in Burt and Barber (1996), Efron and Tibshirani (1993) and Blank et al (1999) as follows:

- B samples of size $m + n$ were iteratively drawn with replacement from the combined sample denoted \mathbf{x} . The first n observations were denoted \mathbf{z}^* and the remaining m observations \mathbf{y}^* .
- $t(\cdot)$, the mean difference was calculated on each of the B replicated samples,

$$t(\mathbf{x}^{*b}) = \mathbf{z}^* - \mathbf{y}^*, b = 1, 2, \dots, B. \quad (\text{Eq.43})$$

- The *Achieved Significance Level* (ASL) or p-value was approximated, defined to be the probability of observing at least that large a value (of the observed mean difference) when the null hypothesis is true,

$$\text{ASL} = \text{Prob}_{H_0} \{t(\mathbf{x}^*) \geq t(\mathbf{x})\} \quad (\text{Eq.44})$$

where $t(\mathbf{x})$ is fixed at its observed value and the random variable \mathbf{x}^* has an empirical distribution, specified by the null hypothesis H_0 . The distribution constitutes a non-parametric estimate of the common population that produced both \mathbf{z} and \mathbf{y} .

$$\text{ASL} = \# \{t(\mathbf{x}^{*b}) \geq t_{obs}\} / B \quad (\text{Eq.45})$$

where $t_{obs} = t(\mathbf{x})$ the observed value of the test statistic (observed mean difference)

Applying the above procedure, ten thousand bootstrap samples ($B=10000$) were drawn with replacement from the combined sample ($m + n$), each time calculating and recording the difference between the gauge rainfall mean and the disaggregated RFEs mean. Both samples were the same size ($m = n = 365$) based on days of the year. Out of 10000 bootstrap samples generated, 4453 had $t(\mathbf{x}^*) \geq 0.17$, (see **Figure 14**) that is, ASL was $4453/10000 = 0.45$. H_0 was accepted with ASL greater than the conventional significance level of 0.05, implying that there is no significant difference between gauge rainfall and disaggregated Meteosat derived RFEs.

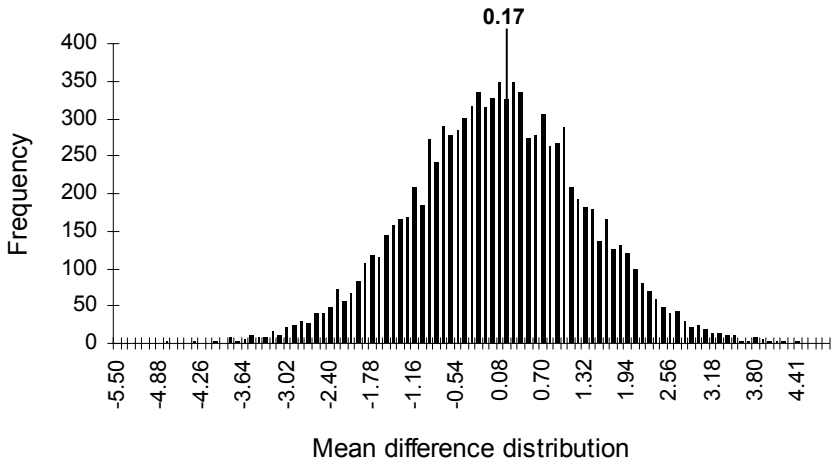


Figure 14. Histogram of bootstrap replications of the mean differences $z-y$ for the test $H_0: F = G$ (Karoï 97/98 season). The observed value ($t_{obs} = 0.17$) is indicated by a vertical line through the distribution.

4.8 PS-2 Simulations of Maize-Based Land-Use Systems using Meteosat

Moulin et al. (1998) provide a detailed review of strategies employed in crop growth models that use satellite-derived data as input for a driving variable, and/or for updating a state variable, and/or as a reference for model re-initialisation or for model re-calibration. In this study, the forcing strategy was adopted; Meteosat-derived dekadal rainfall estimates were used and only the rainfall state variable was updated.

Twelve PS-2 scenarios were run first updating the state variable with observed daily rainfall values then with disaggregated Meteosat-derived RFEs for Karoï in order to obtain two independent samples for equality of means hypothesis test H_0 . Only rainfall data were updated as forcing variables in PS-2 runs. All other state variables were obtained from meteorological and agricultural extension sources. The twelve scenarios were based on the common planting dates (day of year) 274, 284 and 294, and on soil texture classes Loamy Sand (LS), Sandy Loam (SL), Loam (L) and Clay Loams (CL) that occur in the study area. **Table 3** shows the generated Storage Organ Mass (SOM) in kg/ha obtained by using gauged rainfall in comparison with maize SOM values obtained with disaggregated Meteosat-derived RFEs. A difference of 368 kg/ha was observed between the means of the SOM values obtained from PS-2 simulations using the observed rainfall and using the disaggregated RFEs.

Table 3. SOM (kg/ha) obtained by using gauged rainfall in comparison with SOM obtained using disaggregated Meteosat-derived RFEs

Planting Date	Texture	Gauge rain SOM (kg/ha)	Meteosat RFE SOM (kg/ha)
274	Sandy loam (SL)	8.781	6.435
	Loamy Sand (LS)	13.324	10.811
	Loam (L)	7.851	6.180
	Clay Loam (CL)	15.234	12.011
284	Sandy Loam (SL)	7.198	5.849
	Loamy Sand (LS)	12.185	9.988
	Loam (L)	6.838	5.619
	Clay Loam (CL)	14.282	10.466
294	Sandy Loam (SL)	2.136	9.867
	Loamy Sand (LS)	7.270	11.020
	Loam (L)	1.174	9.680
	Clay Loam (CL)	8.857	11.622
	Mean	8.761	9.129
	Difference of means		368

Although the observed difference of the means of 368 kg/ha was relatively small, there was evidence of bias (**Figure 15**) in the sense that SOM values from scenarios involving METEOSAT RFEs for planting dates 274 and 284 were underestimated for all soil texture classes. The opposite occurred for scenarios with planting date 294 and Sandy Loam or Loam soils.

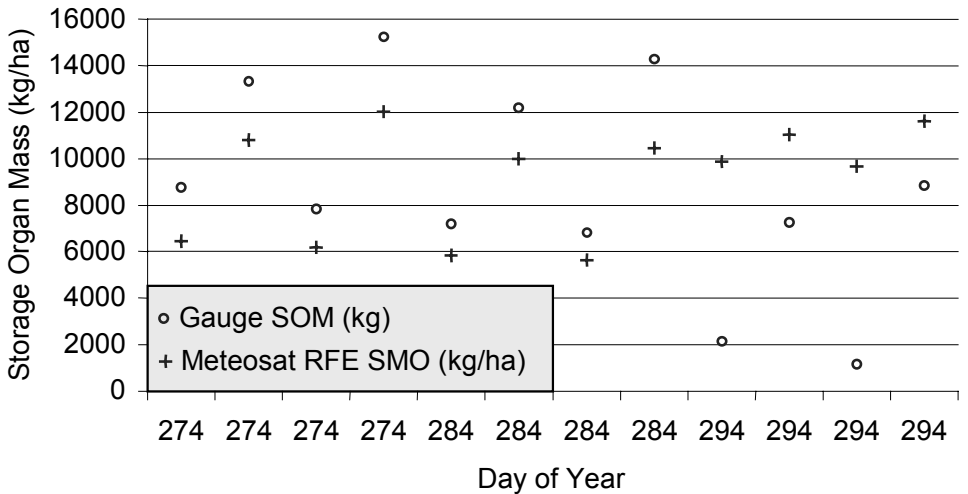


Figure 15. Graph showing underestimation of SOM based on disaggregated Meteosat-derived RFEs for planting dates 274 and 284 for all soil texture classes. Overestimations can be seen for planting date 294 and soil texture classes Sandy Loam and Loam.

However, consistency in growth trends in PS-2 simulations using rainfall data from the two different sources is evident in time-series plots as displayed in **Figure 16**. Time-series growth curves in **Figure 16** show gauge scenarios on the right and disaggregated RFE scenarios on the left.

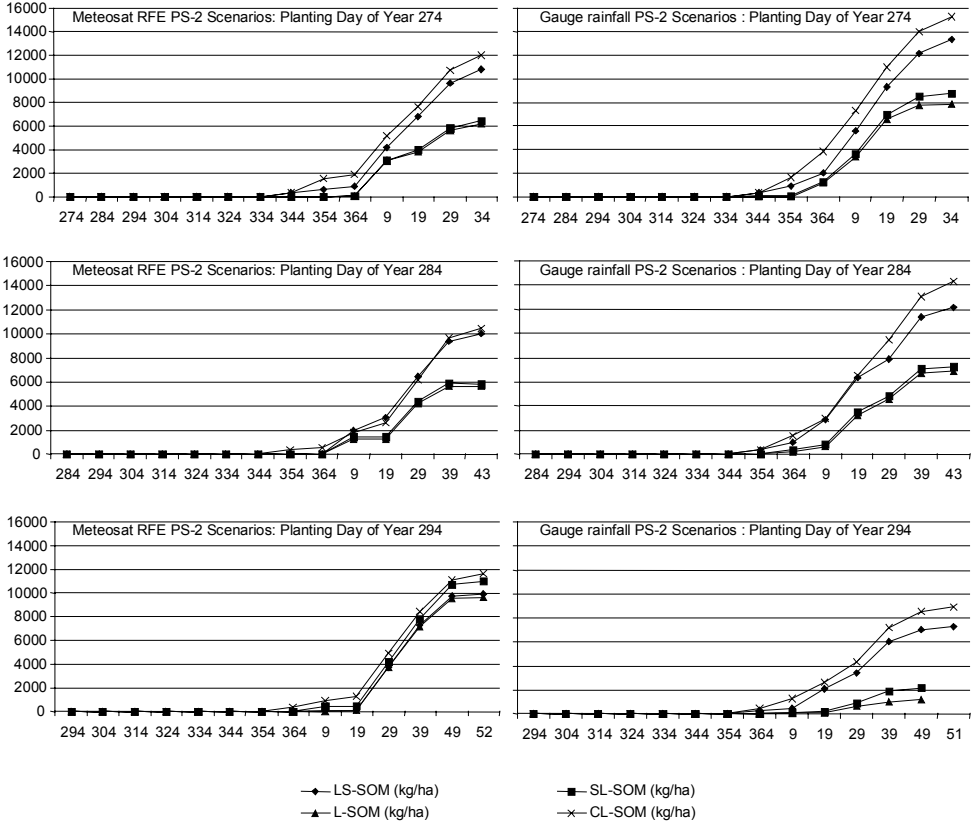


Figure 16. Paired time-series comparing PS-2 simulated SOM from gauged rainfall and Meteosat-derived RFEs for scenarios of four soil texture classes (LS, SL, L and CL) and for three planting dates (274, 284 and 294) within a 25-36 km² pixel size centred at Karoi.

A null hypothesis of no difference in means was again tested to show that no significant difference would exist between Storage Organ Mass (SOM) obtained from the PS-2 model runs using gauge rainfall and those obtained using disaggregated RFEs. The null hypothesis is $H_0: F = G$, where F and G are possibly different distributions of the two independent SOM samples simulated using gauge rainfall or using disaggregated RFEs. The bootstrap hypothesis test method was applied as described earlier in this chapter.

Ten thousand bootstrap replications were generated from the combined gauge and disaggregated RFEs SOM samples each time scoring the difference of the means. **Figure 17** shows a histogram of the distribution of differences between mean SOM values simulated using gauge rainfall data and mean SOM values simulated using Meteosat derived RFEs. 5186 of the generated mean differences had values greater than or equal to the observed mean difference value of -368 kg/ha (ASL = 0.52). $H_0: F = G$ was accepted at 0.05 significance level suggesting that there was no significant difference between SOM predictions based on gauge rain and those based on Meteosat-derived RFEs.

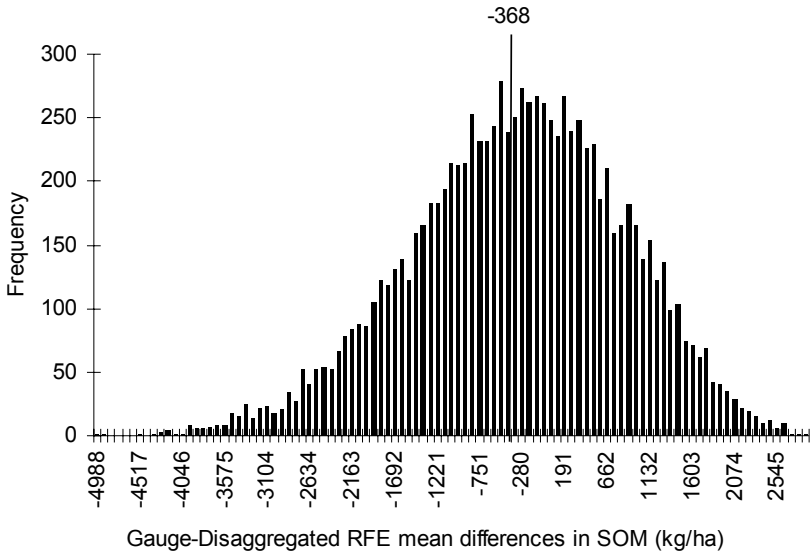


Figure 17. Bootstrap differences of the mean between SOM values simulated using gauged rainfall and disaggregated Meteosat-derived RFEs.

Experimental data for the validation of the predicted water-limited crop production potential are not available. However, re-sampling techniques can be applied on the simulated values, randomly replicating them into a proxy universe from which the distribution can be analysed and confidence intervals of the mean determined.

The bootstrap method was used to generate a normal distribution of the predicted SOM values from which confidence intervals for the mean could be determined. The bootstrap percentile method was used to derive the confidence limits for the mean. The following bootstrap percentile confidence interval derivation is based on Burt and Barber (1996) and Efron and Tibshirani (1993):

For a random variable $\hat{\theta}^*$ drawn from the distribution $N(\hat{\theta}, \hat{s}e^2)$, it follows that:

$$\hat{\theta}^* \approx N(\hat{\theta}, \hat{s}e^2) \quad (\text{Eq.46})$$

Where:

- $\hat{\theta}$ is the sample estimate of the parameter θ
- $s\hat{e}$ is the estimated standard error
- N is the number of measurements making-up the entire population

Then, $\hat{\theta}_{lower} = \hat{\theta} - z^{(1-\alpha)} \cdot s\hat{e}$ and $\hat{\theta}_{upper} = \hat{\theta} + z^{(\alpha)} \cdot s\hat{e}$ are the 100. ∇^{th} and 100. $(1-\nabla)^{th}$ percentiles of $\hat{\theta}^*$.

Alternatively:

- $\hat{\theta}_{lower} = \hat{\theta}^{*(\alpha)} = 100 \cdot \alpha^{th}$ percentile of $\hat{\theta}^*$'s distribution
- $\hat{\theta}_{upper} = \hat{\theta}^{*(1-\alpha)} = 100 \cdot (1-\alpha)^{th}$ percentile of $\hat{\theta}^*$'s distribution

Figure 18 shows histograms of the bootstrap distributions for the respective SOM means. The distributions showed that 95% of SOM values predicted with gauged rainfall data lay between 6375 and 11102 kg/ha with a mean \bar{x} of 8761 kg/ha. 95% of the SOM predictions using disaggregated Meteosat RFEs were bound between 7823 and 10409 kg/ha with the mean \bar{x} = 9129 kg/ha. The lines flanking the distributions in **Figure 18** indicate the 2.5th and 97.5th percentiles whereas the central lines show the calculated bootstrap mean.

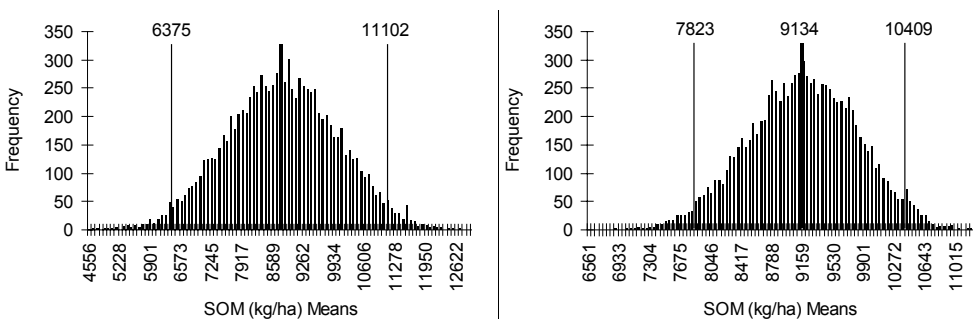


Figure 18. Histograms of 10000 bootstrap replications each of the mean SOM (kg/ha) predicated based on gauged rainfall (left) and based on disaggregated Meteosat-derived RFEs (right). The flanking vertical lines in each histogram indicate the 95% confidence interval values while the central lines indicate the respective means.

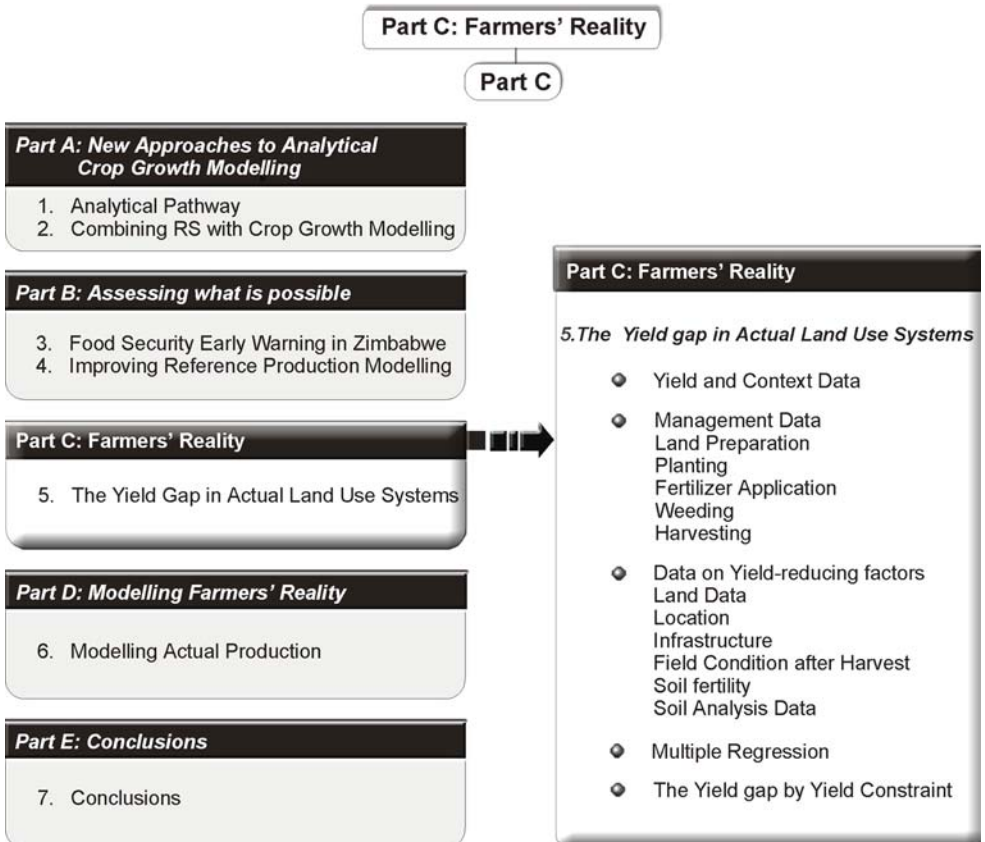
4.9 Discussion

The findings presented suggest that satellite-derived cumulative rainfall can be disaggregated to daily values and used for modelling of water-limited production potentials with sufficient accuracy based on universally valid physical, chemical and biological relationships.

One difficulty affecting the regionalization of reference crop production estimates is that in addition to precipitation, dynamic crop models require other meteorological data that include minimum/maximum air temperatures, relative air humidity and number of sunshine hours (or solar radiation data). The coarse spatial resolution of meteorological satellites does not allow the retrieval of these parameters or their equivalents with sufficient accuracy required for the crop growth models. Meteorological stations in Zimbabwe are not only very sparse but are almost completely absent in the communal lands. This makes interpolation of meteorological data for model input very risky. Recent research efforts have revealed that high spatial and temporal resolution climate surfaces can be generated (Hutchinson, 2000; Price et al, 2000) using Digital Elevation Models (DEM), hydrological maps and some basic meteorological station data. The time constraint has not allowed the author to explore and test application of this approach.

In the proceeding Chapter it is demonstrated that actual yields are far less than the water-limited potential. Yield constraints are studied to acquire insight in their quantified relative contributions to the yield gap. It is shown that the yield gap is caused by a complex combination of various yield-reducing constraints that originate from the environment, the management and the socio-economic setting of the farmers. As discussed earlier, the complexity of the yield constraints in numbers, their nature and their manifestation in the yield prohibits their meaningful inclusion in prediction models.

Part C. Farmers' Reality



5. Case Study 2: The Yield Gap and Causative Constraints in Maize-Based Land Use Systems in Piriwiri and Mupfure Communal Lands, Zimbabwe

In actual farming conditions, farmers' socio-economic circumstances do not allow many mitigating interventions against yield constraints to obtain a high yield level. The result is that actual production is often less than the water-limited potential. Thus, a yield gap develops in the course of the cropping season, between the achievable potential production and the observed actual production at farmers' level.

As mentioned earlier in this thesis, the gap between the water-limited production potential and actual production is caused by a combination of management constraints and natural hazards and/or unfavourable socio-political incidental events. In this case study, actual conditions of maize-based land use systems in two adjacent communal lands, Piriwiri and Mupfure in Zimbabwe were studied. Land, management and yield data were acquired through land use/land ecology surveys and interviews of farmers. Yield constraints were identified and quantified. Note that results represent data from only one season and therefore exclude impacts of the year-to-year variability. A production function and parameter statistics were derived and used to determine the 'mean' and 'best' values for each explanatory parameter, and the quantified impact by yield constraint and its contribution to the overall yield gap were estimated.

35% of the yield gap was contributed by environmental constraints related to the terrain, soil texture and farmers' perception of their soil's fertility. The remaining 65% of the yield gap were contributed by constraints related to management including inorganic and natural fertilizer application, the amount of seed used and various yield-reducing constraints related to crop protection. The actual and calculated best yield values were close and agreed with the simulated water-limited yield potential as described in the previous chapter. Yield gap constraints related to management are also linked to socio-economic circumstances of the farmer. This reality limits the versatility of the method to local conditions. In order to obtain a regional and season-independent perspective of the yield gap, a direct method for estimating actual yield at farmers' level is proposed in the following.

5.1 Study Area

Piriwiri (area = 300 km²) and Mupfure (interchangeably named as Umfuli, area = 1500 km²) communal lands in Hurungwe West District were surveyed. The communal lands, adjacent to each other, run in the southeast to northwest plane above the Sanyati and the Mupfure rivers that form their respective lower boundaries. The Mupfure contributes to the Sanyati, which is a major tributary of the Zambezi river. The study area is bound by the geographic coordinates 17°10'S, 29°13'E and 17°45'S, 29°50'E. These communal lands lie in natural

regions III (agricultural rainfall index: 69 to 50) and are partially designated for semi-intensive and semi-extensive farming. The agricultural rainfall index is a function of dependable rainfall and potential evapotranspiration (Anderson, 1993). The terrain is mainly rolling to hilly rising from 700 to 1100 m.a.s.l. Soils comprise Ustropepts and Ustorthents (Soil Taxonomy) or Leptosols, Regosols, and Cambisols (FAO/Unesco).

A stratified clustered and representative sample scheme was designed in order to obtain an integrated land use systems dataset for the 1996-97 growing season. Stratification was based on four land units adopted from a land unit map based on altitude, geology, landform, drainage, soils, vegetation and land use. Appendix D1 and Appendix D2 show the land unit map of the study area and its legend respectively. It was intended that the land units be sampled equally. In total 167 plots were sampled. **Figure 19** shows the study area with ward demarcations and positions of sampled fields against a backdrop Landsat TM false colour composite image. When a pre-determined sample point fell on a maize field, the owning farmer was sought out and interviewed in the identified field using a checklist designed to obtain yield data, management data and observations from the farmer. However, farmers were not always readily available and this influenced the sample distribution.

The interview was followed by a land use and land ecology survey of the maize field and its surroundings and observations including field infrastructures recorded in a pre-designed relevee sheet. Appendix E1 features a sample farmer-interview checklist and Appendix E2 a sample relevee sheet. The study was carried out two to three months after harvesting when farmers would have yield data of the past (recent) season. Descriptive statistics were used to obtain a general overview of the various factors affecting maize yield in the study area.

5.2 The Weather during the 1996/97 Growing Season

Scattered thunderstorms started in mid-September. Following widespread rains in late October-early November, planting of the maize crop advanced under generally favourable weather conditions. The studied districts had a comparatively late start of rains and planting lagged behind the rest of the country. Widespread and regular rainfall occurred from December onwards. In the Zambezi Valley, several weeks of continued rains in January-February reduced crop yields as crops suffered from waterlogging. The weather was generally cool and dry in April, which facilitated drying of crops and allowed a timely harvest. The 1997 maize crop harvest was slightly above the five-year average.

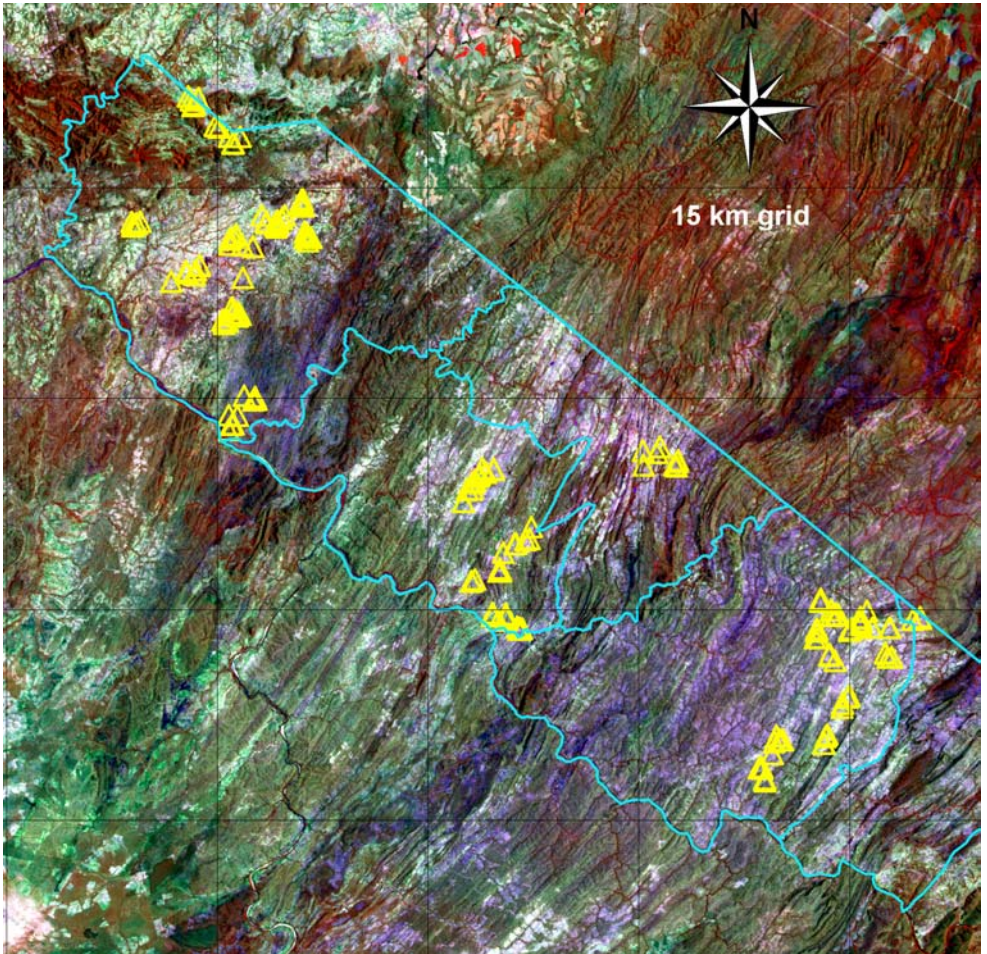


Figure 19. TM Image of the study area (RGB-453; Dec.1994) with administrative (Ward) boundaries and identification of plots sampled.

5.3 Descriptive Statistics

5.3.1 Yield and context data

The distribution of the yield data is shown in **Figure 20**. There are sufficient statistical reasons to state that the data obtained are normally distributed. The Kolmogorov-Smirnov 2-tail test, using as average 2630 and as standard deviation 1762 kg/ha, had a non-significant probability that the data follow a non-normal distribution ($P= 15.7\%$); the Z-Scores are sufficiently aligned along a straight line. Transformation of the yield data was therefore not required to make them normally distributed.

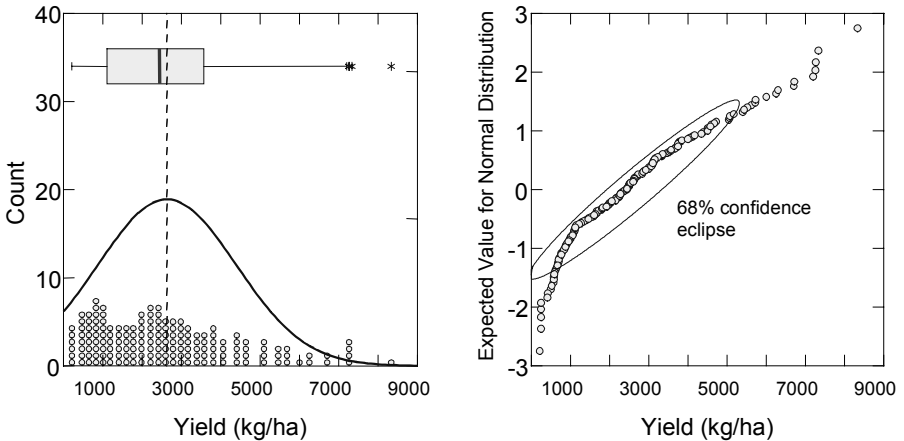


Figure 20. Left: Distributions of yield data and fitted normal distribution curve. Right: Z-Scores of the yield data.

Previous research (An, 2000) suggested that farmer knowledge correlated with maize yield. Based on agronomic education provided by AGRITEX, 75 of interviewed farmers obtained the status of 'Master Farmer'. However, no significant relation with yield was found in this study.

5.3.2 Management data

Land Preparation

Out of 167 farmers, 143 farmers ploughed their field once or twice, mostly with ox-drawn ploughs; 24 practiced non-tillage because of lack of 'affordable' draft power. A study by Hunchu and Sithole (1994) on eight randomly selected districts of Zimbabwe, revealed that 53.3% of farmers owned the draught animals they used. The rest of the farmers either borrowed or hired animals. This number agrees with the 55.8% of farmers that did winter ploughing in one of the communal lands. The ploughing depth was mostly shallow (15-25 cm). Ploughing increased yields on average by about 1000 kg ha^{-1} (Figure 21). In Zimbabwe, "Winter Ploughing" refers to 'early' ploughing, carried out directly after harvesting a previous crop and timed at the end of the rainy season (Figure 22). Only 41 farmers practiced winter ploughing. They achieved significantly higher yields (Figure 23). When winter ploughing was carried out, farmers often carried out a second ploughing as well upon the start of the first rains (23x). The duration from the 'last' ploughing done till planting had however no clear impact on yields (Figure 24). In addition to ploughing, 35 farmers (21%) harrowed their field in order to produce a better seedbed; this had slightly positive impacts on yield ($P=6\%$).

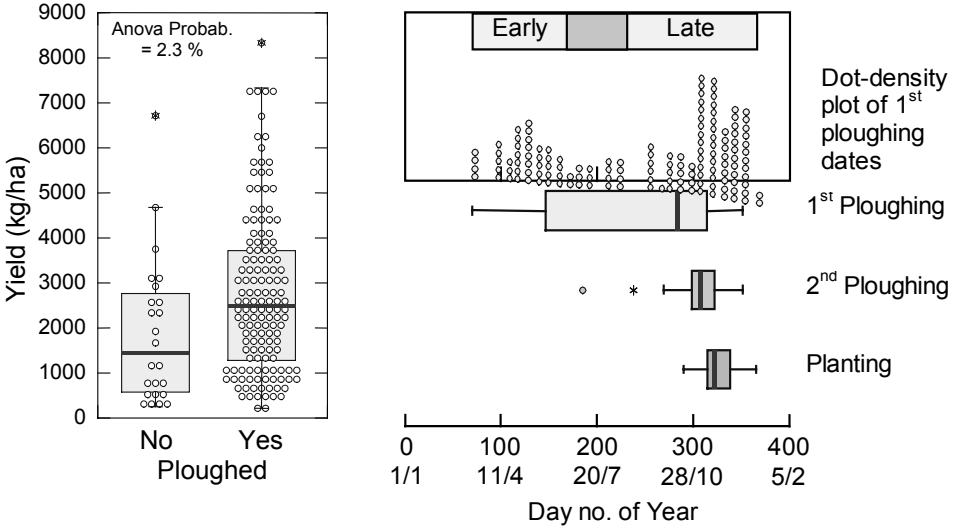


Figure 21. Impact of ploughing on yield.
Figure 22. Ploughing and planting dates.

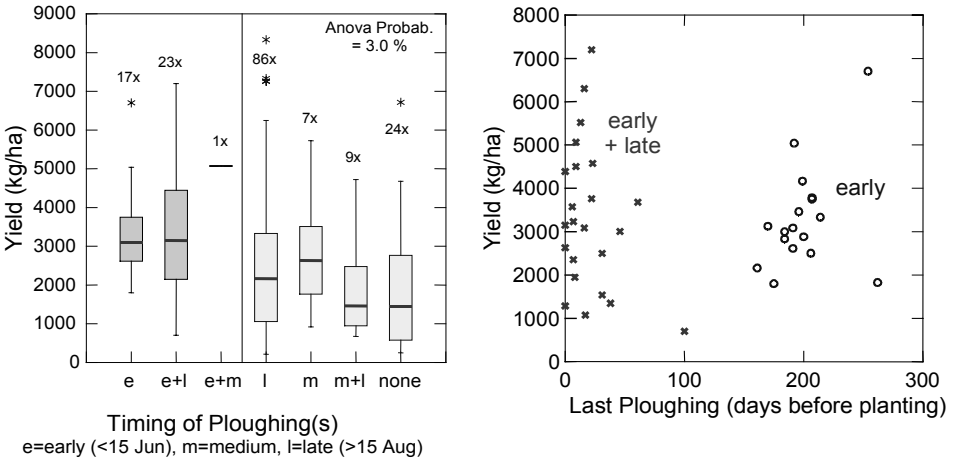


Figure 23. Timings of ploughing vs. Yield.
Figure 24. Timing of the last ploughing vs. yield.

Relating, through regression, three ploughing categories to yield, yielded the regression equation shown below. If winter ploughing was carried out, yields were 1479 kg/ha higher than if zero-tillage was practiced, while yields were only 642 kg/ha higher if only medium and/or late ploughing was done.

Yield (kg/ha) = 1875 + 1479 . (if early ploughing done*) + 642 . (if later ploughing done)**

(n = 167; Adj.R-Sq = 5.9%; ** = sign.at 1%; * = sign.at 10%)

Planting

The farmers planted their crop around the 22nd of November, viz. between 18 October (Julian day nr 292) and 31 Dec (day nr 366). **Figure 25** confirms that this was indeed around the optimum planting date (median day of year 329); the quadratic curve indicates that early planting provided the best yields. The quantity of seed used (25 kg ha⁻¹ on average) had a substantial impact on yields (**Figure 26**); one extra kg of seed resulted in 63 kg of additional yield (N=166; Adjusted R² =13%). Plant density data (estimated after harvesting) were less clearly related to yields; plant spacing varied from 45x15 cm to 100x30 cm. Plot size data in turn explained to some extent the differences in the quantity of seed used; sowing densities were somewhat less on larger plots (2-4 ha) (**Figure 27**).

Seeds were placed by plough or cultivator (116x), harrow (23x), hoe (17x), or planting machine (11x). Animal traction was used when required. Planting by hand (and hoe) was associated with lower yields (**Figure 28**). All farmers planted early maturing hybrid varieties. The type of variety planted did not notably affect yields; **Figure 29** summarizes results of varieties aggregated by seed company (P=53%); in total 11 specific varieties were planted.

In summary, the following impacts of planting method on yields could be quantified:

Yield (kg ha⁻¹) = - 89746 + 55.7 . (seed quantity used; kg/ha **) - 647 . (if planting by hoe *) + 1112 . (if planting by harrow or planting machine **) + [580 . (planting date; day of year *) - 0.922 . (planting date; day of year *)²]

(n = 166; Adjusted R² = 26.1%; ** = sign.at 1%; * = sign.at 10%)

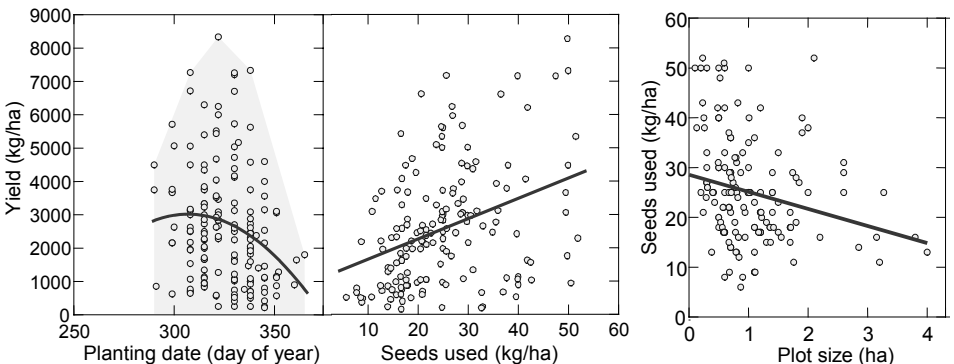


Figure 25. Planting date versus yield.

Figure 26. Sowing density versus yield.

Figure 27. Plot Size versus sowing density.

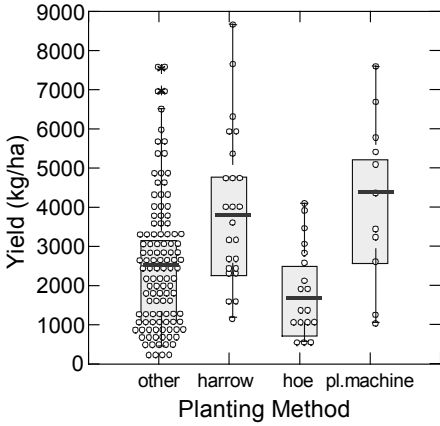


Figure 28. Planting method vs. yield.

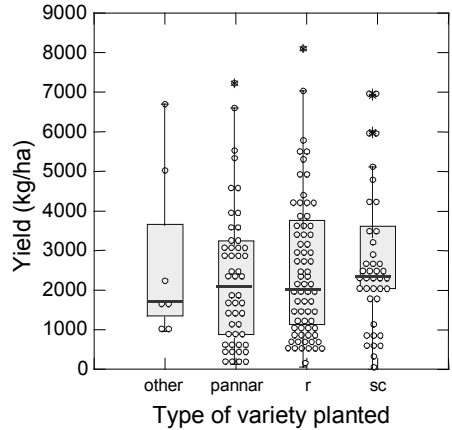


Figure 29. Type of variety planted vs. yield.

Fertilizer Application

Nitrogen deficiency is evident on as much as 80% of the fields in communal lands (Waddington, 1993). Farmers applied Compound ‘D’ (8-14-7-6.5; 70x), Ammonium Nitrate (78x), and/or Farmacyard manure (FYM; 32x; **Figure 30**). Compound-‘D’ was mostly applied at planting (53x) along the plant lines, or alternatively, about 26 days after planting (17x). In all cases the applied dose was about 157 kg ha⁻¹. In earlier studies, timing of fertiliser application was found to be a significant contributor to the yield gap; up to 8% yield reduction has been attributed to late application of basal fertilizer (Shumba, 1990). In this study, response to Compound-‘D’ (**Figure 31**) was as follows for both groups (both had non-significant quadratic components):

$$\text{Yield (kg/ha)} = 2211 + 6.88 \cdot (\text{Compound-‘D’ at planting; kg/ha **}) + 4.08 \cdot (\text{Compound-‘D’ after planting; kg/ha *})$$

(n=167; Adjusted R² = 13.7%; ** = sign.at 1%; * = sign.at 10%)

Most farmers applied Ammonium Nitrate (AN) as a top-dressing, 3 to 9 weeks after planting (average of 45 days), close to individual plants in the planting lines. AN application had a significantly positive effect on yield. The quadratic curve [Yield = 2109 + 18.6 AN – 0.055 AN²], had an Adjusted R² of 11.9% (Max. yield at 169 kg AN ha⁻¹; N=159; **Figure 32**). On average, farmers applied 47 kg AN ha⁻¹. Interaction between AN application rate and application date could not be detected. Farmers applied up to 16,000kg FYM ha⁻¹ (average = 3,300 kg ha⁻¹; **Figure 33**).

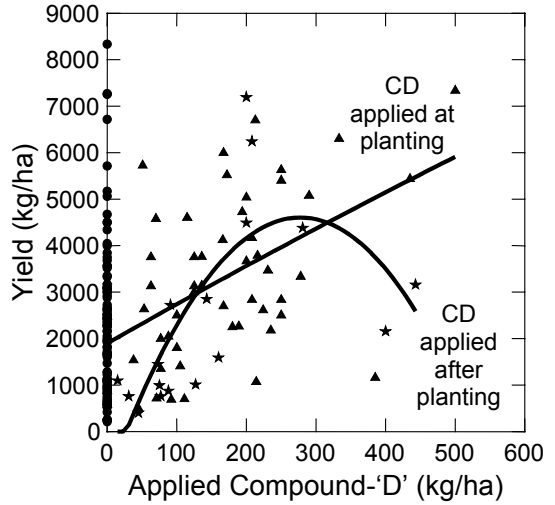
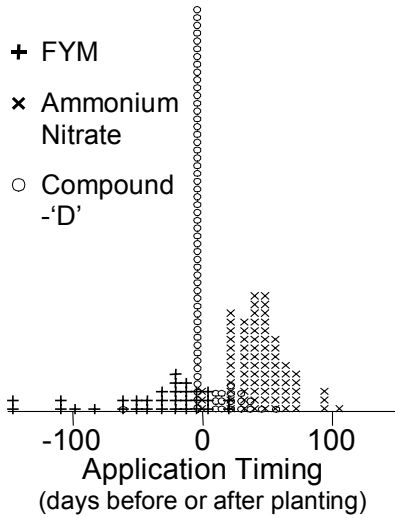


Figure 30. Timing of fertilizer application.

Figure 31. Rate of applied Compound-'D' at planting or later vs. yield.

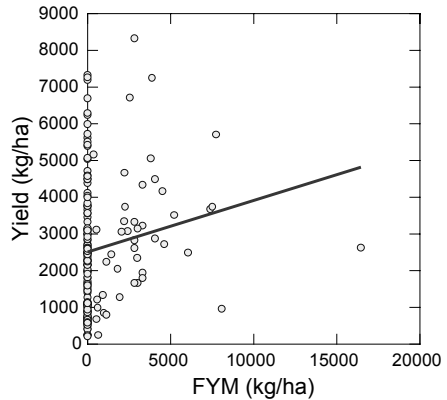
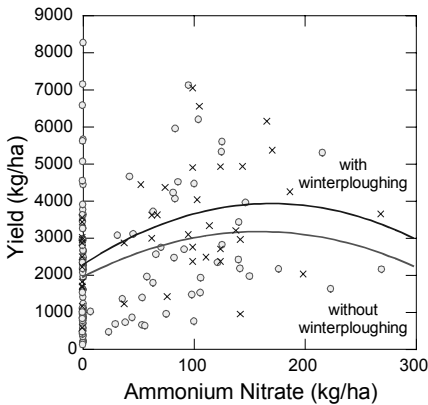


Figure 32. Rate of applied AN vs. yield (with and without winter ploughing).

Figure 33. Rate of applied FYM vs. yield.

Weeding

Farmers weeded their crops 1 to 3 times (**Figure 34**); a higher weeding frequency gave slightly improved yields. In a previous study, Shumba (1990) found that smallholder farmers often weed late and incompletely because of shortage of labour and draught power. Delayed weeding of maize from 14 to 30 days after crop emergence may reduce yields by 20%. In this study, no clear impact of the

timing of weeding on yield could be detected, but using animal traction (cattle) for the 1st weeding was associated with increased yields (see **Figure 35**). Farmers using animal traction availed of a plough, cultivator or ridger.

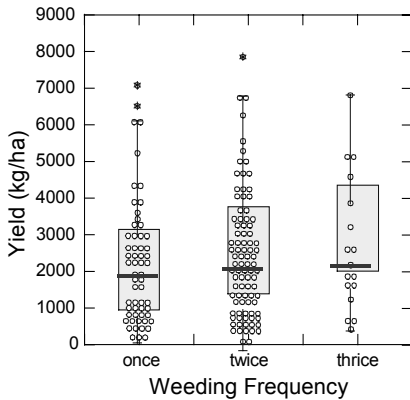


Figure 34. Number of weedings versus yield.

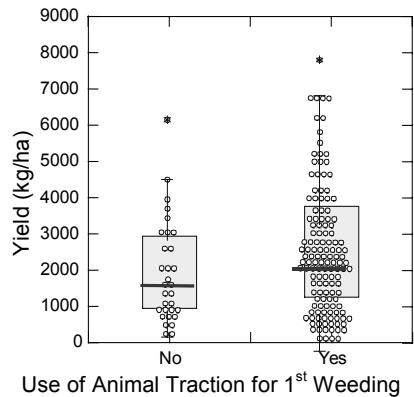


Figure 35. Impact of use of animal power source for weeding on yield.

Harvesting

Harvesting took place after the crop had dried down to a moisture content that permits safe storage. The average length of the growing cycle was 161 days (range 98-314 days). Four farmers waited very long before they harvested their crop; this did not seem to have a negative impact. 'Length of growing period' had a significant (positive) effect on yield but this may be more related with the timing of planting than with the time of harvesting.

5.3.3 Data on yield reducing factors

Among insect pests that occur in Zimbabwe, damage by armoured crickets, maize stalk-borers and termites is considered to be of economic significance (Whingwiri et al, 1992; Page, 1985). The leafhopper is also viewed in serious light as a vector for the maize streak virus. Page (1985) ascribes yearly yield losses of 2 to 7% to diseases but in some localities, one or more diseases may become acute and cause much greater damage.

During the 1996/1997 survey, farmers complained about several yield limiting and yield reducing factors, including wildlife, livestock, weeds, drought, waterlogging, aphids, armyworm, grasshopper, stem-borer, termites, and diseases. On average, farmers estimated their total losses due to these factors at 28% (**Figure 36**) computed as: $[(\text{target} - \text{actual}) / \text{target}]$. Partial losses (contributions by factor) were also estimated. In general, by percent claimed loss, yield was significantly lower by 31.6 kg/ha (N=167; Adjusted $R^2 = 12.1\%$).

The frequency and extent of farmers' complaints about specific loss factors is shown in **Figure 37**. In particular termites, weeds, and drought were regularly indicated as causes of high yield losses. Few and insufficient control measures were carried out to control pests and weeds because farmers could not afford purchase of pesticides and herbicides. Drought stress could hardly be avoided with the current management options available to the farmers. The perceived impacts of termites, weeds, and mid-season dry spells on yields suggest the following functional relation.

$$\text{Yield (kg ha}^{-1}\text{)} = 3418 - 46.73 \cdot (\% \text{ reported yield loss by termites}^{**}) - 37.78 \cdot (\% \text{ reported yield loss by weeds}^{**}) - 28.04 \cdot (\% \text{ reported yield loss by drought}^{*})$$

(n = 167; Adjusted R² = 11.3%; ** = sign.at 1%; * = sign.at 10%)

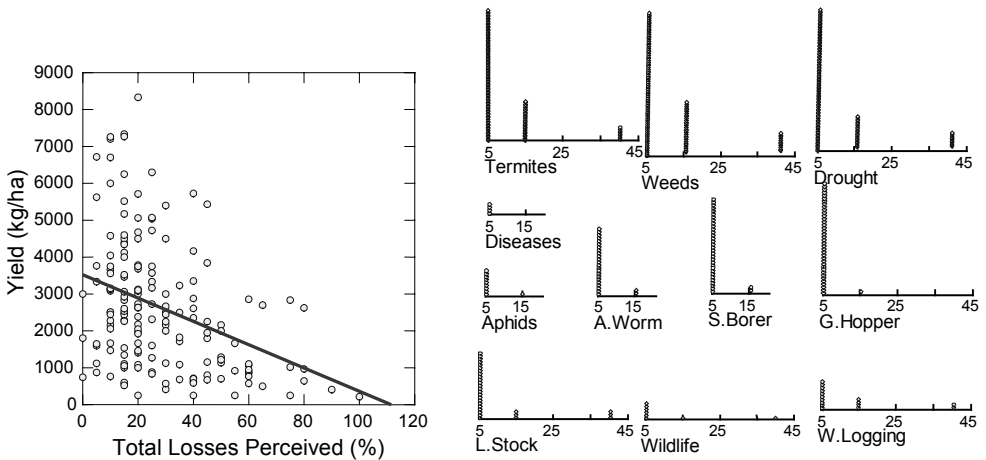


Figure 36. Perceived total yield losses vs. yield.

Figure 37. Frequency and extent that farmers complained about yield losses.

5.3.4 Land data

Location

Plots at higher altitudes produced slightly better (some 115 kg ha⁻¹ for 100 m increase in altitude); the relation was however not significant (P=40.5%). However, step-wise multiple regression revealed that altitude is to be considered in studies of yield variability, as will be discussed in the following section. There was no significant relation between yields and land unit identification (Anova P=98.1).

Infrastructure

Contour ridges were present on 89 plots; their maintenance varied considerably. Where they were present, yields were on average some 400 kg ha⁻¹ higher but this relation was not significant (P=16.1%).

Field condition after harvesting

During the survey, the fraction ground cover was estimated on each field, i.e. the surface fraction occupied by shrubs and forbs, litter, stones, bare soil, anthills and basal cover (total = 100%; **Figure 38**). Notably 'cover by shrubs and forbs' and 'fraction of bare soil' were significantly related to yield (**Figure 39**).

In summary, the following impacts of the two cover elements on yields could be quantified:

$$\text{Yield (kg ha}^{-1}\text{)} = 1900 - 74.68. (\% \text{ cover by shrubs \& forbs } **) + 13.51 . (\% \text{ cover by bare soil } *)$$

(n = 167; Adj.R-Sq = 8.2%; ** = sign.at 1%; * = sign.at 10%)

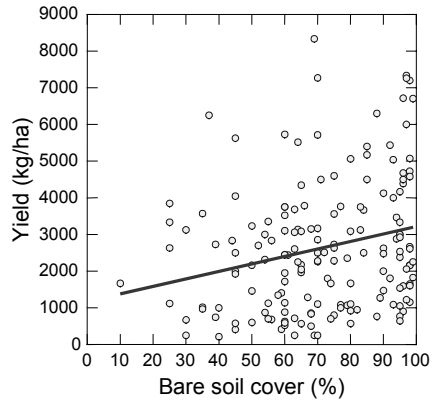
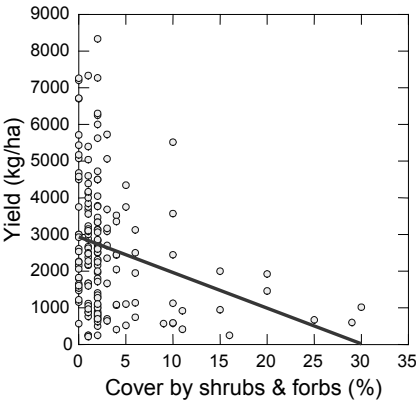


Figure 38. Percent cover by shrubs at harvest versus yield.

Figure 39. Percent bare soil at harvest versus yield.

Soil fertility and infiltration status

The opinion of farmers with regard to the fertility status of their plot is presented in **Figure 40**. The few farmers (12x) who classified their soil as 'good' had significantly better yields (+1243 kg/ha) than those who rated their fields 'moderate' or 'poor' (Anova P=3.0%). Farmer's linked soil fertility with the soil's infiltration rate (Anova P=19.6%). The latter was (crudely) judged by recording the time (seconds) needed for a calibrated cup of water to sag into the soil. However, the so obtained 'infiltration times' were not related to yields (P=62.2%).

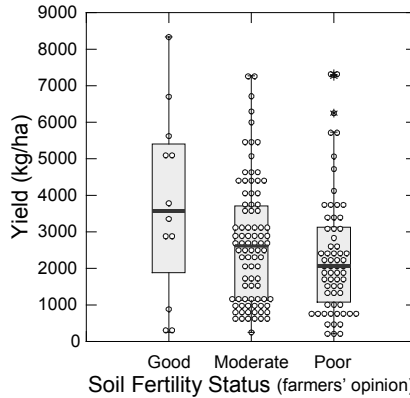


Figure 40. Soil fertility status (farmers' perception) versus yield.

Soil analytical data

Soil samples were taken from the topsoil (0-20 cm) for a broad characterization of the soil material; they were tested at the soils laboratory of the Department of Research and Specialist Services (DRSS) in Harare (**Table 4**).

Table 4. Laboratory tests of soil samples collected in the study area

<ul style="list-style-type: none"> • Soil Texture (Bennett 1985), based on: <ul style="list-style-type: none"> • Clay % (< 0.002 mm) • Silt % (0.02-0.002 mm) • Fine Sand % (0.2-0.02 mm) • Medium Sand % (0.5-0.2 mm) • Coarse Sand % (2.0-0.5 mm) 	<ul style="list-style-type: none"> range 2-59 range 4-48 range 13-68 range 1-44 range 0-19 	<ul style="list-style-type: none"> avg. 17 avg. 20 avg. 40 avg. 17 avg. 6
<ul style="list-style-type: none"> • pH-CaCl₂ range 4-8 		avg. 5.6
<ul style="list-style-type: none"> • % Base Saturation, based on the ratio of: <ul style="list-style-type: none"> • Total Exchangeable Bases per 100 g clay • Cation Exchange Capacity per 100 g clay 	<ul style="list-style-type: none"> range 54-100 range 0.4-24.1 range 0.4-27.4 	<ul style="list-style-type: none"> avg. 94 avg. 5.98 avg. 6.28
<ul style="list-style-type: none"> • Electrical Conductivity (mS/m) 	range 1.9-290	avg. 42

Testing the correlation of the soil analysis data with yield data suggested a significant relation between crop yield and 'medium sand' fraction and soil-pH.

$$\text{Yield (kg/ha)} = 1267 - 27.43 \cdot (\text{medium sand-\%}^*) + 25.65 \cdot (\text{soil-pH}^{**})$$

(n = 167; Adj.R-Sq = 5.3%; ** = sign.at 1%; * = sign.at 10%)

All other soil analytical data were not correlated with the yield data. This was to be expected because:

- Standard soil data have serious limitations for use in land suitability assessments because of unsuited concepts, definitions, collection and analysis procedures (Driessen, 1995). Distortions that arise from laboratory pre-treatment methods (drying, crushing, and sieving) and unsuitable analytical procedure may change the chemical characteristics of the soil rendering the data unusable.
- Soil stoniness and gravel content data are often not (properly) determined. However, gravel content is an important determinant not only of the *effective* rootable soil volume but also for proper assessment of the capacity of the soil to store and convey water.
- Soil-pH (and element content) measurements in laboratories are normally performed on soil material that was first dried, milled, sieved and stored away. At the time of the measurement, it is again hydrated with distilled water or a mild electrolyte solution, usually at a 1:1 to 1:10 soil-to-water ratio. Such laboratory data are not representative of the soil-pH of the undisturbed field soil.

5.4 Multiple Regression

Based on the results of descriptive statistics (**Table 5**), a list of independent variables was selected for consideration in an approximate production function obtained through step-wise multiple regression. The resulting function is presented in **Table 6**. The low “Adjusted R-Square” of 51.7% may in part be caused by site-specific variability that remained unaccounted for, e.g. the observed pattern of localized rainfall.

The stepwise multiple regression analysis suggests the following notable changes in the deductions from descriptive statistics:

- The altitude at which plots were located became a significant explanatory variable.
- Different responses between Compound-D and Ammonium Nitrate (including their timing) could no longer be detected at significant levels.
- The fact that winter ploughing and planting method did not appear in the final regression equation was caused by a strong correlation between winter ploughing and planting method with chemical fertilizer application rates (**Figure 41** and **Figure 42**).

Table 5. Summary of results obtained through descriptive statistics

Yield (kg/ha) is: <i>(each explanatory variables is tested individually)</i>		
+ 1479	if	early ploughing done
+ 642	if	later ploughing done
+ 55.7	x	kg/ha seed used
- 647	if	planting by hoe
+ 1112	if	planting by harrow or planting machine
+ 580	x	planting date (day of year)
- 0.922	x	planting date ²
+ 6.88	x	kg/ha Compound-'D' at planting
+ 4.08	x	kg/ha Compound-'D' after planting
+ 9.0	x	kg/ha Ammonium Nitrate
+ 0.140	x	kg/ha FYM
+ 836	if	animal traction is used for the 1 st weeding
- 46.73	x	% yield loss by termites
- 37.78	x	% yield loss by weeds
- 28.04	x	% yield loss by drought
+ 1.15	x	altitude (masl; n.sign.)
+ 400	if	contour ridges were present (n.sign.)
- 74.68	x	% cover by shrubs and forbs
+ 13.51	x	% bare soil cover
+ 1243	if	the soil fertility is considered 'good'
- 27.43	x	fraction of medium sand in the topsoil (%)
+ 25.65	x	soil pH-CaCl ₂

Table 6. Established overall production function (N=160; Adj.R-Sq=51.7%)

Yield (kg/ha) = - 67631	P (2 Tail)
+ 41.804 x kg/ha seed used	0.000
- 849.722 if planting by hoe	0.006
+ 424.195 x planting date (day of year)	0.071
- 0.674 x planting date ²	0.061
+ 3.733 x kg/ha applied Compound-D and AN	0.000
+ 0.181 x kg/ha FYM	0.004
+ 754.622 if animal traction is used for the 1 st weeding	0.007
- 28.597 x % yield loss by termites	0.006
- 36.867 x % yield loss by weeds	0.001
- 32.321 x % yield loss by drought	0.004
+ 2.225 x altitude (masl)	0.026
- 44.385 x % cover by shrubs and forbs	0.055
+ 703.828 x if the soil fertility is considered 'good'	0.063
- 26.282 x fraction of medium sand in the topsoil (%)	0.018
+ 167.350 x soil pH-CaCl ₂	0.090

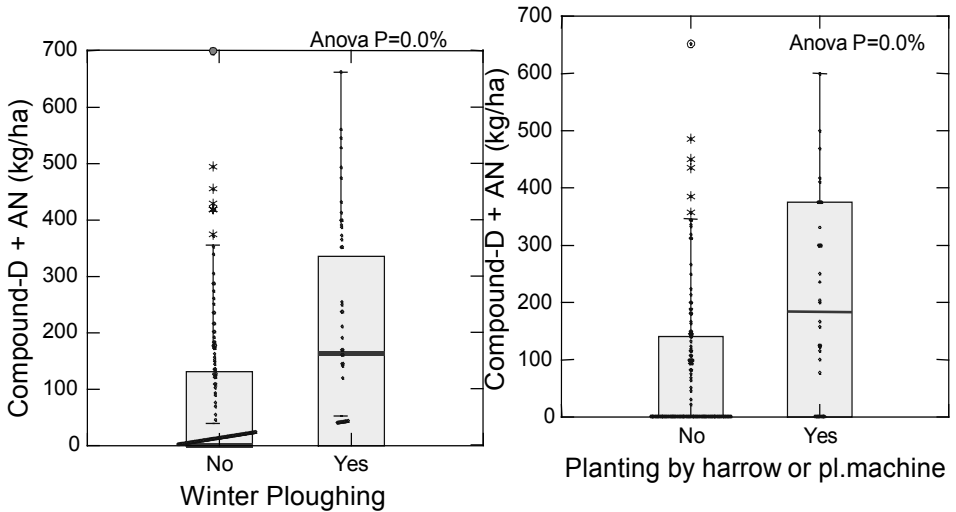


Figure 41. Relation between winter ploughing and chemical fertilizer application rates.

Figure 42. Relation between planting method and chemical fertilizer application rates.

5.5 Yield Gap by Yield Constraint

Using the production function and parameter statistics, 'mean' and 'best' values were derived for each explanatory parameter (Bie, 2000), and the quantified impact by yield constraint as well as its contribution to the overall yield gap were estimated (**Table 7, Figure 43**). Estimates of the respective contributions are based on comparisons of the average yield level with the best yield value reported from the 167 surveyed sites.

The multiple regression analysis showed that limiting land unit specifications, notably soil pH-CaCl₂, medium sand soil texture, soil fertility (as perceived by the farmer) and altitude were accountable for 35% of the yield gap. The remaining 65% of the yield gap were attributed to management factors. Management factors that contributed more than 5% each to the yield gap included application of compound-D and AN, FYM and amount of seed used. Condition of the maize field after harvest, planting (method and timing), weeding method, and yield loss (by weeds, termites and drought) each contributed less than 5% to the yield gap. The estimated total yield gap in Piriwiri and Mupfure Communal lands was considerable: 5705 kg ha⁻¹.

Table 7. Impact by yield constraint and its estimated contribution to the overall yield gap

Based on 160 sets of plot data

Yield (kg/ha) =	Parameter Statistics				Mean+2SD	Best value?	x Coefficient		Yield Gap	
	Min	Max	Mean	St.Dev.			Mean	Best		
-67631 constant			1			1	-67631	-67631		
41.804 x kg/ha seed used	6	52	25.006	10.045	45	45	1045	1885	840	15%
-849.722 if planting by hoe	0	1	0.125	0.35		0	-106	0	106	2%
424.195 x planting date (day of year)	290	365	325	15.342		315	66666	66744	78	1%
-0.674 x planting date ²			105922			99026				
3.733 x kg/ha Compound-D and AN	0	652	109.66	147.365	404	404	409	1510	1100	20%
0.181 x kg/ha FYM	0	8065	808.12	1691.742	4192	4192	146	759	612	11%
754.622 if animals used for weeding	0	1	0.812	0.392		1	613	755	142	3%
-28.597 x % loss by termites	0	40	6.75	9.011		0	-193	0	193	3%
-36.867 x % loss by weeds	0	40	7.562	9.745		0	-279	0	279	5%
-32.321 x % loss by drought	0	40	6.781	9.271		0	-219	0	219	4%
2.225 x altitude (m.a.s.l)	668	1210	882.99	103.124	1089	1089	1965	2424	459	8%
-44.385 x % shrubs and forbs	0	29	2.969	4.435		0	-132	0	132	2%
703.828 x if the soil is 'good'	0	1	0.075	0.264		1	53	704	651	12%
-26.282 x medium sand (%)	1	42	16.906	9.773		1	-444	-26	418	8%
167.35 x soil pH-CaCl2	4	8	5.606	1.025	7.656	7.66	938	1281	343	6%
Calculated:							2831	8403	5573	
Actual mean:							2628			
Actual best:								8333		
Actual gap:									5705	

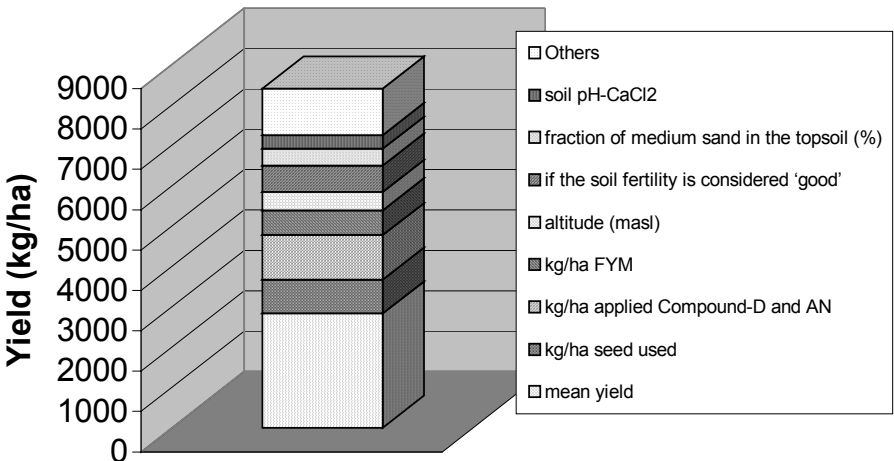


Figure 43. Contributions of major constraints to the yield gap.

Part D. Modelling Farmers' Reality

Part D: Modelling Farmers' Reality

Part D

Part A: New Approaches to Analytical Crop Growth Modelling

1. Analytical Pathway
2. Combining RS with Crop Growth Modelling

Part B: Assessing what is possible

3. Food Security Early Warning in Zimbabwe
4. Improving Reference Production Modelling

Part C: Farmers' Reality

5. The Yield Gap in Actual Land Use Systems

Part D: Modelling Farmers' Reality

6. Modelling Actual Production

Part E: Conclusions

7. Conclusions

Part D: Modelling Farmers' Reality

6. RS Canopy Temperature in Modelling Actual Production (PSn) *QuZhou, North China Plain*

- ◆ Crop canopy temperature retrieval
- ◆ Validating the temperature difference phenomenon
- ◆ Updating the temperature difference variable in the PSn Model
- ◆ Estimating day-equivalent canopy temperatures
- ◆ Model results and validation

6. Case Study 3: Using Remotely Sensed Canopy Temperatures in Modelling Actual Crop Production in Quzhou County, North China Plain

6.1 Crop Canopy Temperature Retrieval

Remote sensing has become an established tool in the assessment of crop growth. Hand-held equipment and infrared thermometers and the thermal infrared scanners aboard aircraft or satellites provide measurements of emitted radiation from which canopy temperatures can be derived. In this case study, crop canopy temperatures derived from the NOAA-AVHRR data are used to estimate the sufficiency of water uptake by the crop using the temperature difference between canopy and surrounding air as discussed in chapter 2.

$$cf(water) = \left[\frac{INTER - \left(\frac{\Delta T * VHEATCAP}{AERODR} \right)}{LATHEAT * TRO * CFLEAF * TC} \right] \quad (\text{Eq.23})$$

The retrieval of canopy temperatures from satellite data is based on the Stephan-Boltzman black body emission equation:

$$R = \sigma \varepsilon_0 T^4 \quad (\text{Eq.47})$$

Where:

- R is radiation emitted by the surface ($W m^{-2}$)
- $\sigma = 5.67 \times 10^{-8} W m^{-2} K^{-4}$ (the Stephan-Boltzman constant for instantaneous derivations; $0.0049 J m^{-2} d^{-1} K^4$ for daily derivations)
- ε_0 is emissivity of the surface
- T is surface temperature $[K]$

The emissivity term in the equation is a measure of the efficiency with which the surface emits energy. A perfect emitter, the black body, has an emissivity of 1. The black body is a theoretical concept whose behaviour does not exist in nature. The emissivity of most natural bodies lies between 0.91 and 0.98 in the thermal wave region 8-14 μm (Qin and Karnieli, 1999).

Accurate retrieval of surface temperature is complicated if measurements are made by sensors aboard satellite platforms far from the ground. Atmospheric attenuation processes including absorption, upward atmospheric radiance and bi-directional reflection of downward atmospheric radiance affect transmission of the emitted radiation. Absorption of water vapour is considered to be the most important factor influencing radiance transfer in the thermal spectral range (Bastiaanssen, 1995; Qin and Karnieli, 1999).

Direct methods used to correct radiometric surface temperature for atmospheric interference include the use of radiation transfer models that apply radio soundings, satellite vertical sounders and climatological data (Parodi, 2000, Bastiaanssen, 1995). Indirect methods apply the split-window technique or use in-situ temperature measurements for calibration. The split-window technique approximates differential water vapour absorption in the 10 to 13 μm range, assuming that surface emissivity is constant over this spectral region. The technique eliminates effects of atmospheric water vapour absorption and emission. The concept exploits the different absorption characteristics of the atmosphere within two different but close wavelengths. The algorithms consider a linear combination of thermal channels and estimate a surface temperature corrected for atmospheric effects. The split-window technique is most commonly applied to the NOAA Advanced Very High Resolution Radiometer (AVHRR) satellite channels 4 and 5 as a way to estimate surface temperature from multi-thermal band sensors.

Detailed reviews of split-window algorithms are provided by Caselles et al (1997), Qin and Karnieli (1999) and by Parodi (2000). The general split-window algorithm takes the following form:

$$T_0 = c_{42} * (\text{Ch}_4\text{BT})^2 + c_4 * \text{Ch}_4\text{BT} + c_{45} * \text{Ch}_4\text{BT} * \text{Ch}_5\text{BT} + c_{52} * (\text{Ch}_5\text{BT})^2 + \text{Offset} \quad (\text{Eq.48})$$

Where:

T_0 is surface temperature [K]

Ch_4BT and Ch_5BT are brightness temperature maps for the AVHRR channels 4 and 5, [K]

c_i are regression coefficients that correct for atmospheric water vapour.

The term "Offset" is the regression offset that corrects for surface emissivity in the AVHRR channels 4 and 5 and for the attenuation by gases and aerosols.

The split-window algorithm developed by Coll and Caselles (1997; in Parodi, 2000) was used to estimate maize crop canopy temperatures in Quzhou County in the North China Plain for the crop season of 1999. **Appendix B** presents a step-by-step description of the canopy temperature mapping procedure.

It was not possible to obtain cloud-free NOAA-AVHRR imagery for the Zimbabwe communal lands study site. Typically, rainfall in Southern Africa is dominated by convective (thunderstorm) activity. Thunderstorms develop in the early afternoon creating cloudy conditions by the time of the afternoon NOAA satellite overpass. However, 23 images for 1999 of reasonably cloud-free AVHRR data for the North China Plain area were obtained under the auspices of the SULAMA¹ project.

¹ Towards Sustainable land Management (SULAMA) is a cooperative research and training project of Wageningen University, ITC and China Agricultural University (CAU, Beijing) in the North China Plain, Peoples Republic of China.

SULAMA is a collaborative research effort between Wageningen University and China Agricultural University, Beijing, People's Republic of China. The latter have an experimental set-up in the North China Plain where researchers conduct field trials, inter alia on maize production potentials. The Chinese colleagues kindly provided experimental production and yield data and correlated weather data recorded from an automatic recording station within the experimental site. In addition, planted areas and yields of surrounding administrative counties were provided for validation and calibration of the PS-n simulations.

Figure 44 shows time-series of AVHRR-derived instantaneous canopy temperatures and ambient air temperatures (top) and the "Normalized Difference Vegetation Index" (NDVI, bottom). The instantaneous temperature values were derived for a pixel containing the Quzhou Research Station, equipped with automatic weather measuring instruments including those for measuring maximum and minimum air temperatures. Ambient air temperatures were recorded in a 2 metre high screen at 14h00 local time. Cloud-free pixels containing the Quzhou experimental fields could be retrieved for 23 dates during the crop season from Julian day numbers 158 (7th June 1999) to 267 (24th September 1999).

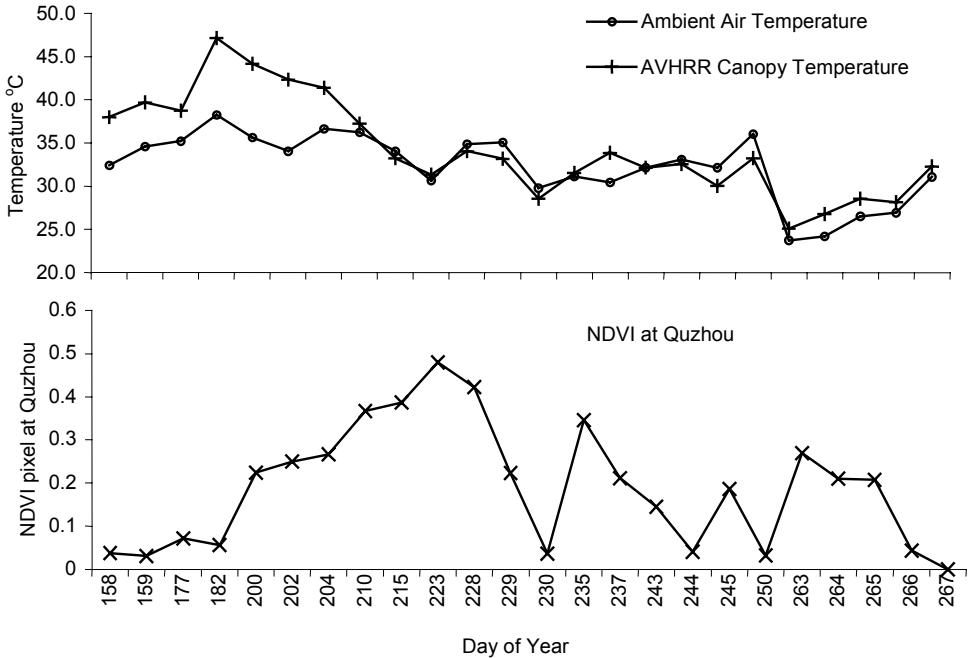


Figure 44. Time-series of AVHRR-derived canopy temperature and ambient air temperature measured at a location inside the AVHRR pixel (top) and the Normalized Difference Vegetation Index (NDVI) for the same pixel (bottom).

The time-series shows differences between the instantaneous afternoon (13h00-15h00 NOAA 14 overpass) crop canopy temperature and ambient air temperature of up to 8.6°C. This is attributed to the fact that vegetative cover is still sparse in the first 30 days after germination of the maize crop. Consequently, there is more exposed soil and the measured surface temperature would be higher than the ambient air temperature at 2 metres height. This explanation seems to be confirmed by the pattern of the Normalized Difference Vegetation Index (NDVI) time-series for the same pixel as presented in the bottom part of **Figure 44**. Surface temperatures remain higher than ambient air temperatures until the NDVI reaches a maximum value coinciding with a fully closed canopy. Thereafter, fluctuations are (almost) entirely attributed to transpiration.

6.2 Validating the Temperature-Difference Phenomenon

In-situ canopy temperatures measured to validate corresponding AVHRR derived temperatures were not available. Indirect validation could be achieved by proving that observed differences between ambient air temperatures and AVHRR derived canopy temperatures would have been due to the cooling of the crop canopy brought about by transpiration. Rejecting the null hypothesis $H_0: F = G$ at a conventional significance level of 0.05 would show proof of a significant difference between the two temperature sources. The alternative hypothesis $H_A: F \neq G$ stating a significant difference between ambient air temperature and the AVHRR-derived temperature would be adopted. The statistic tested was the difference of means $t(\mathbf{x}) = \bar{z} - \bar{y}$ between AVHRR derived canopy temperature denoted independent sample z and ambient air temperature denoted independent sample y of sizes m and n from possibly different distributions F and G respectively. The difference between the two means was 2.19°C.

Bootstrap re-sampling was applied since both sample sizes were small ($m = n = 23$) and could not satisfy the assumptions for conventional hypothesis testing. In section 4.7.2 an explanation is provided of bootstrap replication to create a proxy universe by randomly drawing B samples of size $(m + n)$ from a pooled dataset of z and y .

The NOAA-AVHRR satellite's orbits drift over time, which causes as systematic change of illumination conditions and local time of observation. Therefore, whilst air temperature measurements are recorded daily at 14h00, the satellite overpass time will vary anywhere between 13h00 and 15h00. Large and rapid day-to-day ambient air temperature variations may occur mainly due to variations in solar radiation. The bootstrap replication procedure was therefore applied on temperature data pairs of the same date (re-sampling with-rows) in order that important temporal effects may not be obscured. **Table 8** shows a "snapshot" of the AVHRR-derived temperatures and the ambient air temperatures by date in the left part and in the right part, the same dataset re-sampled with-row (across column) to create 10000 replicates while maintaining the temporal variability (across rows).

The bootstrap percentile method described in section 4.8 was applied to determine the 95% confidence interval of the mean temperature differences. **Figure 45** shows the distribution of bootstrap re-sampled differences between the means of the observed ambient air temperatures (14h00 recording) as recorded by the automatic weather station and corresponding instantaneous AVHRR-derived canopy temperatures. The solid vertical lines flanking both sides of the distribution indicate the 2.5th and 97.5th percentiles representing the 95% confidence interval. The dotted vertical line shows that the observed mean temperature difference of 2.19°C lies in remaining significant 5% of the distribution.

Table 8. The left part shows AVHRR-derived canopy temperatures and observed air temperatures measured at 2m above ground within the approximate 1 km² pixel according to the date. The right part shows values obtained with bootstrap re-sampling within-rows retaining the temporal variability of temperatures across the season

Date	Day of Year	Temperature (°C)		Temperature (°C)	
		AVHRR	Air at 2m	Within-row Bootstrap re-samples	
				AVHRR	Air at 2m
7/6/99	158	39.66	34.56	39.66	34.56
8/6/99	159	37.96	32.39	32.39	37.96
1/9/99	244	31.00	33.11	31.00	33.11
.
.
.
9/23/99	266	29.00	26.91	29.00	26.91
24/9/99	267	32.10	31.05	31.05	32.10
	Mean	33.94	36.60	Mean:	32.62
	Difference		2.19	Difference (repeat & score: B=10000)	-0.31

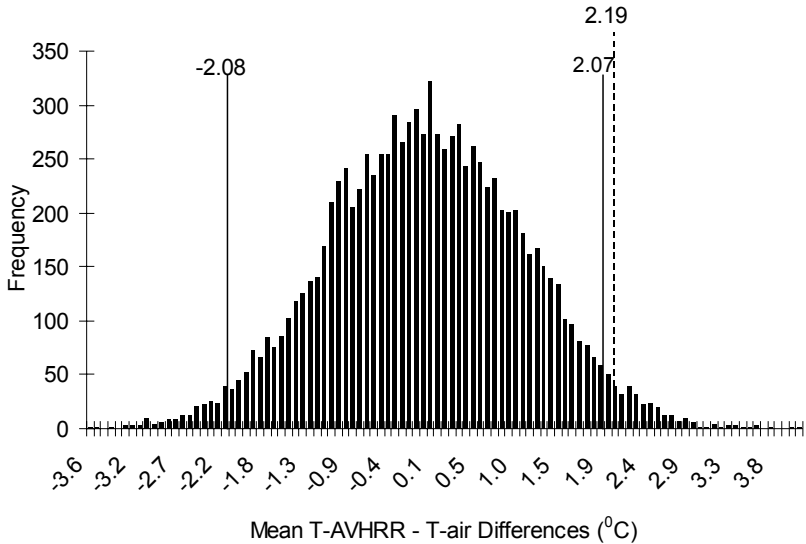


Figure 45. Bootstrap distribution of differences between the means of the AVHRR-derived canopy temperature and ambient air temperature. The flanking vertical solid lines show the temperature differences of the means at 2.5th and 97.5th percentiles. The dotted line shows that the observed mean temperature difference of 2.19^oC lies in the significant 5% of the distribution.

Out of 10000 bootstrap samples drawn ($B=10000$) only 194 were equal to or greater than the observed mean difference of 2.19^oC. Thus, the Attained Significance Level - ASL (Efron and Tibshirani, 1993) was 0.02. The null hypothesis $H_0: F = G$ was rejected at 0.05 significance level suggesting that the differences in ambient air and AVHRR-derived canopy temperatures were significant and caused by crop transpiration. In the next section it is demonstrated that the temperature difference data can be used in a crop model to predict actual production at farmers' level with reasonable accuracy by applying the water sufficiency coefficient $cf(\text{water})$ as defined by Equation 23.

6.3 Updating the Temperature Difference Variable in the PS-n Model

6.3.1 Parallel processes feeding data into the PS-n model

Figure 46 below presents a relational diagram of the methodology for deriving canopy temperatures from AVHRR imagery and integrating them in the PS-n model. The flow diagram shows two parallel processes that feed data into the PS-n model. The right side of the flow diagram describes the canopy temperature retrieval process from AVHRR imagery using the split-window technique as documented in Appendix B. The left side of **Figure 46** describes input constants and initial conditions as well as the meteorological data required by PS-n model program outlined in Appendix A.

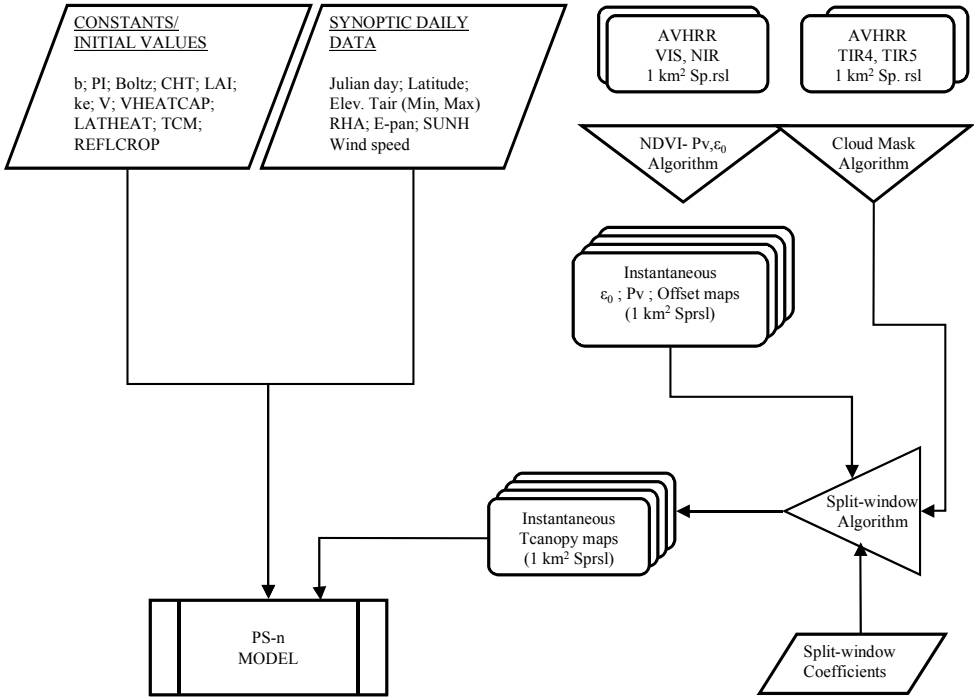


Figure 46. Relational diagram of the integration of AVHRR-derived crop canopy temperatures in the PS-n model for updating the temperature difference forcing variable.

6.3.2 Estimating day-equivalent canopy temperatures

As only 23 cloud-free AVHRR images were obtained for the 1999 crop-season, it was necessary to fill in the days when canopy temperature data were unavailable. A linear interpolation procedure was applied to obtain proxies for missing values. After this, adjustments were made to estimate daily values from instantaneous values using a correction term as explained in Part A of this thesis (Equations 18 and 19).

6.4 Model Results and Validation

In the summer growing season the main crop in Quzhou and surrounding counties is maize. The North China Plain consists of flat terrain at 40 m.a.s.l with uniform, re-washed loess (loam) soils. It was therefore assumed that ambient temperatures measured at the automatic weather station would not deviate very much from the same in neighbouring pixels within the County and could be used in temperature difference calculations for representative pixels. Nine representative pixels around

and including Quzhou Research Station were retrieved from AVHRR-derived surface temperature maps. As the AVHRR images obtained for the 23 dates were not entirely free of cloud on all dates, nine cloud-free pixels were selected for further analysis.

Figure 47 shows the time-series of temperature differences between ambient temperatures as recorded at the automatic weather station and corresponding AVHRR-derived canopy temperatures for the nine selected cloud-free pixels. A common trend is evident with higher temperature differences (-10 to +10) at the beginning of the crop season when there is little leaf mass, stabilizing (-3 to +5) once a full canopy has been established.

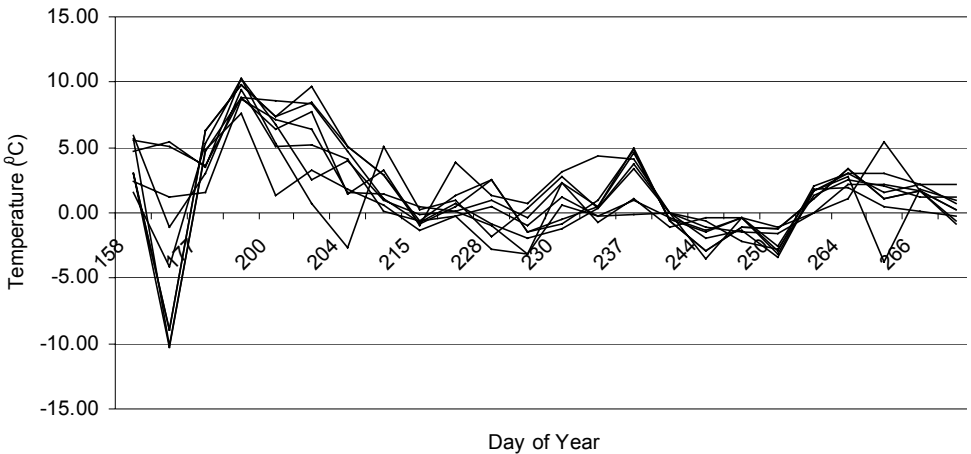


Figure 47. Time-series of differences between ambient air temperatures measured at the Quzhou Automatic Weather Station and instantaneous crop canopy temperatures derived from the NOAA-AVHRR afternoon-pass of image data for selected neighbouring pixels.

The PS-n model was run using canopy temperature data to update the 'TEMPDIFF' (temperature difference) forcing variable for each of the nine pixels including the pixel containing the Quzhou site. **Figure 48** shows the nine output curves of simulated (PS-n) storage organ development and one observed (measured) experimental storage organ development curve for a rain-fed maize trial plot (dashed curve). All simulated curves show good similarity and closeness with the curve for the storage organ development observed at the experimental plot.

Table 9 shows the total Storage Organ Mass (SOM) values in kg ha^{-1} simulated with the PS-n model using canopy temperature data from the selected nine pixels in Quzhou County. The SOM output value for the pixel containing the Quzhou Research Station was 8066 kg ha^{-1} . A mean SOM value of 8151 kg ha^{-1} was

calculated for the nine PS-n simulations. The observed SOM value from the water-limited (no irrigation, sufficient nutrients and no other yield constraints) experimental maize field was 8453 kg ha^{-1} . The difference between the observed and modelled storage organ yield mean was a minor 302 kg ha^{-1} (4%).

Table 9. Comparison of SOM (kg ha^{-1}) simulated by the PS-n model using the AVHRR-derived temperatures from nine representative pixels with SOM values observed at Quzhou experimental fields. The mean simulated SOM value was within 302 kg/ha or 4% of the observed value

Simulated Maize SOM (kg ha^{-1}) compared with observed values from Quzhou County, 1999	
AVHRR Pixel Coordinate	PS-n Simulations: SOM (kg ha^{-1})
36°52' N; 115°00' E (Quzhou Auto-weather station)	8066
36°38' N; 115°05' E	8023
36°42' N; 114°53' E	8790
36°47' N; 115°02' E	7862
36°49' N; 114°58' E	7907
36°50' N; 114°58' E	7948
36°43' N; 114°52' E	8344
36°44' N; 114°58' E	8357
36°46' N; 114°57' E	8059
PS-n Mean SOM (kg ha^{-1})	8151
Observed SOM (kg ha^{-1})	8453
Difference (kg ha^{-1})	302

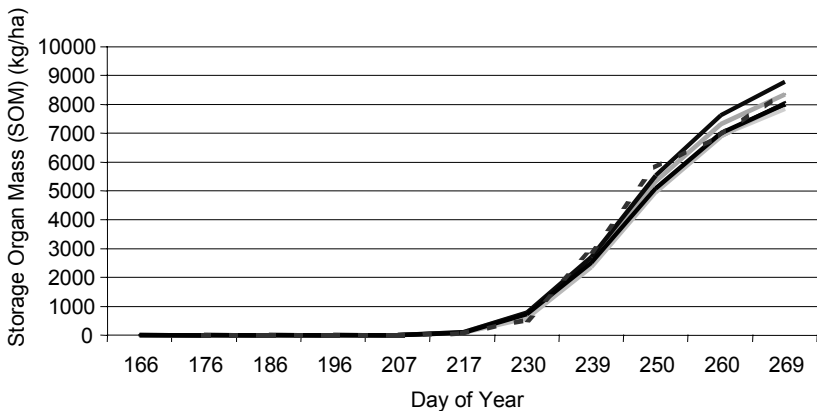


Figure 48. Storage organ growth curves simulated with the PS-n model on the basis of the canopy-ambient air temperature difference.

6.5 Discussion

Although in-situ canopy temperatures were not available to determine the accuracy level of AVHRR-derived canopy temperatures, it was possible to reject the null hypothesis equating ambient air temperature with AVHRR-derived canopy temperatures using the re-sampling tool.

Further confirmation is obtained from the PS-n model output of storage organ mass that is close to the observed and from the quantitative similarity of the simulated curves with the observed curve. The next step in establishing actual yield would involve aggregation techniques over a defined area of interest. One commonly used method for aggregating crop production data involves averaging of simulation results across spatial grid cells in a GIS environment (Thornton et al, 1997; Venus, 1999). Alternatively, one might apply Monte Carlo integration to aggregate simulation results selected by stochastic sampling (Hansen and Jones, 2000) similar to the re-sampling techniques as used in this study to generate a proxy universe from a small sample. Both approaches require reliable data/estimates of cropped areas for the relevant season. This is a major difficulty in the communal lands of Zimbabwe as already explained.

Part E. Conclusions

Part E: Conclusions

Part E

Part A: New Approaches to Analytical Crop Growth Modelling

1. Analytical Pathway
2. Combining RS with Crop Growth Modelling

Part B: Assessing what is possible

3. Food Security Early Warning in Zimbabwe
4. Improving Reference Production Modelling

Part C: Farmers' Reality

5. The Yield Gap in Actual Land Use Systems

Part D: Modelling Farmers' Reality

6. Modelling Actual Production

Part E: Conclusions

7. Conclusions

Part E: Conclusions

- ◆ Conclusions

7. Conclusions

Combining dynamic crop growth modelling with remote sensing allows to make regionalized estimates of reference as well as actual production and yield levels that are based on universally valid relations, reproducible, transportable and acceptably accurate.

Comparing reference production with actual production dynamically reveals the compounded effect of all yield constraints on a Land Use System as it develops over a crop season. Monitoring the development of the yield gap is a key factor in effective early warning.

Understanding the environmental conditions and farmers' socio-economic circumstances that constitute yield constraints is necessary in order to institute developmental interventions in crop production. Statistical analysis of geo-referenced observations of biophysical land/field infrastructures and field operations can be obtained from farmer interviews. Farmer interviews are especially valuable in revealing perceptions of the relative impacts of individual constraints.

The difference between remotely sensed crop canopy temperature and the corresponding ambient temperature at the time of the satellite overpass can be linked to the daily actual rate of transpiration. This relation allows adjustment of the actual rate of assimilation and thence of actual crop growth. Although promising results were obtained from estimations over the fairly homogeneous maize-based Land Use Systems (terrain, soils, Land Use) in the North China Plain, the transportability of the method has yet to be tested for areas of heterogeneous Land Use Systems such as those found in the communal lands of Zimbabwe.

A number of difficulties speak against the application of the Actual Production Situation (PS-n) model in Zimbabwe:

- Regional canopy temperature data can be affordably obtained only by indirectly involving complex algorithms and multi-spectral visible and thermal infrared data obtained from satellite sensors. Thus the data need high spectral and high radiometric properties.
- Canopy temperature data for the PS-n model are required at (minimum) daily time interval, thereby requiring a matching temporal resolution of the satellite overpass.
- The Advanced Very High Resolution Radiometer (AVHRR) aboard the NOAA polar-orbiting satellite series, as the name suggests, senses data at a very high radiometric resolution (1023 levels of contrast) in 5 spectral bands. The satellite has a temporal resolution of at least one day. This sensor therefore meets the first two requirements of radiometric, spectral and temporal resolutions for canopy temperature retrieval.

- However, an interesting pattern emerged while surveying NOAA-AVHRR data over Zimbabwe for the 1996-1999 growing seasons as part of an attempt to retrieve daytime canopy temperatures: almost all daytime pass images in the crop season were overcast. This suggests that the mid-afternoon satellite orbit over Zimbabwe would correspond with the pick of thunderstorm activity typical of the climatic characteristics of the region. Thus, although the NOAA-AVHRR sensor provides data of a temporal resolution that meets the PS-n time-step requirement, a higher temporal resolution sensor would have been preferable to capture a cloud-free window.
- In the communal lands of Zimbabwe, maize-based Land Use Systems are heterogeneous in terms of physical and management characteristics. Maize fields are generally small, often less than half a hectare and lie on hilly and undulating terrain with a variety of soils. The maize crop is often intercropped with smaller proportions of sunflower, sorghum or other crops. Even though maize is the dominant crop in the rainy season, high spatial resolution data would be required for crop canopy temperature retrieval. The NOAA-AVHRR sensor has a spatial resolution of 1km x 1 km at nadir.
- Technology has advanced in hyperspectral data provision from geo-stationary meteorological satellites at quarter-hourly temporal resolutions. The European Meteosat Second Generation satellite has been designed to capture data with these properties at a spatial resolution similar to that of the NOAA-AVHRR. Possibilities of pixel un-mixing using the discriminatory properties of hyperspectral data should be investigated to counter limitations posed by low spatial resolution.
- The National Early Warning Units (NEWU) can benefit by testing with the PS-n model with the Meteosat Second Generation data.

8. References

- An, N. T., 2000. Assessing spatial constraints leading to maize yield gaps. M.Sc.-thesis, ITC, Enschede, The Netherlands.
- Anderson, P. J., 1993. Physical Resource Inventory of the Communal Lands of Zimbabwe. Bulletin 60., Natural Resources Institute, Chatham, UK.
- Barros, J. M., 1997. Quantitative Analysis of Selected Land-Use Systems. Ph.D.-thesis, WAU, Wageningen, The Netherlands. 169 pp.
- Bastiaanssen, W. G. M., 1995. Regionalization of surface flux densities and moisture indicators in composite terrain. Integrated Land, Soil and Water Research. Ph.D. - thesis. WAU, Wageningen, The Netherlands. 273 pp.
- Bastiaanssen, W. G. M., 1998. "A remote sensing surface energy balance algorithm for land (SEBAL). 1. Formulation." *Journal of Hydrology*: 212-214.
- Bennett, J. G., 1985. A Field Guide to Soil and Site Description in Zimbabwe. Technical Handbook No.6. Department of Research and Specialist Services, Harare, Zimbabwe,.
- Bie, C. A. J. M. de, 2000. Comparative Performance Analysis of Agro-ecosystems. Ph.D-thesis, ITC, Agriculture Conservation and Environment Division, Enschede and Wageningen University, The Netherlands. 232 pp.
- Blank, S., C. Seiter and P. Bruce, 1999. Re-sampling Stats in Excel Users Guide. Arlington, Resampling Stats, Inc.
- Bogert, P., P. Mahau and F. Becker, 1995. The spatial interpolation of agro-climatic data. Agrometeorology Working Series Paper no. 12. Rome, FAO.
- Bonifacio, R., G. Dugdale and J.R. Milford, 1993. Sahelian rangeland production in relation to rainfall estimates from METEOSAT. *International Journal of Remote Sensing* 14: 2695-2711.
- Brink, C., 1996. The estimation of the area under maize using Area Frame Sampling and Remote Sensing. Conference proceedings on the Applications of Remote Sensing and Geographic Information Systems in Resource Assessment in Africa (Harare, March 1996). 242-244. Harare.
- Burt, J. E., and G.M. Barber, 1996. Elementary Statistics for Geographers. Second Edition. Guilford Press, New York. p. 573-598
- Caselles, V., C. Coll and E. Valor, 1997. Land surface emissivity and temperature determination in the whole HAPEX-Sahel area from AVHRR data. *International Journal of Remote Sensing*, Vol. 18, No. 5:1009-1027.
- Coll, C. and V Caselles, 1997. A split window algorithm for land surface temperature from advanced very high-resolution radiometer data: validation and algorithm comparison. *J. Geophys. Res.*, 102(D14), 16697-16713.
- Curran, P. J., 1988. The Semivariogram in Remote Sensing. *Remote Sensing of Environment* 24: 493-507.
- Doorenbos, J. et al, 1979. Yield Response to Water. FAO Irrigation and Drainage Paper 33. Rome. 193 pp.

- Driessen, P. M., 1995. Lecture Notes on the Adequacy of Soil Data. ITC, Enschede, The Netherlands. 66 pp.
- Driessen, P. M. and N.T. Konijn, 1992. Land Use Systems Analysis. WAU, Dept of Soil Science and Geology, Wageningen, The Netherlands. 230 pp.
- Eastman, J. R., 1996. The Spatial Manifestation of ENSO Warm Phase Events in Southern Africa, Conference proceedings on the Applications of Remote Sensing and Geographic Information Systems in Resource Assessment in Africa (Harare, March 1996). Harare.
- Efron, B. and R. Tibshirani, 1993. An Introduction to the Bootstrap, Chapman and Hall. New York, NY 10001-2299. 436 pp.
- Flitcroft, I. D., J.R. Milford and G. Dugdale, 1989. "Relating point to area average rainfall in semiarid West Africa and the implications for rainfall estimates derived from satellite data." *Journal of Applied Meteorology* 28: 252-266.
- Goss, M., 2001. Soil aeration and plant growth. University of Guelph, Ontario, Canada.
- Grimes, D. I. F., 1993. Use of rainfall estimates in hydrological modelling. First International Conference of African Meteorological Society, Nairobi, Kenya.
- Grimes, D. I. F., R. Bonifacio and H.R.L. Loftie, 1998. Rainfall Estimation Workbook. Natural Resources Institute. Chatham, UK.
- Groen, M. M. de, 2001. Modelling interception and transpiration at monthly time steps. Introducing daily variability through Markov chains. Delft, IHE Delft, The Netherlands.
- Hansen, J. W. and J.W. Jones, 2000. Scaling-up crop models for climate variability applications. *Agricultural Systems* 65: 43-72.
- Hunchu, P. and P.N. Sithole, 1994. Rates of Adoption of New Technology and Climatic Risk in the Communal Areas of Zimbabwe, ACIAR/SACCAR workshop, Harare.
- Hutchinson, M. F. and J.D. Corbett, 1993. Spatial Interpolation of Climate Data using Thin Plate Smoothing Splines. FAO Agrometeorological Series Working Paper 13. Rome.
- Hutchinson, M. F., 2000. ANUSPLIN Users Guide. Canberra, The Australian National University.
- Iqbal, M. (Ed.), 1983. An introduction to Solar Radiation. Academic Press, Toronto Canada.
- Jackson, R. D., 1982. Canopy temperature and crop water stress. *Advances in Irrigation* 1: 43-85.
- Jackson, R. D., W.P. Kustas and B.J. Choudhury, 1988. A re-examination of the crop water stress index. *Irrigation Science* 9: 309-317.
- Jones, P. G. and P.K. Thornton, 1997. Spatial and temporal variability of rainfall related to a third-order Markov model. *Agricultural and Forest Meteorology* 86: 127-138.
- Jones, P. G. and P.K. Thornton, 1999. Fitting a third-order Markov rainfall model to interpolated climate surface. *Agricultural and Forest Meteorology* 97: 213-231.
- Jones, P. G. and P.K. Thornton, 2000. MARKSIM: Software to generate daily weather data for Latin America and Africa. *Agronomy Journal* 92: 445-453.
- Journel, A. G. and C.J. Huijbregts, 1978. Mining Geostatistics. Academic Press, New York.

- Kalluri, S. N. V. and J. R. G. Townshed, 1998. A Simple Single-layer Model to Estimate Transpiration from Vegetation using Multi-spectral and Meteorological Data. *International Journal of Remote Sensing* 19: 1037-1053.
- Lebel, T., J.D. Taupin, and N. D'Amato, 1997. Rainfall monitoring during the HAPEX-Sahel. 1. General rainfall conditions and climatology. *Journal of Hydrology* 188-189: 74-96.
- Lebel, T. and L. le Barbe, 1997. Rainfall monitoring during the HAPEX-Sahel. 2. Point and areal estimation at the event and seasonal scales. *Journal of Hydrology* 188-189: 97-122.
- Marschner, H., 1996. Mineral nutrition of higher plants. Second Edition. Academic Press, New York.
- Milford, J. R., V.D. McDougall and G. Dugdale, 1994. Rainfall estimation from cold cloud duration. Proceedings of Niamey Workshop, December 1994, ORSTOM, Niamey.
- Moulin, S., A. Bondeau and R. Delecolle, 1998. Combining Agricultural Crop Models and Satellite Observations from Field to Regional Scale. *International Journal of Remote Sensing* 19: 1021-1036.
- NSW Agriculture, 1998. Nutrient disorders of greenhouse Lebanese cucumbers. www.agric.nsw.gov.au/reader/7388. New South Wales Agriculture, Australia.
- Page, S. L. J. (1985). Pests and Diseases of Crops in Communal Areas of Zimbabwe. British Overseas Development Administration. UK.
- Parodi, G. N., 2000. AVHRR Hydrological Analysis System (AHAS). ITC Water Resources Division. Enschede, The Netherlands.
- Price, D. T., D.W. McKenny, I.A. Nalder, M.F. Hutchinson and J.L. Kesteven, 2000. A comparison of two statistical methods for interpolation of Canadian monthly mean climate data. *Agricultural Forest Meteorology*. 101: 81-94.
- Qin, Z., and A. Karnieli, 1999. Progress in the remote sensing of land surface temperature and ground emissivity using NOAA-AVHRR data. *Int. J. Remote Sensing* 20, 12: 2367-2393.
- Rosenberg, N. J., 1983. Microclimate, the Biological Environment, Second Edition, John Wiley & Sons, New York.
- Rukuni, M. and C.K. Eicher, 1994. Zimbabwe's Agricultural Revolution. University of Zimbabwe, Harare.
- SADC-RRSP - Regional Remote Sensing Project, 1998. The Database of the SADC Regional Remote Sensing Project; Working Paper Series No. 6. Merchant House, 43 Robson Manyika, P.O. Box 4046, Harare, Zimbabwe.
- Saney, G., J. Verdin, and R. Smith, 2001. Crop yield estimate comparison between two methods: Energy Balance EWBMS and Water Balance (WRSI). FEWS NET, USGS/EROS data Centre.
- Scoones, I. et al., 1996. Hazards and Opportunities. Farming Livelihoods in Dryland Africa. Lessons from Zimbabwe. IIED, London. 267 pp.
- Seed, A. W. and G.L. Austin, 1990. Sampling errors for raingauge-derived mean areal daily and monthly rainfall. *Journal of Hydrology*, 118: 163-173.

- Shumba, E. M. et al., 1990. Maize and Groundnut Yield Gap Analysis for Research Priority Setting in the Smallholder Sector of Zimbabwe. *Zimbabwe Journal of Agricultural Resources*: 105-113.
- Snijders, F. L., 1991. Rainfall monitoring based on Meteosat data - a comparison of techniques applied to the Western Sahel. *International Journal of Remote Sensing* 12: 1331-1347.
- Soer, G.J.R., 1980. Estimation of regional evapotranspiration and soil moisture conditions using remotely sensing crop surface temperature. *Remote Sensing Environment*, 9: 27-45.
- Thornton, P. K., W.T. Bowen, A.C. Ravelo, P.W. Wilkens, G. Farmer, J. Brock and J.E. Brink, 1997. Estimating millet production for famine early warning: an application of crop simulation modelling using satellite and ground-based data in Burkina Faso. *Agricultural and Forest Meteorology*, 83: 95-112.
- Venus, V., 1999. Towards a Framework for Maize Yield Forecasting; A Comparison of Two Promising Methods., M.Sc.-thesis, ITC, Enschede, The Netherlands.
- Waddington, S. R., 1993. Annual Report 1993, CIMMYT Maize Agronomy - Southern Africa, Harare, Zimbabwe. p. 33-53.
- Walker, P. J. C., 1989. *Famine Early Warning Systems*. Earthscan Publications Ltd, London. 196 pp.
- Whingwiri, E. E. et al. 1992. *Small Scale Agriculture in Zimbabwe. Book One. Farming Systems, Policy and Infrastructural Development*, Rockwood Publishers, Harare, Zimbabwe.
- Wit, C. T. de and F.W.T. Penning de Vries (1985). *Predictive Models in Agricultural Production*., Phil. Trans. R. Soc. London B310, London.

9. Appendixes

Appendix A: Outline of the Structure of the PS-n Algorithm

This program consists of three parts:

- (1) PROGRAM INITIALIZATION
- (2) INTERVAL CALCULATIONS, and
- (3) OUTPUT OF RESULTS.

** PART (1): PROGRAM INITIALIZATION **

RUNNR = 1

Fields are dimensioned for the storage of relevant parameters.

Basic weather data:

DIM Tmax(366), TMIN(366), PREC(366), RHA(366), E0(366), SUNH(366),
ET0(366)

Processed weather data and salinity data:

DIM TDAY(366), T24h(366), INTER(366), ECEW(366), ECET(366), ECE(366)

Calculated crop parameters:

DIM SLEAF(366), SROOT(366), SSTEM(366), SSO(366), LIVSLEAF(366),
LAI(366)

DIM TDM(366), LFRDS(366), RDS(366), TRM(366), TEMPDIFF(366)

Tabulated crop parameters:

DIM FRLEAF(20), FRROOT(20), FRSTEM(20), FRSO(20), CRDS(20)

Crop file and soil file labels:

DIM SOILLABEL\$(20), CROPLABEL\$(30)

Irrigation/water management parameters:

DIM cfwater(366), IE(366)

Interpolation values PS-nian approach:

DIM PASSDAY(36), RSTcan(36), LOP(36), ROCH(36), DIFVAL(36),
INTERTcan(366)

A Land Use System is composed of a Land Unit and a Land Utilisation Type.

The Land Unit properties are WEATHER properties and SOIL properties.

The weather data must be read from a file. The total number of weather stations on file is counted and the station names are identified:

GOSUB WEATHERFILE

Next, one weather station is selected and the data read:

GOSUB WEATHERDATA

Soil data are part of the Land Unit description but are not needed in PS-1 analyses. They will be called from file (if needed) after selection of the Production Situation to be analysed. Continue with the Land Utilisation Type, characterised by

CROP data and MANAGEMENT data. First, call the crop file, then select a crop and call the data:

CROFFILE:

GOSUB SELECTCROP

SKIPCROFFILE:

Management information will be entered from the keyboard. This concludes data collection for now. Select the Production Situation to be analysed:

PS SELECTION:

CLS

PRINT : PRINT

PRINT " WHICH PRODUCTION SITUATION DO YOU WISH TO ANALYSE ?"

PRINT : PRINT

PRINT " 1. The biophysical production potential (PS-1)"

PRINT " 2. The water-limited production potential (PS-2)"

PRINT : PRINT

INPUT " SELECT ONE OPTION AND PRESS 'ENTER' "; PSSELECT\$

IF VAL(PSSELECT\$) < 1 OR VAL(PSSELECT\$) > 2 THEN GOTO

PSSELECTION

IF VAL(PSSELECT\$) = 1 THEN

PASTSCENARIO = 1

GOTO SKIPSOILDATA

ELSE

PRINT : PRINT

INPUT " ==> CONVENTIONAL WATER BUDGET CALCULATION 'C' or PS-nIAN

'A"; PS-n\$

END IF

IF RUNNR = 0 THEN

IF PASTSCENARIO <> 1 AND (PS-n\$ <> "a" AND PS-n\$ <> "A") THEN

CLS

PRINT : PRINT

INPUT " DO YOU WISH TO SELECT A SOIL (Y/N)"; SOILSEL\$

IF SOILSEL\$ <> "Y" AND SOILSEL\$ <> "y" THEN

GOSUB CONDUCTIVITY

GOTO SKIPSOILDATA

END IF

ELSE

PASTSCENARIO = 0

END IF

END IF

The soil properties are read from file if the Production Situation <> 1.

GOSUB SELECTSOIL

GOSUB CONDUCTIVITY

SKIPSOILDATA:

The Land Utilisation Type is described by its "key attributes". The crop parameters are known once the crop (variety) has been selected from a menu.

MANAGEMENT/TECHNOLOGY information is now entered from the keyboard:

GOSUB MANAGEMENT

Before the calculations can start, a number of parameter values must be set to zero; other parameters may have an initial value other than zero (e.g. S(org)). Functions and numerical constants must be declared.

GOSUB INITIALISE

IF PS-n\$ = "A" OR PS-n\$ = "a" THEN

GOSUB INTERPOL

END IF

** PART (2): INTERVAL CALCULATIONS **

NEXTCYCLE:

*DETERMINE TEMPERATURES AND RDS AT MID-INTERVAL --**In this step, daily and daytime temperatures (T24h and TDAY) are computed.*

GOSUB DAYLENGTH

GOSUB CANRAD

GOSUB TEMPCALC

Use these AIR temperatures to check for TOO LOW temperature:

IF TMIN(DAY) > TLOW THEN

TCOUNT = 0

ELSE

TCOUNT = TCOUNT + Dt

END IF

IF ((RDS > .9) AND (TMIN(DAY) < -2) AND (TLOW > TMIN(DAY))) OR TCOUNT > 10 THEN

CLS

PRINT

LOCATE 10, 10: PRINT "MINIMUM TEMPERATURE ON DAY"; DAY; "WAS LESS THAN REQUIRED."

LOCATE 12, 10: PRINT "Press any key"

WHILE INKEY\$ = "": WEND

GOTO ANOTHERSCENARIO

END IF

Now calculate intercepted radiation, INTER in J/m2d:

GOSUB INTER

Now, calculate the difference between air temperature and canopy temperature:

GOSUB TEMPDIFF

Correct canopy temperature for TEMPDIFF

TDAY(DAY) = TDAY(DAY) + TEMPDIFF ' This is daytime temperature

T24h = (DL * TDAY(DAY) + (24 - DL) * Tnight) / 24

T24h(DAY) = T24h

Calculate the mid-term RDS using the canopy temperature:

GOSUB MIDTERM RDS

DETERMINE SLA AND LAI --

```
IF RDS = 0 THEN RDS = .01 ' To avoid LOG(0)
SLA = SLAMIN - .5 * (SLAMAX - SLAMIN) * LOG(RDS)
IF SLA > SLAMAX THEN SLA = SLAMAX ' At very low RDS
LAI = LIVSLEAF * SLA * .0001
LAI(RUNDAY) = LAI ' LAI array is only needed for printout!!
```

DETERMINE THE MAXIMUM RATE OF CO2 ASSIMILATION (AMAX) --

```
GOSUB AMAX
CC = EFF * ke * PARCAN
Fgc = DL * (AMAX / ke) * LOG((AMAX + CC) / (AMAX + CC * EXP(-LAI * ke)))
```

DETERMINE CFWATER --

```
IF (PS-n$ = "a" OR PS-n$ = "A") AND VAL(PSSELECT$) <> 1 THEN
IF RUNDAY = 1 THEN
PRINT
PRINT
PRINT " ==> HOW DO YOU WISH TO DEFINE cfwater?"
PRINT
PRINT " 1. against internal reference (TRact / TRref)"
PRINT " 2. Against external reference (TRact / TRmax)"
PRINT
INPUT " ==> Specify your choice (1 or 2)"; cf$
INPUT " ==> cfwater = TRact / TRref (internal) or cfwater = TRact / TRmax
(external) (I/E)"; cf$
END IF
RSDDELTA = INTERTcan(DAY) - TDAY(DAY)
DELTA TR = (RSDDELTA * VHEATCAP / AERODR) / LATHEAT ' in kg/m2sec!
DELTA TR = DELTA TR * CFLEAF ' only the covered fraction transpires 1
kg/m2sec is equivalent to 1 mm/s
TRref2 = INTER(RUNDAY) / LATHEAT ' TRref in kg/m2s
IF TRref2 <= 0 THEN
TRref2 = .01
END IF
TRactsec = TRref2 - DELTA TR ' in mm/s
IF TRactsec < 0 THEN TRactsec = 0
CHOOSECFAG:
IF cf$ = "1" THEN
cfag = TRactsec / TRref2
ELSEIF cf$ = "2" THEN
cfag = TRactsec / (TRM(RUNDAY) * 10)
ELSE
CLS
PRINT
PRINT
PRINT " ==> HOW DO YOU WISH TO DEFINE cfwater?"
```

```

PRINT
PRINT " 1. against internal reference (TRact / TRref)"
PRINT " 2. Against external reference (TRact / TRmax)"
PRINT
INPUT " ==> Specify your choice (1 or 2)"; cf$
GOTO CHOOSECFAG
END IF
IF cfag < 0 THEN cfag = 0
IF cfag > 1 THEN cfag = 1
cfwater = cfag
cfwater(RUNDAY) = cfwater
ELSEIF VAL(PSSSELECT$) <> 1 THEN
GOSUB WATERBALANCE
ELSE
cfwater = 1
cfwater(RUNDAY) = 1
END IF
IF DROUGHTLIMIT >= INT(PSILEAF / 1000 + .5) AND SEED <> 0 THEN GOTO
CROPOUTDRY
After (PSIleaf/1000) consecutive days of zero transpiration the crop perishes.
IF AERENCHYM <> 1 AND WETLIMIT >= 20 THEN GOTO CROPOUTWET
After 20 consecutive days of excessive wetness crops without aerenchym fail.

CALCULATE FGASS AND ALLOCATE FRACTIONS OF FGASS TO PLANT
ORGANS --
GOSUB GAAORG

DETERMINE THE MAINTENANCE RESPIRATION RATE --
GOSUB REFMAINT
GOSUB TEMPCORRECT
GOSUB ACTMAINT
DETERMINE NAA(org) AND DWI(org) OF ALL ORGANS --
GOSUB NETASSORG
GOSUB DRYWTINCREMENT

CALCULATE ORGAN WEIGHTS AND CORRECT FOR DEAD LEAVES --
GOSUB GROSSORG
GOSUB ENDRDS
GOSUB DEADLEAVES

CALCULATE TDM AND TLDM AT THE END OF THE CURRENT INTERVAL --
GOSUB TDMTLDM

ANOTHER INTERVAL ?? --
IF RDS < 1 THEN
DAY = DAY + Dt

```

```

IF DAY > Q THEN ' Q is Julian number of last day in the year
YEARFLAG = 1 ' Using Q permits to use leap years
DAY = DAY - Q
JAARNEW = JAAR + 1
JAAR$ = STR$(JAARNEW)
LENGTE = LEN(JAAR$)
JAAR$ = RIGHT$(JAAR$, LENGTE - 1)
FILE$ = PLEK$ + JAAR$ + ".DAT"
GOSUB NEWYEAR
END IF
RUNDAY = RUNDAY + Dt
IF RUNDAY > Q THEN GOTO TOOLONGONFIELD
GOTO NEXTCYCLE
END IF

```

```

*****
** PART (3): OUTPUT OF CALCULATION RESULTS **
*****

```

```

GOSUB OUTPUTONSCREEN
PRINT : PRINT
INPUT " ==> DO YOU WISH TO PRINT THE RESULTS ON A LINE PRINTER
(Y/N)"; LINEPR$
IF LINEPR$ = "Y" OR LINEPR$ = "y" THEN
GOSUB OUTPUTONPRINT
END IF
PRINT : PRINT
IF PS-n$ = "A" OR PS-n$ = "a" THEN
PRINT : PRINT
INPUT " ==> DO YOU WISH TO STORE DAILY TEMP & TDM DATA IN A FILE
(Y/N)"; STORE$
IF STORE$ = "Y" OR STORE$ = "y" THEN
GOSUB ASCIOUT
END IF
END IF

```

```

*****
** RESUMING OR EXITING THE PROGRAM **
*****

```

ANOTHER SCENARIO:

Appendix B: Land surface Temperature Retrieval

A Procedure based on the Coll and Caselles (1997) and Caselles, Coll and Valor (1997)

Step 1. DETERMINATION OF BARE SOIL – CROP NARROW-BAND EMISSIVITY

Define channel 4 and channel 5 emissivity values for a pure vegetation pixel, ε_v and for a pure bare soil pixel, ε_g .

Minimal data is available from literature, collated in AHAS (Parodi, 2000) help files (de calculator):

Available bare soil emissivity values ε_{ig} :

$\varepsilon_4 \approx \mathbf{0.969 \pm 0.004}$ (for loamy soils as found in the study area)

$\varepsilon_5 \approx \mathbf{0.976 \pm 0.005}$ (for loamy soils as found in the study area)

Specific narrow-band emissivity values for maize (study crop) are not available. However, the following broad-band values are available:

$\varepsilon_{8-14\mu m}$ maize over dry Petric Calcisol soil $\approx 0.968 \pm 0.009$

$\varepsilon_{8-14\mu m}$ maize over wet Petric Calcisol soil $\approx 0.983 \pm 0.005$

$\varepsilon_{8-14\mu m}$ **maize** $\approx (0.968 \pm 0.009 + 0.983 \pm 0.005)/2 \approx \mathbf{0.978 \pm 0.007}$ maize is taken as average of maize over dry soil and maize over wet soil

The above broad-band emissivity values need to be converted to ε_4 and ε_5 values using the expression:

$$\varepsilon_{ig} = (a * \varepsilon_{8-14\mu m}) + b$$

Where:

a and **b** are coefficients (for ε_4 calculations **a** $\approx \mathbf{1.619}$ and **b** $\approx \mathbf{-0.608}$ and for ε_5 calculations **a** $\approx \mathbf{1.467}$ and **b** $\approx \mathbf{-0.458}$).

Approximations for irrigated maize (source: AHAS):

$\varepsilon_{4\text{-maize}} = (\mathbf{1.619 * 0.978}) + (\mathbf{-0.608}) \approx \mathbf{0.975 \pm}$ (maize over wet **Petric Calcisol** soil)

$\varepsilon_{5\text{-maize}} = (\mathbf{1.467 * 0.978}) + (\mathbf{-0.458}) \approx \mathbf{0.977 \pm}$ (maize over wet **Petric Calcisol** soil)

Note! $\varepsilon_4 > \varepsilon_5$. **is always valid**

Step 2. DETERMINATION OF THE EMISSIVITY CORRECTION TERM “*demax*”

Define vegetation structure for the main vegetation/crops i.e. height, H, breadth, L and spacing, S. **For a fully-grown maize crop: H ≈ 2.5 m; L ≈ 0.6 and S ≈ 0.6 m.** Calculate for the emissivity correction term “*demax*”. “*demax*” is a correction for the emissivity non-linearity with NDVI. It is a function of vegetation structure and

satellite view angle. Algorithm is provided by AHAS spreadsheet with input parameters from step 2 (“**demax**” ≈ 0.024 for the study area).

Weight demax according to % land cover:

Example:

$$\text{final "de"} = a_1 * \text{demax}_{(\text{maize})} + a_2 * \text{demax}_{(\text{sorghum})} + a_3 * \text{demax}_{(\text{sunflower})}$$

$$a_1 + a_2 + a_3 = 100\% \text{ land cover}$$

However for the study area (Quzhou, North China Plain), land cover is homogeneously ‘maize’ in the summer growing season. Weighting is not necessary.

Step 3. CALCULATION OF VEGETATION PROPORTION

Determine pure bare soil and pure vegetation pixels from NDVI map. Pure bare soil pixel has the lowest positive NDVI value whereas the pure vegetation pixel has the highest positive NDVI value. Examine and record the albedo values of the pure bare soil and pure vegetation pixels (*ILWIS pixel info*).

Calculate for K. 'K' is the ratio between the difference of the reflectance of the fully vegetated pixel in Channel 2 and Channel 1 by the same difference but for the bare soil pixel. It is an image constant. CH1SUR and CH2SUR are atmospherically corrected reflectance.

$$K = \text{CH2SUR}_v - \text{CH1SUR}_v / \text{CH2SUR}_{bs} - \text{CH1SUR}_{bs}$$

Example for image of Quzhou (study area) 23 Aug 99:

$$\text{CH2SUR}_v \approx 0.340$$

$$\text{CH1SUR}_v \approx 0.119$$

$$\text{CH2SUR}_{bs} \approx 0.170$$

$$\text{CH1SUR}_{bs} \approx 0.150$$

$$\therefore K = 11.05$$

$$\text{NDVI}_{bs} \approx 0.050; \text{NDVI}_v \approx 0.550$$

The vegetation proportion **map** ($L511P_v$), is calculated by the following expression:

$$P_v = 1 - (\text{NDVI} / \text{NDVI}_{bs}) / ((1 - \text{NDVI} / \text{NDVI}_{bs}) - K(1 - \text{NDVI} / \text{NDVI}_v))$$

Step 4. CALCULATION OF NARROW BAND (channels 4 and 5) EMISSIVITY MAPS

Calculate for Channel 4 and Channel 5 (narrow band) emissivity maps:

$$\epsilon_4(\text{map}) = \epsilon_{4bs}(1 - P_v(\text{map})) + (\epsilon_{4v} * P_v(\text{map})) + (4 * \text{demax} * P_v(\text{map}) * (1 - P_v(\text{map})))$$

$$\epsilon_5(\text{map}) = \epsilon_{5bs}(1 - P_v(\text{map})) + (\epsilon_{5v} * P_v(\text{map})) + (4 * \text{demax} * P_v * (1 - P_v(\text{map})))$$

Note! ϵ values lies between 0 and 1

Use “if” statements to mask water and cloud pixels.

Examples:

If (NDVI < 0, $\varepsilon_{4,5} = 1$, $\varepsilon_{4,5}$)

If ($\varepsilon_{4,5} > 1$, 1, $\varepsilon_{4,5}$)

If (Ch5 < threshold Temp, ?, Ch5)

Step 5. CALCULATION OF MEAN AND DIFFERENCE EMISSIVITY MAPS

Calculate for mean emissivity, ε

$$\varepsilon(\text{map}) = \varepsilon_4(\text{map}) + \varepsilon_5(\text{map}) / 2$$

$$\Delta\varepsilon(\text{map}) = \varepsilon_4(\text{map}) - \varepsilon_5(\text{map})$$

Note! $\varepsilon_5 > \varepsilon_4$!

Calculate offset map:

$$\text{Offset}(\text{map}) = 0.56 + a * (1 - \varepsilon) - b * \Delta\varepsilon$$

Constants obtained from Coll and Caselles (1997) graph: **a = 40** (fairly constant), **b = 80** (median value).

Step 6. CALCULATION OF CROP CANOPY TEMPERATURE

Calculate of surface (canopy) temperature from Coll and Caselles (1997) equation.

$$T_0(\text{map}) = c_{42}(\text{Ch}_4\text{BT}(\text{map}))^2 + c_4\text{Ch}_4\text{BT}(\text{map}) + c_{45} * \text{Ch}_4\text{BT}(\text{map}) * \text{Ch}_5\text{BT}(\text{map}) + c_{52} * (\text{Ch}_5\text{BT})^2(\text{map}) + \text{Offset}(\text{map})$$

Coefficients obtained from Coll and Caselles (1997):

$$c_{42} = 0.39$$

$$c_4 = 2.34$$

$$c_{45} = -0.78$$

$$c_5 = -1.34$$

$$c_{52} = 0.39$$

To note in ILWIS! For all maps, "values for domain":

Map	Range	Precision	Practical range
NDVI	-1 - 1	0.001	-2 - 2
ε	0 - 1	0.001	-1 - 2
T_0	250 - 350	0.1	150 - 350

Appendix C: 1998 Weather of Karoi from Interpolated Surfaces

LAT (-16.83°); LON (29.62°E); ELEV (1344m); TAV (19.8°C); AMP (14.9mm)
 REFHT (missing); WNDHT (missing); Meteorological Station (KAROI)

DATE	RAD	T _{MAX}	T _{MIN}	RAIN	DATE	RAD	T _{MAX}	T _{MIN}	RAIN
98001	25.9	28.1	18.9	.0	98032	13.1	27.7	19.2	5.6
98002	30.0	27.4	17.1	31.9	98033	8.5	24.5	18.3	10.9
98003	9.1	24.9	19.8	.6	98034	8.3	24.9	17.5	2.2
98004	20.3	29.0	22.7	.0	98035	6.5	26.1	19.8	8.0
98005	25.1	26.3	17.4	.0	98036	9.4	26.2	20.5	12.7
98006	9.1	23.9	19.2	1.9	98037	28.1	28.9	18.4	.0
98007	26.0	28.1	19.1	.0	98038	13.7	26.8	18.3	6.1
98008	26.1	26.4	22.0	.0	98039	24.9	30.1	19.2	.0
98009	7.3	20.1	18.7	.6	98040	9.0	27.8	19.0	2.2
98010	20.6	23.5	17.2	.0	98041	9.6	31.9	21.9	.3
98011	25.1	24.9	15.5	.0	98042	13.4	29.9	20.3	.0
98012	27.7	26.9	13.2	.0	98043	26.4	28.7	19.1	.0
98013	19.4	23.3	14.3	.0	98044	6.4	27.7	21.9	.2
98014	22.4	25.4	14.8	.0	98045	28.5	27.6	17.0	.0
98015	21.1	26.7	15.8	.0	98046	18.2	24.0	17.8	16.1
98016	26.9	28.0	16.2	.0	98047	25.8	28.0	15.6	.0
98017	24.3	29.0	17.4	.0	98048	23.8	27.3	18.0	.0
98018	25.9	28.9	15.2	.0	98049	14.7	22.7	17.9	40.7
98019	16.2	31.1	16.9	116.9	98050	19.6	24.1	16.3	.0
98020	11.4	26.0	18.1	9.1	98051	22.9	24.8	16.3	.0
98021	23.9	27.6	17.0	3.2	98052	19.5	28.0	18.9	.0
98022	10.5	20.2	16.7	.2	98053	25.8	26.8	20.2	.0
98023	9.5	18.8	16.1	1.8	98054	11.3	25.0	17.1	19.2
98024	21.6	22.9	17.7	8.5	98055	23.6	27.2	14.1	.0
98025	19.5	22.4	14.8	13.1	98056	20.2	21.0	17.2	3.8
98026	26.4	25.6	17.5	2.5	98057	20.1	26.0	17.8	.0
98027	16.1	26.9	19.1	4.7	98058	23.4	24.4	15.8	.0
98028	17.9	27.6	18.3	.5	98059	31.2	28.5	18.0	.0
98029	16.2	25.3	16.8	.7	98060	31.1	27.4	19.1	.0
98030	16.6	28.9	17.9	3.8	98061	31.0	29.1	14.9	.0
98031	22.2	28.9	17.2	7.9	98062	30.9	27.0	15.1	.0

Appendix D1: Land Mapping Units (LMUs) in Piriwiri/Mupfure

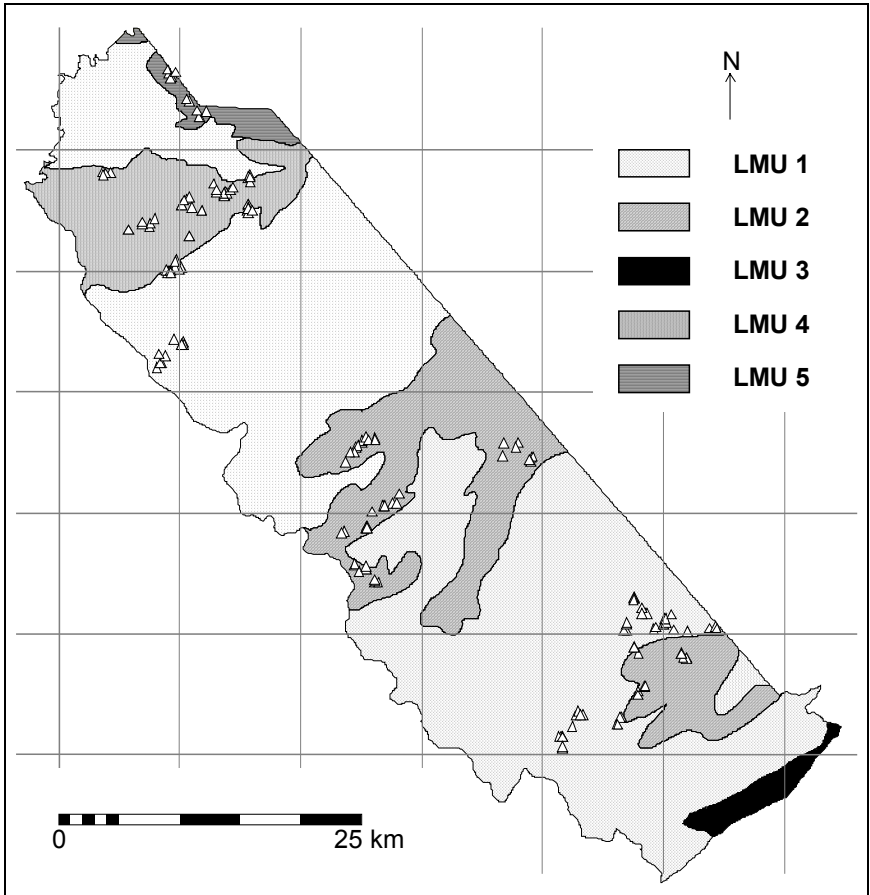


Figure 49. Mapping Units of Piriwiri/Mupfure communal land wards, based on Anderson et al (1987).

Appendix D2: Legend to Land Mapping Units

Table 10. Legend to Land Mapping Units (Appendix D1) of Piriwiri and Mupfure communal lands based on Anderson et al (1987)

LMU	TOPOGRAPHY	GEOLOGY	SOILS	REMARKS
1	Rolling to Hilly	Mainly Piriwiri Phyllites	Very shallow fine sandy loam to clay loam liable capping, over strong brown to yellowish red clay loam to clay	Steep slopes and shallow soils with severe erosion hazard
2	Undulating	Mainly Piriwiri Phyllites	Similar to Land Unit 1, with a small proportion of alluvium	Shallow stony soils, susceptible to erosion
3	Ridge and Valley	Lomagundi quartzites, dolomite, slate and argillites	Variable with the quartzites and dolomites forming sands or loamy sands over yellowish red or red fine sandy loams of variable depth. The argillaceous rocks produce silty soil similar to those over phyllites of Land Units 1 and 2.	Mainly Steep lands
4	Mainly undulating	Sijarira sandstones, slates and conglomerates	Sijarira sediments. Shallow moderately deep medium or fine-grained loamy sands over strong brown to yellowish red medium grained sandy loams or sandy clay loams.	No major physical constraints. 40% arably disturbed, mainly maize and cotton.
5	Complex topography	Tengwe limestone, dolomite and quartzite	Soils of the klippe overthrust comprising arkose, limestone, gneiss, quartzite and tillite.	Partly stony or rocky.

Appendix E1: Sample Checklist***Sample Checklist for Land Use and Land Ecology Survey***

DATE: SERIAL No:
 VILLAGE No: WARD No:
 NAME OF FARMER:
 TYPE OF FARMER: Ordinary Communal Farmer
 Master Farmer
 Advanced Master Farmer

POSSIBLE OPERATIONS:

Op. 1: CLEARING

Was the field cleared as virgin land by farmer? Yes / No
 If Yes, when?
 If No, for how long has the farmer been cultivating the land?

Op. 2: PLOUGHING

- (a) How many Ploughings did farmer make for the 1995/6 maize crop?
- (b) Early Ploughing (at the end of the previous growing season)
When? How? How deep? What Implements?
- (c) Late Ploughing (just before the start of the growing season)
When? How? How deep? What Implements?
- (d) Other Ploughings
When? How? How deep? What Implements?

Op. 3: HARROWING

- (a) Did farmer carry out Harrowing?
How many times? When? How? What Implements?

Op. 4: PLANTING

- (a) Which variety of seed did farmer plant?
When? How? How much per field? What Implements? At what spacing?

Op. 5: FERTILITY MAINTENANCE

- Which fertilizers were applied?
- (a) Compound D
 - (b) Ammonium Nitrate
 - (c) Urea
 - (d) Farm Yard Manure / What type?
 - (e) Lime
 - (f) Ant/Termite Hill soil
 - (g) Crop Residue / What type?

* In each case, specify:

When? How applied? How much / field? What Implements?

Op. 6: WEED CONTROL

(a) How many times was weeding carried out in the field?

1st Weeding; 2nd Weeding; 3rd Weeding

* In each case, specify:

When? How? What Implements?

Name the dominant weeds

Estimate damage/loss of yield (percentage) attributable to weed infestation

Op. 7: PEST CONTROL

(a) Ants/Termites

(b) Stalkborer

(c) Grasshopper/Locusts

(d) Ballworm/Armyworms

(e) Aphids

(f) Other Pests

In each case, **When** was the pest attack? **How? What** implements were used to control pests.

Estimate damage/loss of yield (percentage) attributable to Pests

Op. 8: DISEASE CONTROL

(a) Were there any plant diseases?

When? How? What Implements used to control disease?

Estimate damage/loss of yield (percentage) attributable to Disease.

Op. 9: HARVESTING

(a) **When? How?**

(b) **Actual Yield / field**

(c) **Target Yield / field**

Why difference between Op. 9(b) and Op.9(c)

(d) **Which operations ensure sustainability?**

(e) What were the reasons for higher or lower yields?

(f) Did you burn the field as part of land preparation (i.e before tillage)?

CROP OBSERVATIONS

Observ. 1 (a) Tasselling / Silking

(b) Drought stress

(c) Other Crop Observations

In each case, when? How long? Estimated loss of yield

Any other periods?

SOIL CHARACTERISTICS

(a) Soil depth of field

(b) Fertility status - increasing / stabilising / declining?

(c) Stoniness of field (percentage)

(d) Improvements on the field

What improvements are needed in the field to ensure sustainability?

1/ Infrastructure, 2/ Soil structure, 3/ Purchase of implements, 4/ Operations, 5/ Methods

(e) Infiltration rate field check:

How many seconds does it take 1/2 cup of water to infiltrate into the soil?

Seconds	Class
0-10	1
11-20	2
21-30	3
31-40	4
41-50	5
51-60	6
>60	7

ONLY FOR SELECTED FARMERS

Requirements for good farming

- What are the requirements for Good Farming from your point of view?
- What are the Agritex recommendations for sustainable maize cultivation?
- What is the degree of acceptability or adaptability of the Agritex recommendations for sustainable maize cultivation?

Problems hindering good farming

- Fertilizer availability
- Infrastructure
- Labour problems at peak periods
- Slopy and stony fields
- Anthills in fields
- Other problems related to fields.

Appendix E2: Sample Relevee Data Sheet

I General	Relevee no.:	Photo no.:	Date:	Corresponding field interview Respondent's name:
	LMU:	Run no.:	Photo element:	Field/Plot size (m ²):
		UTM Coordinate:m(X)m(y)		

II Photo characteristics	Texture	VC	C	M	F	S	Others
	Tone	DG	G	W	Others		
	Field pattern	Yes	No	N/A			
	Field shape	I	B	S	Others		
Landsat TM	Colour						
MOMS-2	Colour						

III Terrain	Altitude (m):	Slope (%):	Rock outcrops in field	Slope shape	Field position in area	Relief type
			- present - absent	- irregular - s-shaped - concave - convex - straight	- low - mid - upper	- very flat - almost flat (<2%) - undulating (3-7%) - rolling (8-13%) - hilly (14-20%) - steeply dissected (21-55%) - mountainous (>55%)

IV Soil

Layer	Depth (cm)	Texture (code)	Structure	Colour (wet)	pH (wet)	Mottling (%)	Mottling (colour)	Stoniness (%)
1								
2								
3								
4								

V Land cover/land use

Strata	Height (cm/m)	% Cover	Remarks
Trees			
Shrubs			
Forbs			
Litter layer (0 cm)	N/A		
Basal cover (0 cm)	N/A		
Stoniness (0 cm)	N/A		

VI Cultivated crop species and field status

	Crops grown	Crop residues	Status of field
1			
2			
3			

VII Infrastructure

Bunds	Other physical conservation structures	Wells/ditches	Reservoir	Basins	Others

Area Sketch	Cross-section sketch: Indication of field

VIII. SUSTAINABILITY INDICATORS

Indicate evidence of Sustainability (favourable structure or soil compaction, erosion control or accelerated erosion, fertility enhancement or fertility depletion, moisture conservation or drought stress and low incidence of pests/diseases or high incidence of pests/diseases).

IX. GENERAL REMARKS OR OBSERVATIONS

Appendix F: ITC PhD Dissertation List

1. **Akinyede**, 1990, Highway cost modelling and route selection using a geotechnical information system
2. **Pan He Ping**, 1990, 90-9003757-8, Spatial structure theory in machine vision and applications to structural and textural analysis of remotely sensed images
3. **Bocco Verdinelli, G.**, 1990, Gully erosion analysis using remote sensing and geographic information systems: a case study in Central Mexico
4. **Sharif, M.**, 1991, Composite sampling optimization for DTM in the context of GIS
5. **Drummond, J.**, 1991, Determining and processing quality parameters in geographic information systems
6. **Groten, S.**, 1991, Satellite monitoring of agro-ecosystems in the Sahel
7. **Sharifi, A.**, 1991, 90-6164-074-1, Development of an appropriate resource information system to support agricultural management at farm enterprise level
8. **Zee, D. van der**, 1991, 90-6164-075-X, Recreation studied from above: Air photo interpretation as input into land evaluation for recreation
9. **Mannaerts, C.**, 1991, 90-6164-085-7, Assessment of the transferability of laboratory rainfall-runoff and rainfall - soil loss relationships to field and catchment scales: a study in the Cape Verde Islands
10. **Ze Shen Wang**, 1991: 90-393-0333-9, An expert system for cartographic symbol design
11. **Zhou Yunxian**, 1991, 90-6164-081-4, Application of Radon transforms to the processing of airborne geophysical data
12. **Zuviria, M. de**, 1992, 90-6164-077-6, Mapping agro-topoclimates by integrating topographic, meteorological and land ecological data in a geographic information system: a case study of the Lom Sak area, North Central Thailand
13. **Westen, C. van**, 1993, 90-6164-078-4, Application of Geographic Information Systems to landslide hazard zonation
14. **Shi Wenzhong**, 1994, 90-6164-099-7, Modelling positional and thematic uncertainties in integration of remote sensing and geographic information systems
15. **Javelosa, R.**, 1994, 90-6164-086-5, Active Quaternary environments in the Philippine mobile belt
16. **Lo King-Chang**, 1994, 90-9006526-1, High Quality Automatic DEM, Digital Elevation Model Generation from Multiple Imagery
17. **Wokabi, S.**, 1994, 90-6164-102-0, Quantified land evaluation for maize yield gap analysis at three sites on the eastern slope of Mt. Kenya
18. **Rodriguez, O.**, 1995, Land Use conflicts and planning strategies in urban fringes: a case study of Western Caracas, Venezuela
19. **Meer, F. van der**, 1995, 90-5485-385-9, Imaging spectrometry & the Ronda peridotites

20. **Kufoniyi, O.**, 1995, 90-6164-105-5, Spatial coincidence: automated database updating and data consistency in vector GIS
21. **Zambezi, P.**, 1995, Geochemistry of the Nkombwa Hill carbonatite complex of Isoka District, north-east Zambia, with special emphasis on economic minerals
22. **Woldai, T.**, 1995, The application of remote sensing to the study of the geology and structure of the Carboniferous in the Calañas area, pyrite belt, SW Spain
23. **Verweij, P.**, 1995, 90-6164-109-8, Spatial and temporal modelling of vegetation patterns: burning and grazing in the Paramo of Los Nevados National Park, Colombia
24. **Pohl, C.**, 1996, 90-6164-121-7, Geometric Aspects of Multisensor Image Fusion for Topographic Map Updating in the Humid Tropics
25. **Jiang Bin**, 1996, 90-6266-128-9, Fuzzy overlay analysis and visualization in GIS
26. **Metternicht, G.**, 1996, 90-6164-118-7, Detecting and monitoring land degradation features and processes in the Cochabamba Valleys, Bolivia. A synergistic approach
27. **Hoanh Chu Thai**, 1996, 90-6164-120-9, Development of a Computerized Aid to Integrated Land Use Planning (CAILUP) at regional level in irrigated areas: a case study for the Quan Lo Phung Hiep region in the Mekong Delta, Vietnam
28. **Roshannejad, A.**, 1996, 90-9009284-6, The management of spatio-temporal data in a national geographic information system
29. **Terlien, M.**, 1996, 90-6164-115-2, Modelling Spatial and Temporal Variations in Rainfall-Triggered Landslides: the integration of hydrologic models, slope stability models and GIS for the hazard zonation of rainfall-triggered landslides with examples from Manizales, Colombia
30. **Mahavir, J.**, 1996, 90-6164-117-9, Modelling settlement patterns for metropolitan regions: inputs from remote sensing
31. **Al-Amir, S.**, 1996, 90-6164-116-0, Modern spatial planning practice as supported by the multi-applicable tools of remote sensing and GIS: the Syrian case
32. **Pilouk, M.**, 1996, 90-6164-122-5, Integrated modelling for 3D GIS
33. **Duan Zengshan**, 1996, 90-6164-123-3, Optimization modelling of a river-aquifer system with technical interventions: a case study for the Huangshui river and the coastal aquifer, Shandong, China
34. **Man, W.H. de**, 1996, 90-9009-775-9, Surveys: informatie als norm: een verkenning van de institutionalisering van dorp - surveys in Thailand en op de Filipijnen
35. **Vekerdy, Z.**, 1996, 90-6164-119-5, GIS-based hydrological modelling of alluvial regions: using the example of the Kisaföld, Hungary
36. **Pereira, Luisa**, 1996, 90-407-1385-5, A Robust and Adaptive Matching Procedure for Automatic Modelling of Terrain Relief

37. **Fandino Lozano, M.**, 1996, 90-6164-129-2, A Framework of Ecological Evaluation oriented at the Establishment and Management of Protected Areas: a case study of the Santuario de Iguaque, Colombia
38. **Toxopeus, B.**, 1996, 90-6164-126-8, ISM: an Interactive Spatial and temporal Modelling system as a tool in ecosystem management: with two case studies: Cibodas biosphere reserve, West Java Indonesia: Amboseli biosphere reserve, Kajiado district, Central Southern Kenya
39. **Wang Yiman**, 1997, 90-6164-131-4, Satellite SAR imagery for topographic mapping of tidal flat areas in the Dutch Wadden Sea
40. **Asun Saldana-Lopez**, 1997, 90-6164-133-0, Complexity of soils and Soilscape patterns on the southern slopes of the Ayllon Range, central Spain: a GIS assisted modelling approach
41. **Ceccarelli, T.**, 1997, 90-6164-135-7, Towards a planning support system for communal areas in the Zambezi valley, Zimbabwe; a multi-criteria evaluation linking farm household analysis, land evaluation and geographic information systems
42. **Peng Wanning**, 1997, 90-6164-134-9, Automated generalization in GIS
43. **Lawas, C.**, 1997, 90-6164-137-3, The Resource Users' Knowledge, the neglected input in Land resource management: the case of the Kankanaey farmers in Benguet, Philippines
44. **Bijker, W.**, 1997, 90-6164-139-X, Radar for rain forest: A monitoring system for land cover Change in the Colombian Amazon
45. **Farshad, A.**, 1997, 90-6164-142-X, Analysis of integrated land and water management practices within different agricultural systems under semi-arid conditions of Iran and evaluation of their sustainability
46. **Orlic, B.**, 1997, 90-6164-140-3, Predicting subsurface conditions for geotechnical modelling
47. **Bishr, Y.**, 1997, 90-6164-141-1, Semantic Aspects of Interoperable GIS
48. **Zhang Xiangmin**, 1998, 90-6164-144-6, Coal fires in Northwest China: detection, monitoring and prediction using remote sensing data
49. **Gens, R.**, 1998, 90-6164-155-1, Quality assessment of SAR interferometric data
50. **Turkstra, J.**, 1998, 90-6164-147-0, Urban development and geographical information: spatial and temporal patterns of urban development and land values using integrated geo-data, Villaviciencia, Colombia
51. **Cassells, C.**, 1998, Thermal modelling of underground coal fires in northern China
52. **Naseri, M.**, 1998, 90-6164-195-0, Characterization of Salt-affected Soils for Modelling Sustainable Land Management in Semi-arid Environment: a case study in the Gorgan Region, Northeast, Iran
53. **Gorte B.G.H.**, 1998, 90-6164-157-8, Probabilistic Segmentation of Remotely Sensed Images
54. **Tenalem Ayenew**, 1998, 90-6164-158-6, The hydrological system of the lake district basin, central main Ethiopian rift
55. **Wang Donggen**, 1998, 90-6864-551-7, Conjoint approaches to developing activity-based models

56. **Bastidas de Calderon, M.**, 1998, 90-6164-193-4, Environmental fragility and vulnerability of Amazonian landscapes and ecosystems in the middle Orinoco river basin, Venezuela
57. **Moameni, A.**, 1999, Soil quality changes under long-term wheat cultivation in the Marvdasht plain, South-Central Iran
58. **Groenigen, J.W. van**, 1999, 90-6164-156-X, Constrained optimisation of spatial sampling: a geostatistical approach
59. **Cheng Tao**, 1999, 90-6164-164-0, A process-oriented data model for fuzzy spatial objects
60. **Wolski, Piotr**, 1999, 90-6164-165-9, Application of reservoir modelling to hydrotopes identified by remote sensing
61. **Acharya, B.**, 1999, 90-6164-168-3, Forest biodiversity assessment: A spatial analysis of tree species diversity in Nepal
62. **Akbar Abkar, Ali**, 1999, 90-6164-169-1, Likelihood-based segmentation and classification of remotely sensed images
63. **Yanuariadi, T.**, 1999, 90-5808-082-X, Sustainable Land Allocation: GIS-based decision support for industrial forest plantation development in Indonesia
64. **Abu Bakr**, Mohamed, 1999, 90-6164-170-5, An Integrated Agro-Economic and Agro-Ecological Framework for Land Use Planning and Policy Analysis
65. **Eleveld, M.**, 1999, 90-6461-166-7, Exploring coastal morphodynamics of Ameland (The Netherlands) with remote sensing monitoring techniques and dynamic modelling in GIS
66. **Yang Hong**, 1999, 90-6164-172-1, Imaging Spectrometry for Hydrocarbon Microseepage
67. **Mainam, Félix**, 1999, 90-6164-179-9, Modelling soil erodibility in the semiarid zone of Cameroon
68. **Bakr, Mahmoud**, 2000, 90-6164-176-4, A Stochastic Inverse-Management Approach to Groundwater Quality
69. **Zlatanova, Z.**, 2000, 90-6164-178-0, 3D GIS for Urban Development
70. **Ottichilo, Wilber K.**, 2000, 90-5808-197-4, Wildlife Dynamics: An Analysis of Change in the Masai Mara Ecosystem
71. **Kaymakci, Nuri**, 2000, 90-6164-181-0, Tectono-stratigraphical Evolution of the Cankori Basin (Central Anatolia, Turkey)
72. **Gonzalez, Rhodora**, 2000, 90-5808-246-6, Platforms and Terraces: Bridging participation and GIS in joint-learning for watershed management with the Ifugaos of the Philippines
73. **Schetselaar, Ernst**, 2000, 90-6164-180-2, Integrated analyses of granite-gneiss terrain from field and multisource remotely sensed data. A case study from the Canadian Shield
74. **Mesgari, Saadi**, 2000, 90-3651-511-4, Topological Cell-Tuple Structure for Three-Dimensional Spatial Data
75. **Bie, Cees A.J.M. de**, 2000, 90-5808-253-9, Comparative Performance Analysis of Agro-Ecosystems
76. **Khaemba, Wilson M.**, 2000, 90-5808-280-6, Spatial Statistics for Natural Resource Management

77. **Shrestha, Dhruva**, 2000, 90-6164-189-6, Aspects of erosion and sedimentation in the Nepalese Himalaya: highland-lowland relations
78. **Asadi Haroni, Hooshang**, 2000, 90-6164-185-3, The Zarshuran Gold Deposit Model Applied in a Mineral Exploration GIS in Iran
79. **Raza, Ale**, 2001, 90-3651-540-8, Object-oriented Temporal GIS for Urban Applications
80. **Farah, Hussein**, 2001, 90-5808-331-4, Estimation of regional evaporation under different weather conditions from satellite and meteorological data. A case study in the Naivasha Basin, Kenya
81. **Zheng, Ding**, 2001, 90-6164-190-X, A Neural - Fuzzy Approach to Linguistic Knowledge Acquisition and Assessment in Spatial Decision Making
82. **Sahu, B.K.**, 2001, Aeromagnetics of continental areas flanking the Indian Ocean; with implications for geological correlation and Gondwana reassembly
83. **Alfestawi, Y.**, 2001, 90-6164-198-5, The structural, paleogeographical and hydrocarbon systems analysis of the Ghadamis and Murzuq Basins, West Libya, with emphasis on their relation to the intervening Al Qarqaf Arch
84. **Liu, Xuehua**, 2001, 90-5808-496-5, Mapping and Modelling the Habitat of Giant Pandas in Foping Nature Reserve, China
85. **Oindo, Boniface Oluoch**, 2001, 90-5808-495-7, Spatial Patterns of Species Diversity in Kenya
86. **Carranza, Emmanuel John**, 2002, 90-6164-203-5, Geologically-constrained Mineral Potential Mapping

Samenvatting

Actuele Landgebruikssystemen kunnen met de bestaande gewasgroeimodellen niet adequaat worden ge-analyseerd; de benodigde data, de complexiteit van het algoritme en de vaak aanzienlijke foutenmarge staan zinnige analyse in de weg. Wel is het mogelijk sterk vereenvoudigde systemen te beschrijven, zogenaamde 'produktiesituaties', met eenjarige voedsel- of vezelgewassen en met minimale groeibeperkingen. De minimumconfiguratie is een produktiesituatie, waarin alle beperkingen, die een gebruiker kan elimineren ook inderdaad verholpen zijn. Gewasproductie en oogst worden dan uitsluitend bepaald door de fysiologie van het gewas, en de straling en temperatuur gedurende de gewasgroeicyclus. De met zulke modellen berekende produktie is *niet* de door de landgebruiker gerealiseerde produktie, maar geeft aan welke produktie binnen de gespecificeerde lokatie- en tijd-grenzen mogelijk is: het 'biophysisch produktiepotentieel'.

In veel gebieden wordt plantaardige produktie vooral beperkt door een tekort aan water. Het model van de minimum produktiesituatie is daarom uitgebreid met een waterbudget-routine, waarin het *actuele* waterverbruik door het gewas wordt gekwantificeerd. Het op basis hiervan berekende 'water-beperkte produktiepotentieel' geeft aan hoeveel gewasproductie mogelijk is onder de bestaande condities van straling, temperatuur *en* waterbeschikbaarheid. Dit proefschrift onderzoekt het gebruik van satelliet-gegevens voor het regional schatten van regenvalcijfers. Deze worden vervolgens ingevoerd in berekeningen van het water-beperkte produktiepotentieel.

Zinnige interpretatie van gewasgroei is onmogelijk, indien de sociaal-economische omstandigheden, waaronder de landgebruiker opereert, niet in de beschouwingen worden betrokken. Dit proefschrift onderzoekt of en hoe ideeën en indrukken van landgebruikers kunnen helpen om de oorzaken en opbouw van de 'yield gap' (i.e. het verschil tussen de berekende *mogelijke oogst* en de werkelijk *gerealiseerde* oogst) vast te stellen.

In het verleden kon de werkelijk gerealiseerde oogst alleen worden bepaald middels directe veldwaarnemingen. Dit proefschrift beschrijft een methodiek voor berekening/schatting van werkelijke gewasproductie. Hiertoe wordt de relatieve sluiting van huidmondjes, en daarmee de relatieve assimilatie door het gewas, geschat op basis van o.a. het temperatuurverschil tussen het bladerdek en de omringende lucht. Invoering van de assimilatiebeperking in het gewasgroeimodel staat toe, de regionaal gerealiseerde, werkelijke produktie te berekenen.

Herhaalde metingen in de loop van de gewascyclus maken het mogelijk om op ieder moment te bepalen in hoeverre bestaande cultuurmaatregelen in de praktijk voldoen. Indien voor het verdere verloop van de gewasgroeicyclus *geschatte* of *voorspelde* weergegevens in de berekeningen worden ingevoerd, kan de verwachte gewasgroei gedurende de rest van de groeicyclus worden bepaald en kan –indien nodig- het 'management' tijdig worden bijgesteld.

Curriculum Vitae

I, Denis Rugege, was born on 12 January 1959 in Kabale, Uganda. I completed High School at Makerere College School in 1977. Thereafter, I accepted an internship job in the Central Bank of Uganda. In 1984, I joined the mass exodus out of Uganda avoiding war and political turmoil. In that same year, I enrolled in a B.Sc.-degree programme at the University of Swaziland and completed it at the National University of Lesotho in 1988, with majors in Applied Environmental Sciences and Physics. I returned to Southern Africa to teach Geography and Science at Goronyane High School in the Free State. In October 1991, I joined the Institute of Natural Resources in Pietermaritzburg, South Africa, as a KW Kellogg research intern in natural resource and environmental management. In September 1992, I was awarded a fellowship by the Netherlands Fellowship Programme to study Rural and Land Ecology Survey at ITC in Enschede. I obtained my Post-Graduate Diploma in September 1993 and a Masters Degree in October 1994.

I re-joined the Institute of Natural Resources in October 1994 as a Research Fellow, contributing geo-information management skills to various projects. In February 1997, I started part-time Ph.D.-research on “Regional Analysis of Maize-based Land Use Systems” in the framework of the SAIL funded project “Sharing Scarce Resources – Zambezi valley”. My fieldwork area was in the Piriwiri and Mupfure communal lands in the Zambezi valley, Zimbabwe.

In 1999, I joined the Centre for Environment and Development of Natal University as Coordinator for South Africa in the SAIL-funded regional project “Training and Education in Land Management in Southern Africa – TELMSA”. Recently, the University of Natal developed a new Masters programme in Land Information Management under the TELMSA project framework, with technical assistance by ITC. Teaching started in January 2002; I hold the position of Programme Director.

